Project Report
NASA/A-7

Results of an Exploratory Study to Develop a Model for Route Availability in en Route Airspace as a Function of Actual Weather Coverage and Type

B.D. Martin
J.E. Evans
R.A. DeLaura

24 October 2006

Lincoln Laboratory
MASSACHUSETTS INSTITUTE OF TECHNOLOGY
LEXINGTON, MASSACHUSETTS

Prepared for the National Aeronautics and Space Administration
Langley Research Center
Hampton, Virginia 23681

TECHNICAL REPORT STANDARD TITLE PAGE

1. Report No.	2. Government Accession No.	3. Recipient's Catalog No.
NASA/A-7		

4. Title and Subtitle	5. Report Date
Results of an Exploratory Study to Develop a Model for Route Availability in en Route Airspace as a Function of Actual Weather Coverage and Type	24 October 2006
	6. Performing Organization Code
7. Author(s)	8. Performing Organization Report No.
B.D. Martin, R.A. DeLaura, and J.E. Evans	NASA/A-7
9. Performing Organization Name and Address	10. Work Unit No. (TRAIS)
MIT Lincoln Laboratory 244 Wood Street Lexington, MA 02420-9108	11. Contract or Grant No. NASA Langley
12. Sponsoring Agency Name and Address	13. Type of Report and Period Covered Project Report
NASA Langley Research Center 100 NASA Road Hampton, VA 23681-2199	14. Sponsoring Agency Code

15. Supplementary Notes

This report is based on studies performed at Lincoln Laboratory, a center for research operated by Massachusetts Institute of Technology, under Air Force Contract FA8721-05-C-0002.

16. Abstract

The objective of this exploratory study is to develop a model that relates convective weather (Wx) to a surrogate for capacity in en route airspace—ATC sector route blockage (RB). This Wx-RB model can then be coupled with forecast meteorological validation models to provide a model that translates probabilistic Wx forecasts into forecasts of fractional RB. Modeling route blockage is accomplished by statistically relating RB to Wx parameters in the form of fractional coverage of intensity, thunderstorm type, thunderstorm vertical structure, and parameters associated with Wx fractional coverage.

Practical pattern classification (PPC) techniques have been investigated as candidates for modeling RB as a function of Wx parameters. PPC techniques also provide an estimate of the relative importance of Wx parameters in determining RB.

Results show that modeling of RB based on 2002–03 Corridor Integrated Weather System (CIWS) Wx data has been accomplished reasonably well for low and high RB events (RB < 20%, RB ≥ 80%, respectively). The statistical classification models for Wx events associated with mid-range RB (20% ≤ RB < 80%) require a much larger Wx data sample to be considered accurate representations of the full ensemble of Wx that can impact an ATC en route sector.

17. Key Words	18. Distribution Statement
weather-traffic flow management integration, route blockage, air traffic control, sector capacity reduction modeling, practical pattern classification, Corridor Integrated Weather System	This document is available to the public through the National Technical Information Service, Springfield, VA 22161.

19. Security Classif. (of this report)	20. Security Classif. (of this page)	21. No. of Pages	22. Price
Unclassified	Unclassified	132	

FORM DOT F 1700.7 (8-72) Reproduction of completed page authorized

ACKNOWLEDGMENTS

This exploratory research was sponsored by the National Aeronautics and Space Administration (NASA) under Air Force Contract FA8721-05-C-0002. The authors would like to thank NASA staff members Banavar Sridhar, Steve Green, and William Chan for both their time and interest in this project.

A great deal of thanks goes out to many staff members of MIT Lincoln Laboratory for their assistance and insight. In particular, Dale Rhoda and Margo Pawlak were instrumental in the initial data collection and algorithm development efforts for the study. To Dale and Margo, the authors owe many thanks. A special thanks to Brad Crowe and Adrienne Kieldsing for their extensive analysis of the initial weather cases used in this exploratory research. Guidance from Richard Lippmann regarding practical pattern classification has been greatly appreciated.

ABSTRACT

A major concern in contemporary traffic flow management (TFM) is reducing the adverse impact that convective weather (Wx) has on Air Traffic Control (ATC) en route sectors throughout the National Airspace System (NAS). The Federal Aviation Administration (FAA) is currently seeking to reduce the delays through the use of multi-hour (e.g. 2-, 4-, and 6-hour) probabilistic Wx forecasts, coupled with strategic planning by the FAA traffic flow managers and airline personnel, to determine how en route traffic should be rerouted so as to avoid sector overloads and minimize the magnitude of the delays that occur.

The objective of this study is to develop a model that relates Wx coverage to a surrogate for sector capacity in en route airspace—the ATC sector route blockage (RB). This Wx-RB model can then be coupled with the forecast meteorological validation models to provide a model that translates the probabilistic Wx forecasts into forecasts of fractional RB for jets in en route airspace.

Twenty major events occurring in 2002–03 Wx season have been used in this study. These Wx events differ in storm type, intensity, and vertical structure as measured by the Corridor Integrated Weather System (CIWS). The Wx spatial patterns collected are treated as sample functions for the overall ensemble of Wx that can impact a given ATC en route sector. Ten ATC sectors within the National Airspace System (NAS) have been selected for study based on differing geographic location, size, route orientation, and varying route complexity. From the sampled Wx data that affects each of the chosen ATC en route sectors, the RB for the sector has been calculated using a modified version of the route blockage algorithm available through Lincoln Laboratory's Route Availability Planning Tool (RAPT).

An important issue addressed is the role of weather radar echo tops in addition to radar reflectivity in determining RB. We compared RB computed considering both storm reflectivity and echo tops with the RB considering only the storm reflectivity terms and found that the estimated sector capacity loss can be significantly reduced by considering echo tops as well as storm reflectivity in assessing the operational impact of Wx.

The task of modeling RB is accomplished by statistically relating RB to the 2002–2003 Wx data in the form of fractional coverage of high radar reflectivity cells, Wx type, and Wx vertical structure (echo tops) within an ATC en route sector. A variety of Practical Pattern Classification (PPC) techniques have been investigated as candidates for modeling the compiled distributions of RB in an ATC sector as a function of the Wx parameters. The PPC techniques also provide an estimate of the relative importance of the various Wx parameters in determining the RB of an ATC en route sector.

Results show that modeling of ATC sector RB has been accomplished reasonably well for the low blockage events (RB in an en route sector less than 20%). Apparent success is due to the large number of sampled Wx events associated with low RB. This sampling effort allows the PPC algorithms to reasonably model the distribution of low RB events as a function of Wx parameters. The statistical classification models for Wx events associated with higher blockage (RB greater and equal to 20%) occur much less frequently and require a greater (e.g., 10 fold) number of Wx data samples to be operationally useful. Work is underway to accomplish the analysis of RB and fractional Wx coverage routinely for a substantially larger number of Wx events in the CIWS domain.

TABLE OF CONTENTS

LIST OF ILLUSTRATIONS

LIST OF ILLUSTRATIONS
(Continued)

LIST OF ILLUSTRATIONS
(Continued)

LIST OF ILLUSTRATIONS
(Continued)

LIST OF ILLUSTRATIONS
(Continued)

LIST OF TABLES

LIST OF TABLES
(Continued)

LIST OF TABLES
(Continued)

1. INTRODUCTION

In this report, we describe the results of an exploratory study to develop a model that can be used to translate probabilistic convective weather forecasts into forecasts of a surrogate for sector capacity—the fraction of jet routes that would be blocked—within an en route sector (RB). The principal objectives of the study were to

1. develop a methodology for relating RB to the parameters characterizing convective weather (Wx), such as the fractional coverage of storm reflectivity, radar echo tops, and the type of convective storms, and

2. assess results of the methodology applied to 10 en route sectors from the highly congested Great Lakes and Northeast Corridors using 20 recorded Corridor Integrated Weather System (CIWS) Wx data sets.

The study also makes recommendations for a follow-on study to extend the model development to consider all of the en route sectors in NAS and use of many more weather data sets to reduce the statistical variability and reduce the effect of predictor overlap that is evident in these initial exploratory results.

1.1 RELATIONSHIP OF THIS STUDY TO THE USE OF PROBABILISTIC CONVECTIVE WEATHER FORECASTS IN TRAFFIC FLOW MANAGEMENT

A major concern in contemporary traffic flow management (TFM) for the US National Air System (NAS) is reducing the adverse impact that Wx has on Air Traffic Control (ATC) sectors throughout the National Airspace System (NAS). The FAA is currently seeking to reduce the delays through the use of multi-hour Wx forecasts coupled with strategic planning by the FAA traffic flow managers and airline personnel to determine how en route traffic should be rerouted so as to avoid en route sector overloads and minimizing the magnitude of the delays that occur.

Specifically, the current FAA/airline "strategic" TFM planning process focuses on 2 to 6 hour lead times with the greatest emphasis on the 4 and 6 hour plans. This is currently being accomplished by the use of the Collaborative Convective Weather Forecast (CCFP) [Fahey and Rodenhuis (2004), Sims and Rodenhuis (2004)] and the Strategic Planning Team (SPT) teleconferences every 2 hours as described in Huberdeau and Gentry (2004). The CCFP may be regarded as a probabilistic forecast of spatial coverage by 40 dBZ echos (equivalent to a Video Integrator Processor (VIP) level 3) that is coarsely quantized into three fractional coverage intervals:

Low 25–49% coverage
Medium 50–74% coverage
High 75%–100 % coverage

Additionally, the CCFP provides an estimate of the forecaster confidence[1] that the actual Wx coverage at the forecast time will exceed the minimum criteria of 3000 square miles coverage by VIP level 3 radar returns.

There have been ongoing operational concerns from the FAA traffic flow managers and airline dispatchers with the accuracy and operational interpretation of the CCFP. It is generally agreed the Wx locations cannot be accurately forecast (e.g., to within a few km) 4 to 6 hours in advance at this time [National Resource Council (2003)]. Rather, it has been recommended that the FAA focus on development of probabilistic forecasts of fractional weather coverage. Active research is underway [see, e.g., Megenhardt et al. (2002)] to develop alternative, less quantized probabilistic Wx forecasts.

As shown in figure 1-1 [from Zobell (2004)], it is essential to be able to translate the weather forecasts into capacity forecasts. Zobell's paper states, "While we can say for sure that the presence of Wx can decrease capacity, there is much about the effect of weather on capacity that is not well understood, and more research is needed."

[1] As of 2005, the confidence probability itself is quantized into two categories: low: 25–49% and high: 50%–100%

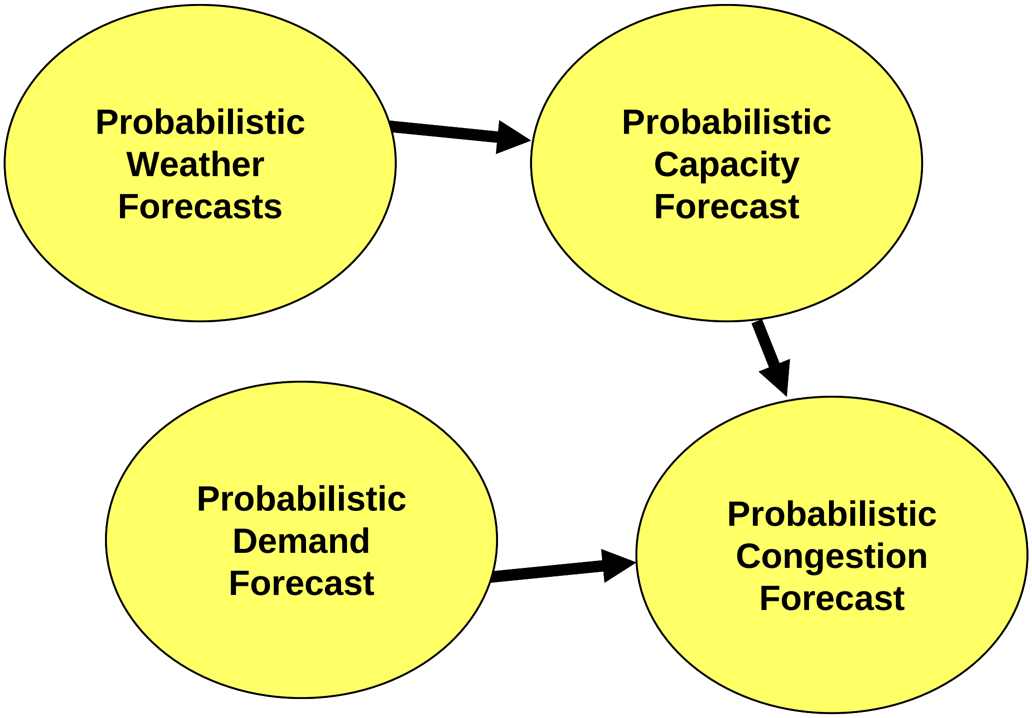

Figure 1-1. Relationships between probabilistic weather forecasts, probabilistic demand forecasts, and a probabilistic congestion forecast that could be used for traffic flow management [from Zobell (2004)]. This study focuses on the translation of probabilistic weather forecasts into probabilistic capacity forecasts.

One of the important elements of capacity is the complexity of the traffic flows as discussed in Histon et al. (2002), where it is shown that Wx disrupts the normal structure of aircraft traffic flow such that complexity increases and throughput decreases.

Given that there is no generally accepted model for the number of aircraft that can be handled by a controller (or, an en route sector) as a function of coverage by Wx, this study has focused on a closely related metric which is the number of normal jet routes that are blocked by Wx. The RB metric is felt to be a reasonable approximation of capacity in highly congested airspace since miles-in-trail (MIT) spacing of aircraft on routes in individual ATC sectors is frequently used to limit capacity during Wx.

The purpose of this study (Wx-RB) is to explore the feasibility of translating measured Wx parameterizations into measures of RB. As shown in the next section, this Wx-RB model can be coupled with the forecast meteorological validation models to provide a model that translates the probabilistic forecasts into forecasts of RB.

The task of modeling RB as a function of actual Wx is accomplished through the use of spatial distribution or fractional coverage of Wx intensity, Wx type (i.e., size, organizational structure, spatial distribution, etc.), and Wx vertical structure within an ATC sector.

While it is currently difficult to forecast several hours in advance the exact locations of Wx cells precisely, it will be possible to forecast with some appreciable skill, the broad characteristics of the storms that are likely to occur in a region – the percent of likely sector coverage by high reflectivity cells, the likely echo tops spatial distribution, the types of storms likely to occur, and given an organized line storm type, the likely orientation. There is often spatial order in the orientation of storms, in the direction of storm motions, and in the distribution of storm types. In some regions of the country, there are geographic features that effect storm initiation, type, and orientation. Hence, the approach taken in this study is to develop separate models for each ATC sector that relate the RB for that sector to the Wx storm characteristics (coverage by high reflectivity cells, the likely echo tops spatial distribution, the types of storms, and given an organized line storm type, the line orientation)

1.2 RELATIONSHIP OF RB-WX RELATIONSHIP TO THE ESTIMATION OF ROUTE BLOCKAGE GIVEN A WX FORECAST

From elementary probability theory, the probabilistic forecast of RB given a probabilistic weather forecast, F, can be determined from:

$$P(RB|F) = \int P_1(RB|\underline{W}_C)\, P_2(\underline{W}_C|F)\, d\underline{W}_C \qquad (1)$$

Where:

> $P(RB|F)$ is the probability distribution of RB in an ATC sector given a Wx forecast with parameters F (i.e., the probabilistic forecast of RB).
>
> $P_1(RB|\underline{W}_C)$ is the probability that route blockage is RB given that actual Wx parameters are $\underline{W}_C$ (a vector). The elements of $\underline{W}_C$ for this study includes the fractional coverage of Wx intensity, type of Wx, and the fractional coverage of the cells whose radar echo tops exceed certain thresholds.
>
> $P_2(\underline{W}_C|F)$ is the probability (density) that the actual Wx parameters are $\underline{W}_C$ given that the Wx forecast of parameters F was made. The model for $P_2(\underline{W}_C|F)$ is developed from meteorological validation of the probabilistic forecast [see, e.g., Mahoney, et al. (2002)]

By integrating the product of the P_1 and P_2 terms with respect to the continuous variable $\underline{W}_C$, one obtains the probabilistic forecast of RB conditional on F. An advantage of determining $P(RB|F)$ by the above approach as opposed to empirically assessing the actual RB for many issued forecasts, is that only meteorological validation needs to be redone [that is, the model for $P_2(\underline{W}_C|F)$ is regenerated] when the forecast methodology is changed. Additionally, the route blockage model [$P_1(RB|\underline{W}_C)$] can be used for many different probabilistic forecast algorithms as long as the various forecasts generate estimates of the weather parameters, $\underline{W}_C$, used for $P_1(RB|\underline{W}_C)$.

In figure 1-2, we show an example of the probability distribution function for $\underline{W}c$ as a function of F [i.e., this is the integral of $P_2(\underline{W}_C|F)$ with respect to $\underline{W}c$] for the 4-hour CCFP circa 2002.

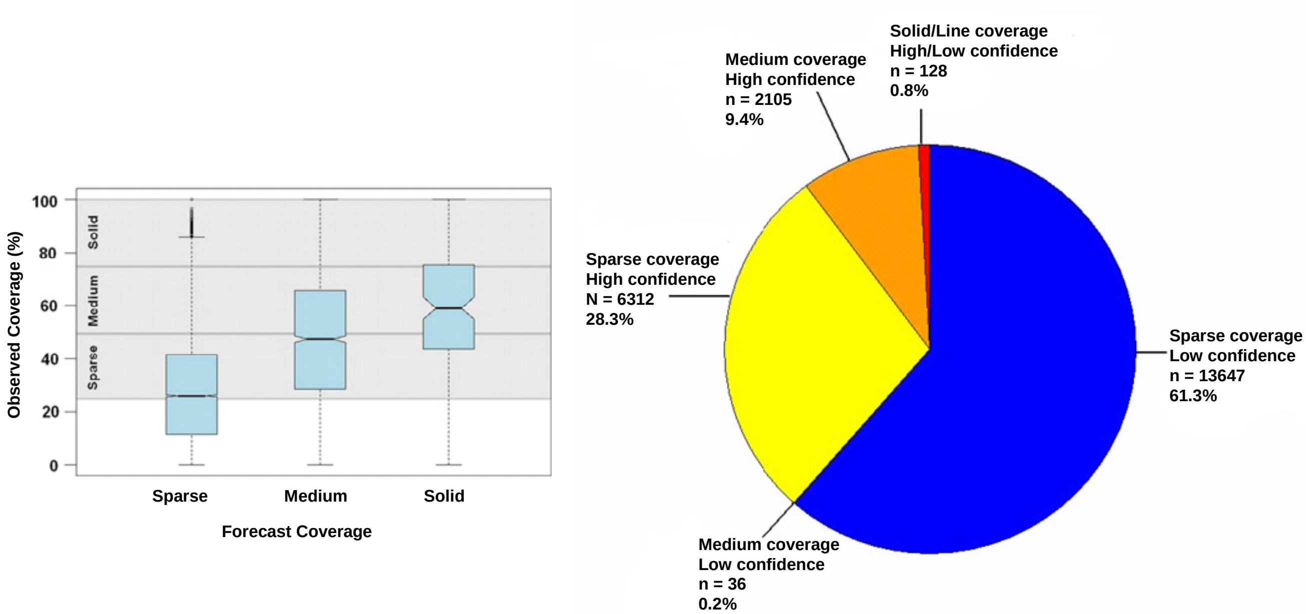

Figure 1-2. Left: "Box plot" representation of the probability distribution function for coverage ($\underline{W}_c$) for the 2005 2-, 4-, and 6-hour CCFP forecasts as a function of the CCFP forecast parameters. The line inside each box represents median values; the bottom and tops of boxes are the 25% and 75% quartile values, respectively. The ends of the bottom and top "whiskers" are the 5% and 95% quartiles. Points above and below the whiskers are in the lower and upper 5% of the distribution respectively. Note that the median value of actual weather coverage corresponding to the frequently produced "Sparse" coverage forecast (vast majority of forecasts making up the blue and yellow portions of the pie chart to the right) barely falls within the lower limit of what is defined as sparse coverage (25%). Medians of the "Medium" and "Solid" CCFP forecasts do not verify against observed Wx coverage. It should also be noted that the weather coverage metric used in these plots significantly overstates the actual area covered by VIP level 3 equivalent echoes [see Mahoney, et al. (2004) and section 2.6].

1.3 CONCEPTUAL APPROACH TO DEVELOPMENT OF A WX-RB MODEL

A key first task in the development of models for the RB in an ATC sector as a function of actual Wx parameters was the identification of an appropriate Wx data set. Major Wx events in the CIWS domain during 2002–03 have been examined and the CIWS product data archives retrieved. These active Wx days consist of convective events differing in storm type, intensity, and vertical structure. Determination of the Wx type, intensity, and vertical structure was accomplished using products generated by the demonstration Corridor Integrated Weather System (CIWS) system operated by MIT Lincoln Laboratory [see Robinson, et al. (2004) for a description of these products]. The measured CIWS Wx spatial patterns at various times (spaced 5 minutes apart) during the analysis period are treated as a sample function from the overall ensemble of Wx that impacts a given ATC sector.

Ten ATC sectors including those from the Chicago (ZAU), Cleveland (ZOB), Indianapolis (ZID), and Washington (ZDC) ARTCCs were selected for study based on differing geographic location, size, route orientation, and varying route complexity.

For each time sample of the Wx spatial pattern in each of the chosen ATC sectors, the route blockage (RB) is calculated using a modified version of the route blockage algorithm for the Route Availability Planning Tool (RAPT) which is currently in operational use for departures from the New York City airports [see DeLaura and Allan (2003) for a description of RAPT].

Other than CIWS, current forecast systems display both probabilistic and deterministic fields of Wx intensity from a 2-D perspective, without information on Wx vertical characteristics. An important issue addressed in the study is the role of the echo tops in addition to radar reflectivity in determining the fractional route blockage. As noted subsequently, we find that the use of storm echo top data in addition to storm reflectivity is critical in accurately assessing sector route blockage.

A statistical data base consisting of the actual Wx fractional coverage parameters and computed RB for each sector was constructed given the various Wx events. Various practical pattern classification techniques have been investigated as candidates for predicting the RB in an ATC sector as a function of the Wx parameters. The performance of the models in correctly predicting the RB given a set of Wx values was evaluated quantitatively on a set of measured Wx-RB data samples that is different from the set of measured Wx-RB data samples used to develop the models.

1.4 REPORT ORGANIZATION

The report proceeds as follows. In the next section, we discuss the methodology for the study including the Wx data, the ATC sectors and routes considered, and computation of route blockage from the Wx data. Statistical pattern classification algorithms used to generate sector specific models of route blockage as a function of Wx parameters (e.g., reflectivity, echo tops, type of Wx) will be discussed. This section also provides some summary statistics on the measured route blockage and Wx data used as well as discussing several issues associated with the modeling and, the use of the models with forecast meteorological validation results. Section 3 discusses the modeling results for RB classification of the 10 ATC sectors of interest. Section 4 provides conclusions while section 5 makes recommendations for follow on studies. An appendix at the end of this report provides expanded model results for the individual ATC sectors.

2. DATA AND METHODOLOGY

2.1 METEOROLOGICAL DATA

For this Wx-RB modeling study, 20 Wx events where examined, each having significant operational impact within the coverage region of the CIWS. Table 2-1 provides the starting date for each event, with associated storm organization, weather types, and impacted Air Route Traffic Control Centers (ARTCCS). Weather events were chosen based on widespread impact on the National Air System (NAS), diversity of weather type, and diversity of vertical structure within individual storms.

TABLE 2-1
Case data for 20 active Wx days used in the Wx-RB study. Cases were chosen primarily from the 2003 Wx season. Information includes date, organization, weather type, and impacted ARTCCS.

Date	Organization	Wx Type	Impacted ARTCCS
020822	Both	Line, Embedded, Isolated	ZAU, ZOB, ZNY, ZBW
030319	Organized	Line, Embedded	All CIWS ARTCCS
030420	Organized	Line, Isolated	ZAU, ZOB, ZNY
030501	Both	Line, Isolated, Embedded	All CIWS ARTCCS
030505	Unorganized	Embedded	All CIWS ARTCCS
030509	Both	Isolated, Embedded	ZAU, ZID, ZOB, ZDC, ZNY
030531	Both	Line, Embedded, Isolated	ZID, ZOB, ZDC, ZNY,ZBW
030608	Organized	Line, Embedded	ZAU, ZID, ZOB ZDC, ZNY
030611	Organized	Line, Embedded	All CIWS ARTCCS
030614	Both	Line, Isolated	All CIWS ARTCCS
030626	Organized	Line, Embedded	ZAU, ZID ZOB
030706	Organized	Line, Isolated	All CIWS ARTCCS
030709	Organized	Line, Isolated	ZAU, ZID, ZOB, ZDC, ZNY
030721	Organized	Line Isolated	All CIWS ARTCCS
030731	Both	Line, Isolated, Embedded	ZAU, ZID, ZOB ZDC
030804	Both	Line, Isolated	All CIWS ARTCCS
030822	Both	Line, Isolated	ZID, ZOB, ZDC,ZNY, ZBW
030826	Both	Line, Isolated, Embedded	All CIWS ARTCCS
030829	Both	Line, Isolated, Embedded	All CIWS ARTCCS
030901	Organized	Line, Isolated, Embedded	ZAU, ZID, ZOB,ZDC, ZNY

The parameters of $\underline{W}_C$ include storm intensity, type, and vertical extent. These quantities are derived from the CIWS output fields of the high-resolution vertically integrated liquid (VIL) product, the Regional Convective Weather Forecast (RCWF) Wx classification[2], and the CIWS Echo Tops product respectively. Summaries of the characteristics of the CIWS products are provided below. More complete information on CIWS and its weather products is provided in the CIWS operational benefits report [Robinson, et al. (2004)] and the CIWS product description report [Klingle-Wilson and Evans (2005)].

Intensity of a thunderstorm is characterized by the CIWS high-resolution VIL product that is based on Next Generation Weather Radar (NEXRAD) radar reflectivity. Given each NEXRAD within the CIWS domain (see figure 2-1), VIL mosaics are created at a temporal resolution of 5 minutes with geographic location and intensity of precipitation mapped to a 1-km resolution horizontal grid. The calculated VIL are mapped to the Nation Weather Service (NWS) 6-level Video Integrator Processor (VIP) standard for weather and precipitation using the methods defined in Troxel and Engholm (1990). Level 1 intensities are associated with weak convection, light turbulence, and rainfall less than 0.2 inches per hour. Level 6 categorize the most intense thunderstorms that can contain severe turbulence, large hail, lightning, and rainfall amounts exceeding 7.0 inches per hour. Levels 2 through 5 fall between these intensity limits [Rhoda and Pawlak (1999)]. Figure 2-1 shows an example of thunderstorm intensity as portrayed by the CIWS NEXRAD VIL product. The strongest portions of thunderstorms are colored in red and correspond to level-6 VIL intensities.

[2] The Wx classification product is generated internally by the RCWF algorithm and is not provided currently to the ATC users of the RCWF.

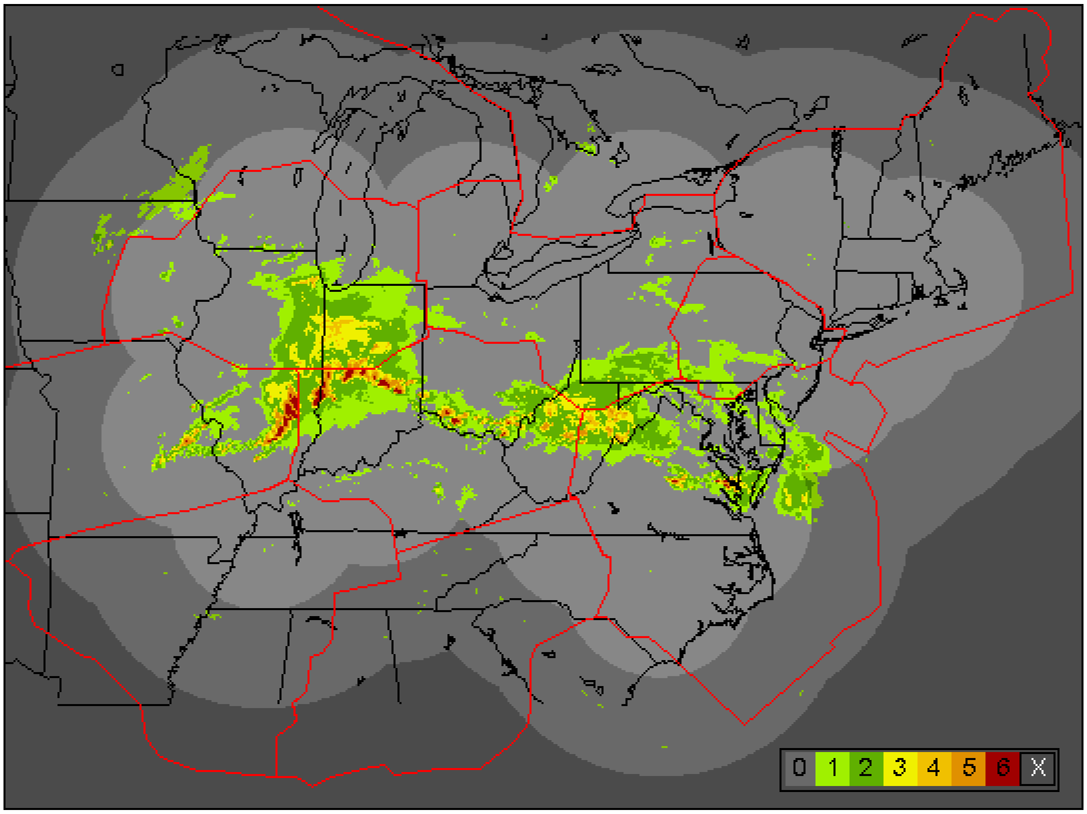

Figure 2-1. Extent of the CIWS domain and the corresponding NEXRAD radar coverage. Best radar coverage within the domain is indicated by the lightest shade of grey. Wx on 10 May 2003 – 16:07:28 UTC provides an example of the 6-level intensities available through the CIWS NEXRAD VIL product. Level-6 intensities in the VIL product are colored red and represent the strongest thunderstorm cores. Bright red contours are the ARTCC boundaries.

The classification of precipitation into Wx type is an internal feature of CIWS Regional Convective Weather Forecast (RCWF) algorithm [Wolfson, et al. (2004)]. Convective Wx type classification is used to optimize the performance of the RCWF forecast. At the time of this study, the RCWF classification technology defined 5 Wx types differing in size and motion characteristics. The five RCWF Wx types were available at the time this study was complete and include “line,” “small cell,” “large cell,” “stratiform precipitation,” and “embedded.” The 6th Wx type “weak cell” was added in summer of 2004. Figure 2-2 provides a flow diagram of RCWF Wx classification and visual representation of the five Wx types used in this study. See Dupree et al. (2002) for a discussion of the Wx classification algorithm.

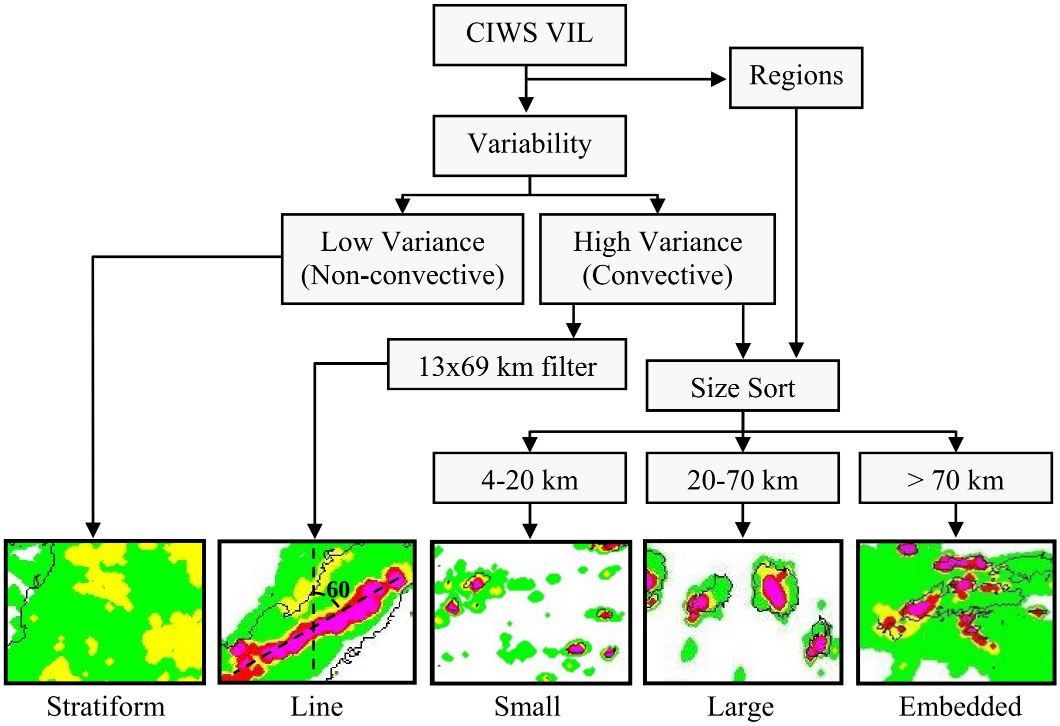

Figure 2-2. Flow diagram of the CIWS RCWF Wx type classification algorithm. Lower images provide a visual representation of the five Wx types classified by the RCWF algorithm.

M.I.T. Lincoln Laboratory studies have shown that the vertical structure of a storm relative to the altitude of an aircraft is a very important factor in determining whether a convective storm will block a route in en route space. In particular, Rhoda et al. (2002) showed that aircraft over Memphis center typically fly over Wx if the aircraft altitude is at least 5 kft above the storm's radar detectable top. DeLaura et al. (2006) found that aircraft deviations were directly attributable to the aircrafts original flight plan intersecting Wx with high-altitude tops. These results appear to have been borne out as well in the CIWS testing although the explicit relationship of flight altitude to storm radar echo tops for storm over flights is not quantified in Robinson et al. (2004).

The spatial pattern of the vertical extent of thunderstorms is characterized by the CIWS Echo Tops mosaic product. Figure 2-3a illustrates the CIWS method of interpolating echo top heights and figure 2-3b provides a pictorial representation of the echo top within a convective cell. For more information on the Echo Tops mosaic product, see Wolfson et al. (2004).

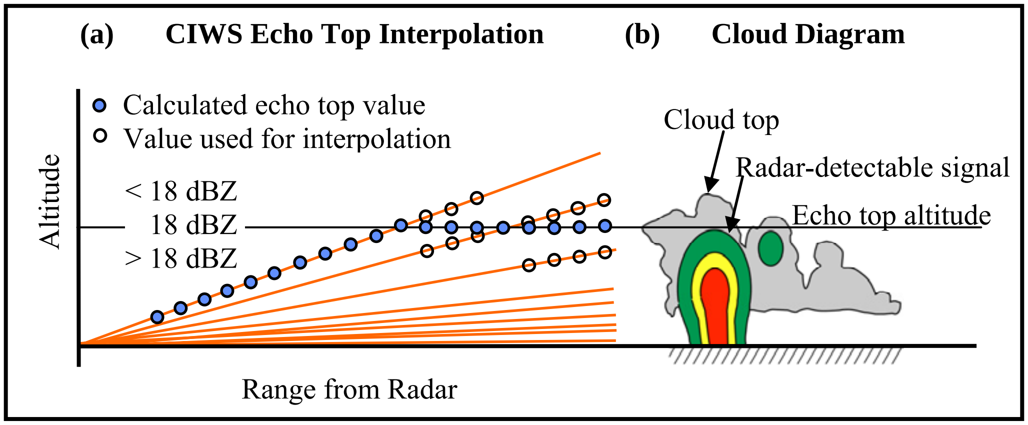

Figure 2-3. (a) Interpolation technique for computing the CIWS Echo Tops product. Method allows for smooth interpolation between beams. (b) Cloud diagram indicating cloud intensity and echo top height of the signal detectable by radar.

Thus, the CIWS products provide the spatial distribution of the Wx parameters (i.e., intensity, type, and echo tops) over an ATC sector. For the Wx-RB modeling study, several combinations of the CIWS products have been used as inputs to statistical classification algorithms that seek to optimally predict the RB of an ATC en route sector. Given that the intent of the study is to provide a model that can be used for probabilistic Wx forecasts, the spatial distribution of Wx within an ATC sector is characterized by the fractional Wx coverage and features associated with that coverage. Fractional Wx coverage is defined as the area a Wx coverage parameter encompasses with respect to the total area of the ATC sector. The Wx parameters derived from the CIWS product data, the parameters that make up $\underline{W}_C$, are as follows:

1. Fractional Wx coverage of VIL greater than or equal to VIP level 1 *(level1+wx)*

   The *level1+wx* parameter accounts for the widest fractional coverage of Wx within an ATC sector. Its purpose is to incorporate, as a group, all storm types and intensities that might have an operational impact on an ATC sector. Storms or clusters of storms can consist of different types and strengths. For example, a convective storm can consist of Wx portions classified as type line associated with the storm core and type stratiform associated with cirrus outflow of a convective anvil. Intensities of this storm can range from level-1 through level-6. *Level1+wx* has been constructed to parameterize the fractional Wx coverage of the conglomerate of storm intensities and types.

2. Fractional Wx coverage of VIL greater than or equal to VIP level 3 *(level3+wx)*

   Level3+wx parameterizes the fractional Wx coverage associated with heavy precipitation and intense storm cores. *Level3+wx* is the parameter bounding Wx intensities typically avoided by commercial and noncommercial aircraft in all phases of flight [Rhoda et al. 1999].

3. Fractional coverage of Wx with echo tops greater than or equal to 25 kft *(etops25+)*

The *etops25+* parameter helps separate low altitude storms from high-altitude storms. Regions of weather within a region of *etops25+* would be expected to impact aircraft on high jet routes within the en route domain.

4. Fractional Wx coverage of VIL greater than or equal to VIP level 3 with echo tops greater than or equal to 25kft *(l3andet25)*

   L3andet25 parameterizes the fractional coverage of the high-reflectivity storm cores with associated tall vertical extent. Storm regions bounded by *l3andet25* would expect to result in high-altitude aircraft deviations and high-altitude jet route closures.

5. Fractional coverage of Wx classified as type line *(line)*

   Line parameterizes the fractional coverage of Wx classified by CIWS RCWF as type line. As seen in figure 2-2, line types are elliptical in shape and have a broad extent of area coverage when compared to the other convective storm types. *Line* bounds the single storm type that is considered organized due to consistency in movement, growth/decay, and orientation of the line storm type.

6. The average azimuth orientation of the line types that fractionally cover a sector *(orientation)*

   Given all storm type classified as line within an ATC sector of study, *orientation* is the average azimuth angle of the longest elliptical length. *Orientation* lies between 0 and 180 degrees azimuth. Zero is attributed to the instances where no *line* type is present. Therefore, N-S or S-N oriented line storms get the 180-degree designation.

7. Fractional coverage of Wx classified as type small *(small)*

   Convective cells of diameter in the 4–20 km range, typically known as "popcorn" convection, make up convective elements in the fractional Wx coverage defined as *small*. Types bounded by the *small* parameter are disorganized with no disenable orientation.

8. Fractional coverage of Wx classified as type large (*large)*

   Cells of diameter in the 40–70 km range make up convective elements in the fractional Wx coverage parameter defined as *large*. Bounded by the *large* are convective elements still considered disorganized—without orientation, but are larger and more persistent in their development than the small Wx types.

9. Fractional coverage of Wx classified as type stratiform *(stratiform)*

   The *stratiform* parameter bounds the fractional Wx coverage of a sector not associated with the deep convective elements of a storm core. *Stratiform* is associated with both condensation resulting from weak vertical forcing and condensation at upper levels of the troposphere as a result of outflow from a towering anvil. *Stratiform* bounds the Wx type considered benign except in areas directly downwind of intense thunderstorms where turbulence within the stratiform outflow may be a concern.

10. Fractional coverage of Wx classified as type embedded *(embedded)*

    The fractional coverage of unorganized cells larger than 70 km are what make up the elements contained in the *embedded* parameter. The embedded types consist of strong convective elements that have a smaller spatial spread than the small and large type but are not continuous enough in intensity to be considered type line. Because of this discontinuity, an orientation cannot be determined. Embedded types typically have stratiform around the periphery of their convective elements.

11. Dominant Wx type of classified fractional coverage (*wx-type*)

    Given the above five classifications of fractional Wx coverage, *wx-type* is a categorical parameter which determines, of the Wx types having impact in an ATC sector at a particular instance in time, which type makes up the majority of fractional Wx coverage. *Wx-types* include line storms, small convection, large convection, stratiform and embedded cells. Instances do exist where the Wx within a sector has not been classified by the CIWS algorithm. These instances are typically associated with benign Wx events and are categorically defined as a *wx-type* of "none."

2.2 AIR TRAFFIC CONTROL SECTOR DATA

Ten ATC sectors have been chosen for the Wx-RB modeling study. Figure 2-4 shows the ATC sectors of interest chosen due to their differences in geographic location, size, route orientation, and route complexity. These ATC sectors include high-traffic areas seen as major choke points within the Indianapolis (ZID) and Cleveland (ZOB) centers, major north-south/south-north transit routes within sectors of the Washington (ZDC) center, and one of the Chicago (ZAU) center sectors responsible for transcontinental air traffic over the Midwest. Route information has been extracted from each ATC sector.

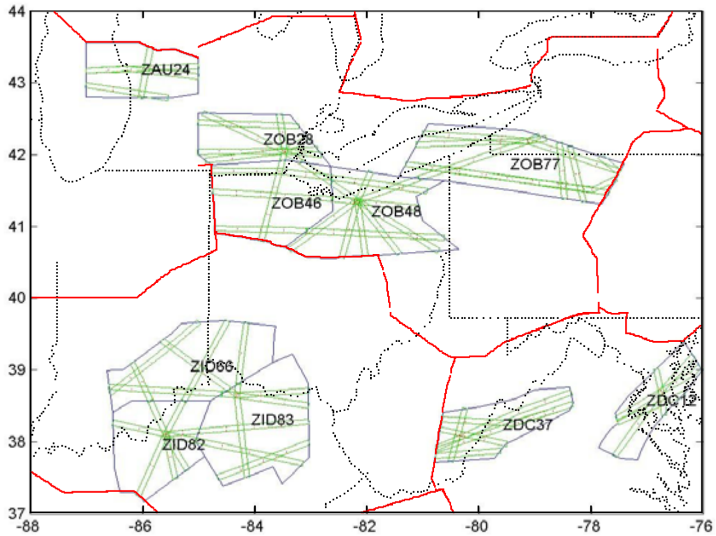

Figure 2-4. ATC sectors chosen within the NAS for their differences in geographic location, size, route orientation, and route complexity. Sectors also fall entirely within the CIWS domain. Represented are high-altitude en route sectors within the Indianapolis Center (ZID), Cleveland Center (ZOB), Washington Center (ZDC), and Chicago Center (ZAU). Principal high-altitude jet routes in the various en route sectors are plotted in green.

Of the ten ATC sectors, a total of 60 high jet route segments (figure 2-4) comprise the route data made available for Wx-RB modeling study.

2.3 CALCULATION OF ROUTE BLOCKAGE (RB) FOR ATC EN ROUTE SECTOR

Given the route information and the measured meteorological quantities for a time sample provided by CIWS, the route blockage (RB) is estimated for each individual route within a sector. The individual route blockages are then combined to provide an average route blockage score for the individual sector. We will now describe how the individual route blockages are determined and how those are used to generate an average route blockage for the sector.

The metric used to determine the blockage of individual routes is a version of the blockage score made available through the RAPT route blockage algorithm. Routes within an ATC sector are divided into lengths of roughly 55 km and assigned a width of 8 km. Route segments can be seen in the ATC sector images of the appendix. For example, figure A.1-1 in section A.1 of the appendix shows the bounds of route segments as denoted by red dotted lines within a route of ATC sector ZAU24. Route segmentation provides the RAPT modified algorithm a spatial area for the computation of a segment blockage score.

Wx components ingested by the RAPT modified algorithm are the CIWS enhanced VIL and Echo Tops products. Given a route segment, the equation for segment blockage is the following:

$$\text{Segment Blockage} = a\cdot\text{intensity} + b\cdot\text{extent} + c\cdot\text{non-extent} - d\cdot\text{echo tops} \qquad (2\text{-}1)$$

Coefficients a, b, c, and d in the above equation have been heuristically determined through study of departure operations for the New York airports and interaction with air traffic managers and controllers.

The first term, intensity, is calculated using a location-weighted sum of all VIL pixels bounded by a route segment. In this term, VIL is taken as its 256-value representation as provided by CIWS. The 8 km wide route segments are equally divided along their length into five weighted sub-segments. Location weights are applied based on a VIL pixel's proximity to the center of the route segment. VIL pixels that fall within the innermost sub-segment receive the largest weight.

The second term, extent, applies to the fractional coverage within a route segment of intense VIL that is greater than or equal to the NWS VIP level-3 equivalent. This term boosts the blockage score in a manner that is proportional to the lateral extent of intense Wx across a segment.

The third term, non-extent, applies to benign or Wx free areas that lie within a route segment. This term decreases the route segment blockage score based on the fractional amount of a route segment that is considered "open."

The final term, echo tops, boosts or lowers the blockage score based on the Wx vertical extent into a sub-segment. Because this study is concerned with the en route space, the echo tops term is modified to determine the effect Wx has on high jet routes. In this form, blockage scores for a route segment are aggressively reduced if the calculated mean of echo tops within a segment fall below 32 kft. If the mean echo tops in a segment are above 36 kft, the blockage score is aggressively enhanced. This echo tops term can effectively cancel out blockage scores associated with high VIL levels, but low-altitude convective cells. Figure 2-5 shows how the blockage score of a route segment is affected depending on the mean echo-top height encountered.

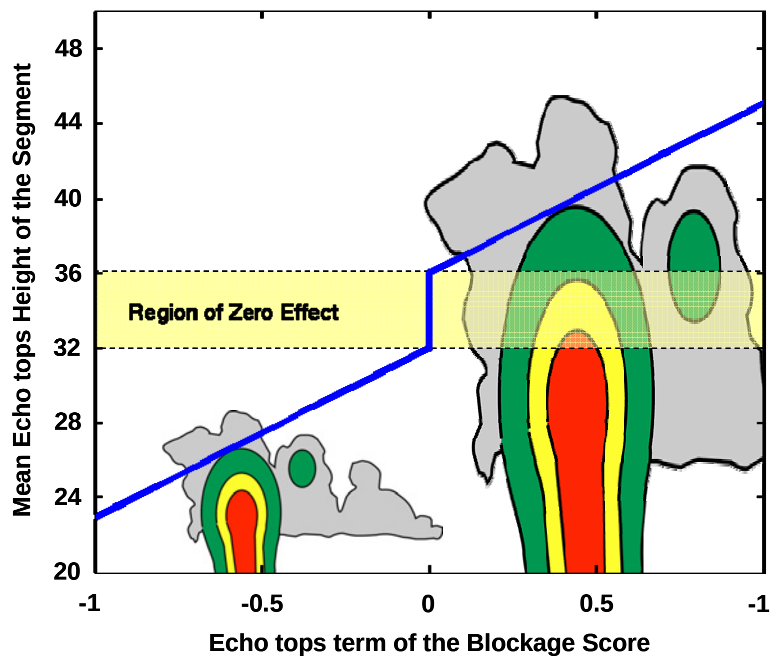

Figure 2-5. Illustration showing the effect echo tops have on the blockage score of a route segment. Full Echo tops term of the blockage score is positioned along the abscissa (d·echo tops). Echo top heights (kft) are plotted along the ordinate. For mean heights greater the 36 kft, the blockage score is enhanced by the echo tops term. For mean heights below 32 kft, the term drops the score. Mean heights within the shaded region will not affect the blockage score. The blue line is the calculated echo tops term as a function of the mean echo tops height within a route segment.

Route segment blockage scores as calculated above are clipped to fall between the values of zero and one. A score of zero indicates that a route segment is completely open where a score of one indicates that a route segment is completely closed.

Each route within an ATC sector is assigned the blockage score equal to the maximum score of its route segments.

The ATC sector's RB is the sum of the blockage score as determined above divided by the total number of routes within a sector[3]. This determination of RB is expressed as a percentage. Take for example, an instance where ATC sector ZID83 has a calculated RB of 100% as seen in the Wx-RB analysis tool of figure 2-6. Given that ZID83 consists of six high jet routes, with at least one segment within each route being fully blocked, segment blockages of one for each route contribute to the 100% RB.

[3] In section 5, we recommend that a follow-on to this exploratory study include computation of the sector route blockage include weighting the individual route blockage scores by the (time varying) fractional fair weather demand for the various routes at that time.

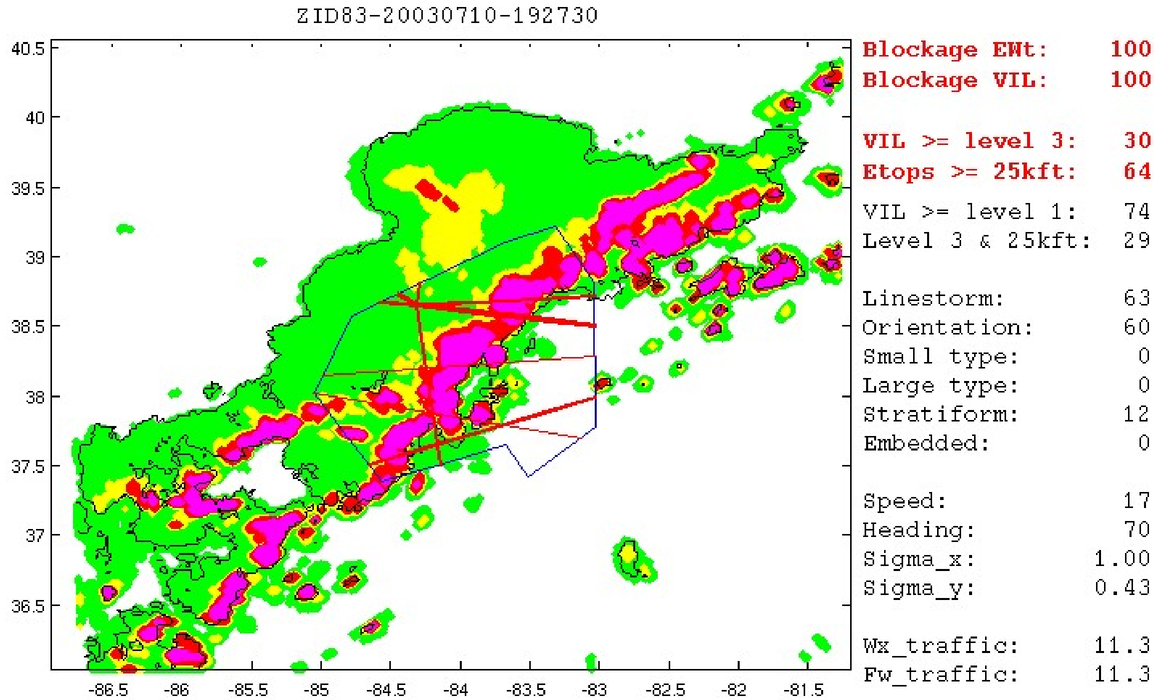

Figure 2-6. Analysis tool developed for the Wx-RB modeling study shows an example of 100% RB for ZID83 as calculated 20030710_19:27:30 UTC. Percentage in the top right-hand corner labeled "Blockage EWt" is the echo-top weighted blockage score (d of the full echo-top term not equal to 0). Score directly below labeled "Blockage VIL" indicates the blockage score calculated solely based on VIL (d equal to 0). Remaining information is the parameters derived from the CIWS VIL, RCWF, and Echo Tops products. At this time, all routes are blocked as indicated by an RB of 100%.

From the 20 active Wx days selected for the Wx-RB modeling study, RB scores have been computed for the 10 chosen ATC sectors at a temporal frequency of 5 minutes matching the CIWS data output interval. This resulted in 6,798 sets of Wx parameters and RB scores being calculated for each ATC sector. The scores have been combined with the derived suite of Wx parameters to match RB scores with the corresponding Wx parameters. The combined data for each ATC sector were then edited to remove Wx free time samples from the data base from the sets. The edited data base was presented to Lincoln Laboratory's LNKnet Practical Pattern Classification software for the modeling of RB. The next section summarizes the classification routines used in the effort to model RB as a function of the Wx parameters.

2.4 LNKNET PRACTICAL PATTERN CLASSIFICATION

LNKnet software has been developed to simplify the application of statistical, neural network, and machine learning pattern classifiers [Kukolich and Lippmann (2004)]. In the Wx-RB modeling study, the desired classification of RB is based on statistical pattern recognition algorithms applied to the set of Wx parameters discussed in section 2.1. LNKnet has been used to perform two functions. The first is to determine the explanatory power of each of the derived Wx parameters over the variations seen in the RB. The second is to model RB as a function of the explanatory Wx parameters. Based on the recommended methodology described in the LNKnet documentation, the data sets for each ATC sector have been split into training and testing subsets. Given that less than 10,000 patterns have been compiled for each ATC sector, per sector subsets consisting of 80% of the edited data have been used for the purposes of training classification routines. The remaining 20% were reserved for per sector testing of the developed classifiers.

Of the classification routines made available through the LNKnet software package, the three best performers of the Wx-RB modeling study will be presented and performance results discussed in the appendix section. These routines include a Neural Network classifier, a Likelihood classifier, and a Nearest Neighbor classifier. Kukolich and Lippmann (2004) provides detailed information on these classification routines.

A key component of the LNKnet software package is Feature selection. Feature selection allows for the reduction of input features used in a classification experiment. In terms of the Wx-RB study, the purpose of feature selection is to determine the explanatory power of the derived Wx parameters and select those parameters that minimize the overall error rate made during classification of RB. These parameters can be presented for classification in order of determined importance or as a subset of Wx parameters that minimizes the error rate made during classification. To determine the statistical significance of feature selection, error rates are compared between the full ordered set of Wx parameters and the reduced combination of parameters that provides the lowest error. Given the total number of patterns presented during training of both sets, improvement in the error is only significant if the difference is greater than roughly two standard deviations where

$$\sigma = 100[p(1-p)/N]^{1/2},$$

where p is the mean error computed between training of the full ordered set and reduced combination of Wx parameters and N is the number of patterns presented in training.

A requirement of the LNKnet software package is to provide the dependent variable (i.e., RB) quantized into a set of classes. The number of classes is dependent upon the number of input patterns supplied. One can envision that as the number of experimental data points becomes infinite, the number of classes could be selected to nearly resemble a continuous distribution of the dependent variable.

For this exploratory phase of the development of a Wx-RB model, the 6,798 weather parameter-RB scores per ATC sector requires a relative coarse discrete binning of the dependent variable RB. Brute force methods have been applied to find a discrete binning interval that maximizes the number of class presented to LNKnet, while at the same time minimizing the overall error rate produced during the classification process. Based on a number of experiments with different RB bin sizes, a discrete, linearly spaced binning interval of 20% has been chosen for this exploratory study. This discrete binning of RB provides LNKnet with a total of five classes, RB intervals of [0–20%), [20–40%), [40–60%), [60–80%), and [80–100%], in which to model RB as a function of measured Wx parameters.

2.5 STATISTICAL BREAKDOWN OF RB AND WX PARAMETERS

With each Wx parameter combined over all ATC sectors, figure 2-7 shows the sample probability distributions (PDs) for each Wx parameter used in the Wx-RB modeling study. The PDs are derived from a data set where "Wx free" measurements were deleted. "Wx free" measurements consist of time slices with a zero fractional Wx coverage of the *level1+wx* or *level3+wx* within an ATC sector. The distribution of Wx parameter *orientation*, a parameter specific to line storms, is not considered in determining "Wx free" measurements. The resulting edited data is made up of 26,955 measured Wx instances over all ATC sectors.

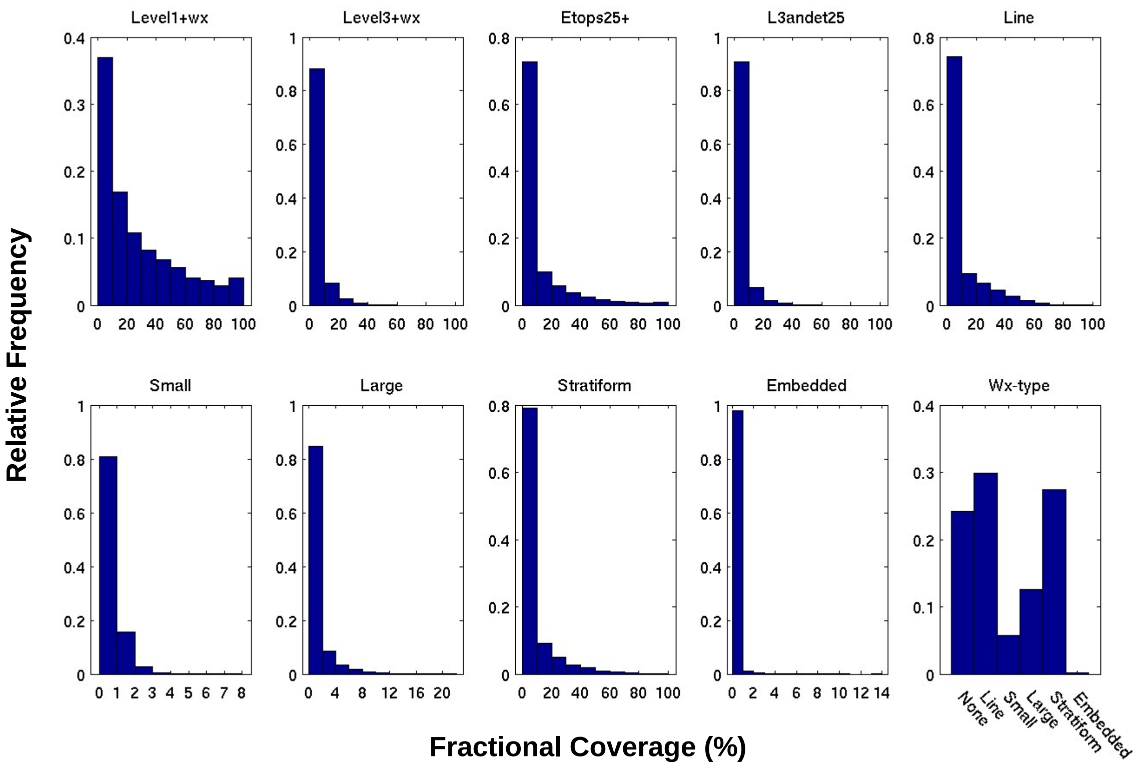

*Figure 2-7. Probability distributions (PDs) of the Wx parameters derived for WX-RB modeling (*orientation *parameter specific to* line *excluded). Ordinate axis indicates relative frequency. For the plots of fractional Wx coverage, abscissa indicated the fractional coverage as a percentage. The plot in the lower right corner shows the PD of the categorical parameter WX-type. Notice that x and y axes have limits that differ in range from plot to plot.*

An important feature to notice is the non-Gaussian, steep Gamma-like distribution of each Wx parameter involving fractional Wx coverage. The majority of the data sampled through the 20 active Wx events is heavily skewed toward low fractional coverage within an ATC sector. When the data are examined on a sector-by-sector basis, these distributions shift slightly depending on the coverage area of the sector and data density, but retain the same skewness. Of the *wx-type* parameter, relative frequency of occurrence is highest for storm type line. The *wx-type* "none" of the distribution is associated with benign-low reflectivity Wx that the RCWF weather type classification algorithm does not assign a type. These events contribute to a zero RB percentage.

Blockage distributions for each ATC sector are reflective of the distributions seen in figure 2-7. Given that low fractional coverage dominates the 20-day, active Wx sampling effort, lower blockage scores make up the bulk of the RB data of each sector. Figure 2-8 provides the discrete PDs of RB for the ten ATC sectors. The discrete bins of RB make up the five classes that will be presented to the LNKnet software package. The data consists of the same edited data as seen in figure 2-7, only in this figure patterns are separated by sector. What is apparent is that for each ATC sector, patterns contributing to the 0–20% RB have been heavily sampled in comparison to the others.

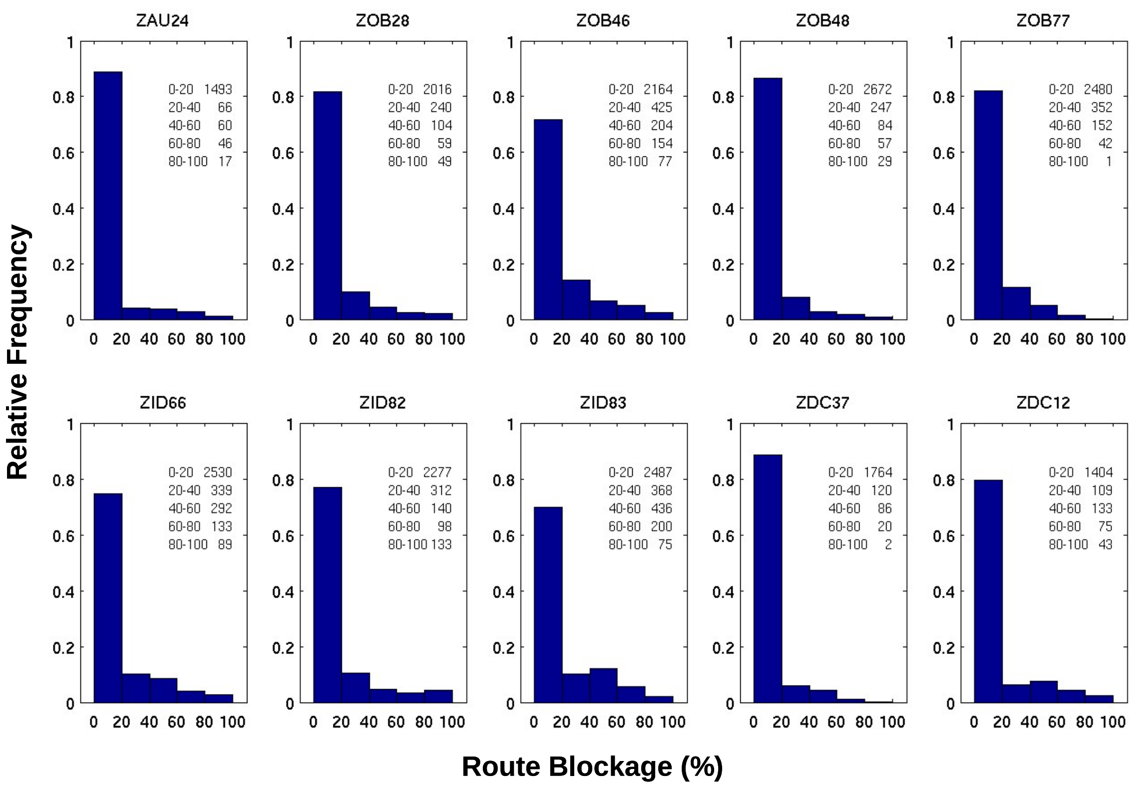

Figure 2-8. Discrete probability distributions of RB for each ATC sector. The ordinate axis indicates the relative frequency of occurrence of RB, given the edited data sets for each sector. The abscissa is the RB expressed as a percentage. The legend represents histogram counts for the discrete bin intervals of RB that will make up the classes needed by the LNKnet software package.

2.6 ROUTE BLOCKAGE SENSITIVITY

2.6.1 Blockage Variability Between Sectors for "Similar" Weather Events

As seen in section 2.2, ATC sectors differ in spatial size; they also differ in route complexity and route orientation. An important postulate of this study has been that for similar Wx events, the impact of such events will differ from ATC sector to ATC sector. Not only will the impact depend upon the characteristic of a sector, but impact will depend on the local variability in the spatial pattern of Wx as well[4]. To demonstrate how the route blockage impact within the ten ATC sectors under study differ for "similar" weather events, a sub-sample of the data has been made consisting of Wx events similar in weather type, sector fractional coverage, and vertical extent.

The sub-sample consists of 1,652 recorded instances of storm type *line* impacting the ten ATC sectors. Each *line* type in the sub-sample holds a general east-west orientation (between 70° and 110° azimuth), with a fractional coverage of between 30% and 50%, and *etops25+* exceeding a fractional coverage of 10%. These features of *line* type are typical of medium-intensity line storms. Figure 2-9 represents the RB PDs for each ATC sector, given the similar types of line storm impacts.

[4] For example, some sectors (e.g., ZOB77 and ZAU24) are near a major lake while others (e.g., ZDC37) contain mountains.

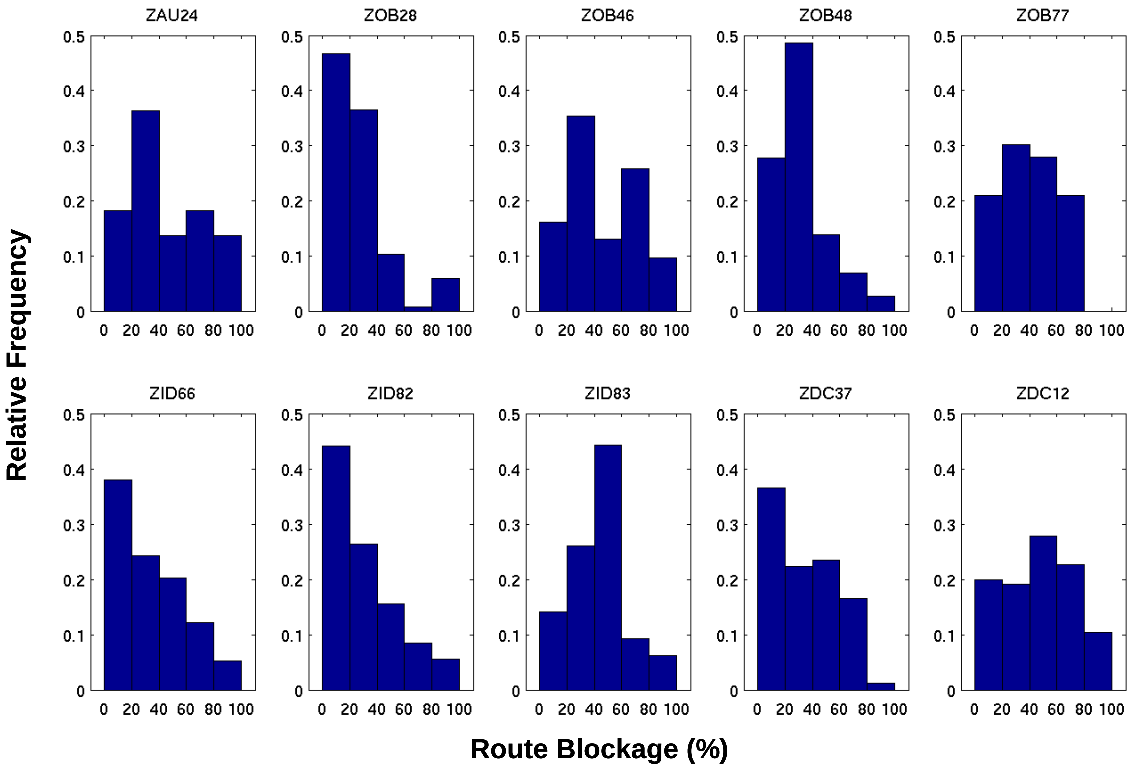

Figure 2-9. Probability distributions of RB of each of the 10 ATC sectors, given a sub-sample of storm type line. *Abscissa displays RB percentages in 20% incremental bins, the ordinate displays the relative frequency. Distributions of blockage differ from sector to sector as a result of their differences in size, route complexity, and orientation.*

Distributions of RB differ from sector to sector given the specific type of line storm events. The RB of ZOB28, ZOB48, ZID66, ZID82, and ZDC37 are skewed toward lower blockage percentages. ZID83 has a RB PD that weakly resembles a Gaussian distribution. The ZID83 mean RB is 46% with $\sigma = \pm 21\%$. ZAU24, ZOB77, and ZDC12 have relatively flat RB distributions. ZOB46 appears multimodal with local maxima at the [20–40%) and [60–80%) intervals. While this line storm sub-sample is limited to 1652 occurrences, differences in the distributions emphasize that estimates of capacity degradation resulting from Wx are directly attributable to ATC sector size, route orientation, and regional effects on line storm characteristics.

2.6.2 Blockage Sensitivity to Criteria Used to Determine Blockage

Another important issue is the role of the echo tops in addition to radar reflectivity in determining route blockage.

The CCFP validation studies to date [Mahoney, et al. (2002) and Mahoney (2004)] and the Enhanced Traffic Flow Management System (ETMS) principally consider only storm reflectivity in determining regions of significant weather.

In figure 2-10, we compare the sector route blockage computed considering both storm reflectivity and echo tops using all of the terms in equation (2-1) with the sector route blockage considering only the storm reflectivity terms in equation (2-1).

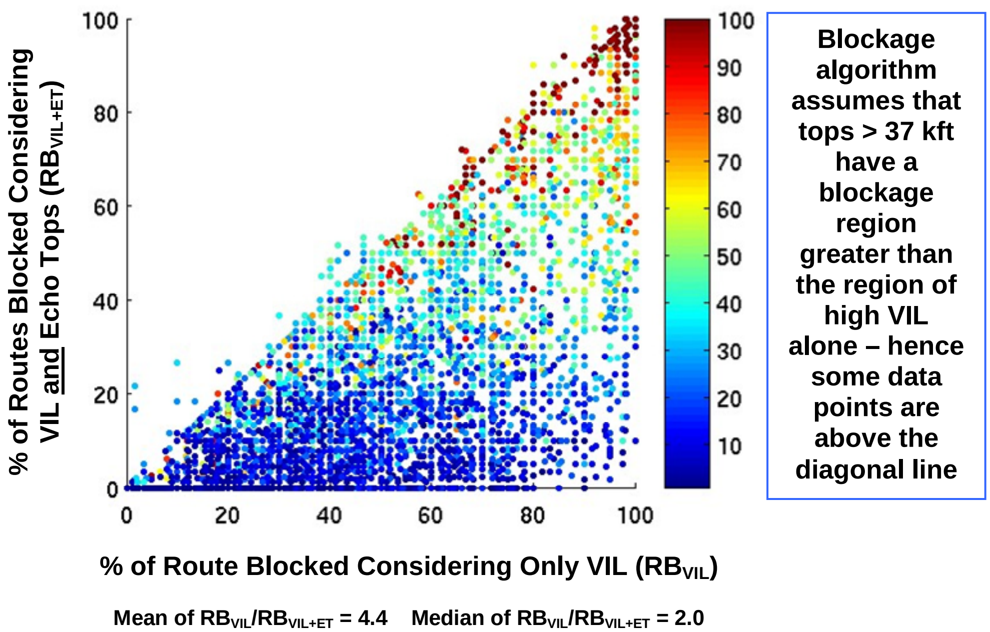

Figure 2-10. Comparison of ATC sector route blockage scores given only storm reflectivity versus route blockage scores considering storm reflectivity and storm radar echo tops for all cases where there was some Wx within a sector with reflectivity of VIP level 3 or higher and echo tops higher than 25 kft. The percentage of routes blocked if one considers only storm reflectivity is about twice that determined considering both storm reflectivity and storm echo tops. Colors assigned to each datum indicate the area coverage of high echo tops (>25 kft) within the sector.

We see that the consideration of storm echo tops as well as storm reflectivity reduces the estimated loss of capacity (as measured by the ATC sector route blockage scores) due to Wx by roughly a factor of two on the average. There are a number of individual cases (those on the main diagonal) where the consideration of echo tops makes no difference. Additionally, since echo tops greater than 38 kft increase the blockage score, there are some cases where the consideration of echo tops leads to a greater route blockage. However, overall, it is clear that the consideration of echo tops in determining route blockage in en route airspace is very important.

It should be noted that a number of the operational cases of substantive CIWS delay reduction benefits were derived from traffic flow manager (TMU) users identifying opportunities for aircraft to fly over storms from the CIWS products in situations where TMU users stated that they had not been able to identify such opportunities previously using the weather products provided by the ETMS and Weather and Radar Processor (WARP) weather products [Robinson et al. (2004)].

These results in figure 2-10 show that it is very important that TFM decision support systems used in Wx consider echo tops forecasts as well as storm reflectivity forecasts in making computations of the forecast capacity (per figure 1-1)[5].

2.6.3 Wx Fractional Coverage Sensitivity to Criteria for Defining the Spatial Extent of Convective Weather That Is of Operational Concern

In section 1, we saw that route blockage distributions can be estimated using a convolution of functions involving actual Wx parameters $\underline{W}_C$. It is important that the same definition of $\underline{W}c$ be used in determining both functions.

Unfortunately, the current CCFP coverage statistics (figure 1-2) are not computed using the actual coverage of 40 dBZ/VIP level 3 equivalent reflectivity, which essentially is the definition of $\underline{W}_C$ used in our study.

Rather, for CCFP validation as accomplished from 2000 to 2004, the weather coverage is computed for a "convective constrained area" (CCA) weather field that basically fills in all pixels within a 40 km box around any single pixel that had a VIP level 3 equivalent reflectivity. The paper by Mahoney et al. (2004) compares the spatial reflectivity fields generated by this procedure to the original reflectivity fields.

In figures 2-11 to 2-13, we compare the fractional weather coverage computed by the CCFP validation approach to the fractional weather coverage we computed using the CIWS VIL product. We see that the coverage computed using the current CCFP validation approach typically is proportional to the actual weather coverage with a slope that varies from 1.9 to as much as 20 depending on the sector and the type of Wx. That is, the use of the 40 km boxes overestimates the actual $\underline{W}_C$ coverage in a number of cases by a factor >10.

[5] The CIWS system commenced providing explicit radar echo tops forecasts in May of 2005.

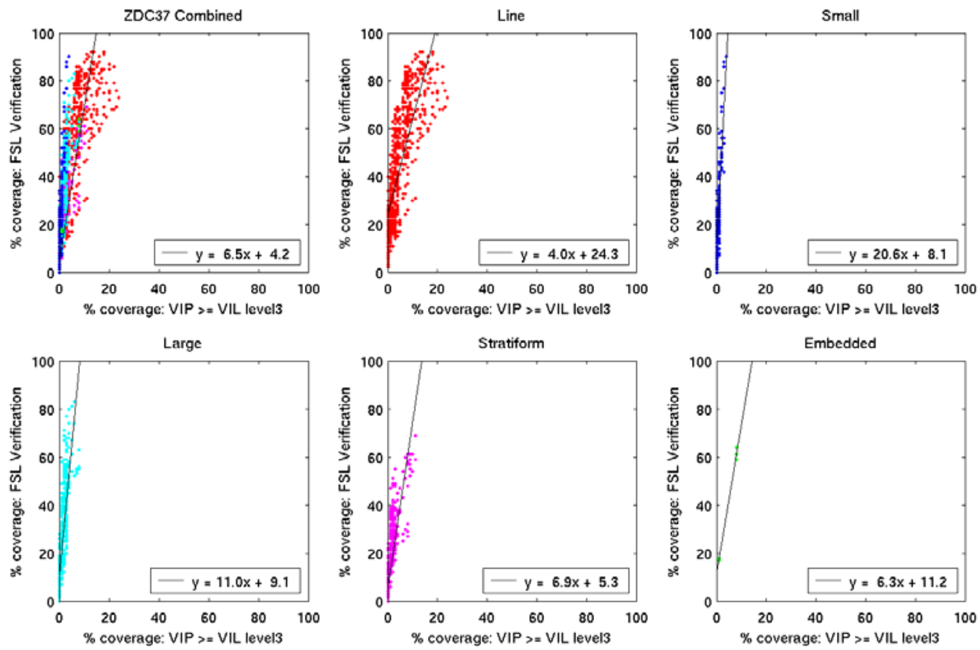

Figure 2-11. Comparison of actual high-resolution VIL coverage within ZDC sector 37 with coverage of 40 km boxes using maximum VIL anywhere within the box for various types of weather. There were very few embedded cases. Note that the use of 40 km boxes increases coverage by a factor of 4–20, depending on the type of weather.

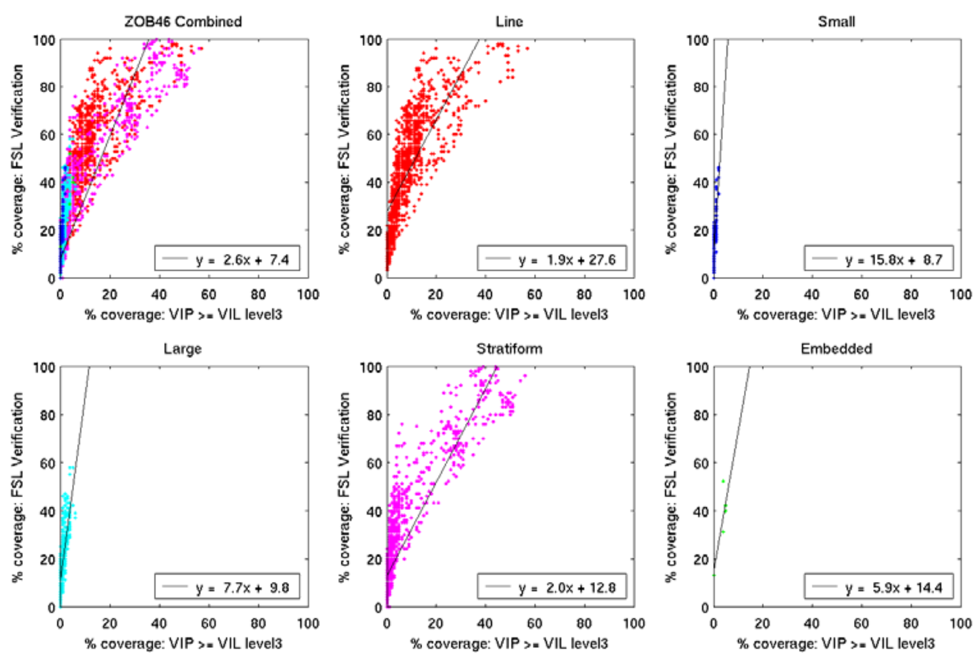

Figure 2-12. Comparison of actual high-resolution VIL coverage within ZOB sector 46 with coverage of 40 km boxes using maximum VIL anywhere within the box for various types of weather. There were very few embedded cases. Note that the use of 40 km boxes increases coverage by a factor of 1.9–15.9, depending on the type of weather.

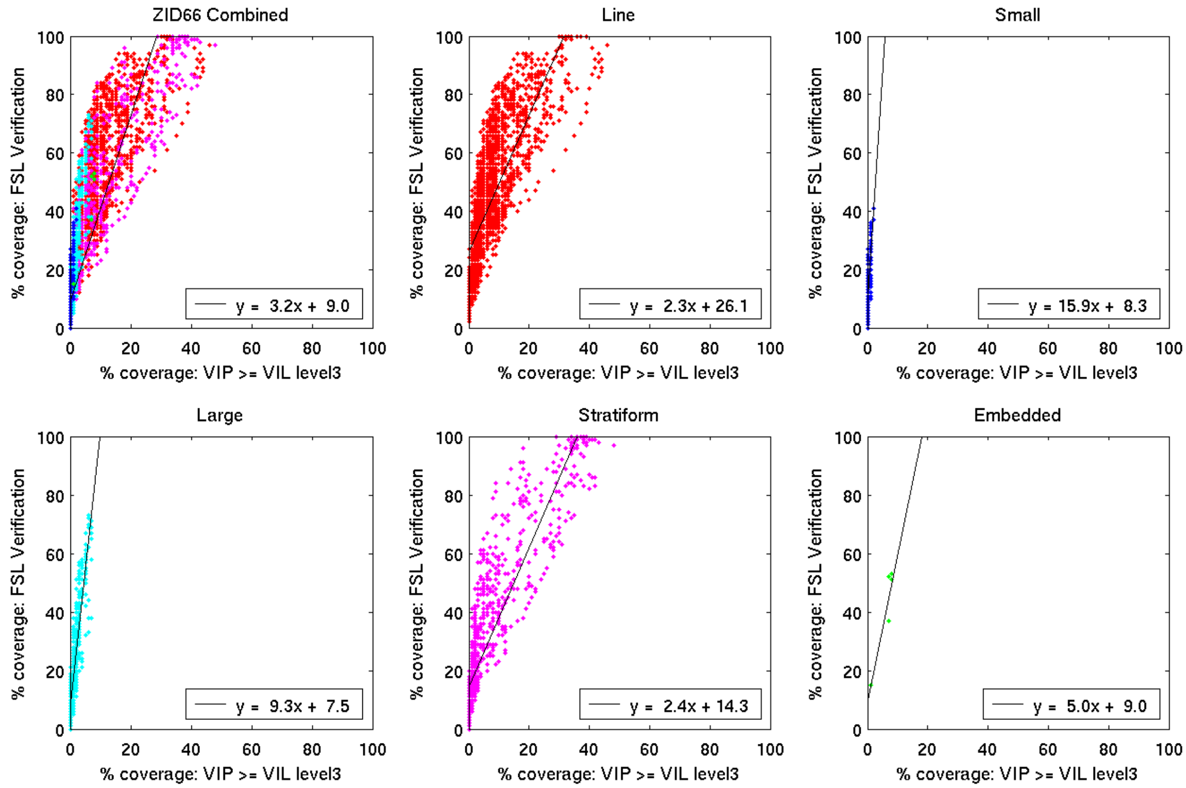

Figure 2-13. Comparison of actual high-resolution VIL coverage within ZID sector 66 with coverage of 40 km boxes using maximum VIL anywhere within the box for various types of weather. There were very few embedded cases. Note that the use of 40 km boxes increases coverage by a factor of 2.3–15.9, depending on the type of weather.

Hence, if one seeks to apply the WX-RB models developed here to CCFP validation data, it will clearly be necessary to adjust for the differences in the definition of $\underline{W_C}$. We have recommended to the FAA that the CCFP validation be reported with actual weather VIP level-3 fractional coverage as well as the CCA fractional coverage.

3. RESULTS

For the Wx-RB modeling study, the ten chosen ATC sectors have been modeled independently utilizing the large number of pattern classification routines made available through the LNKnet software package. Of these routines, the Gaussian mixture, Multi-layer Perceptron (MLP), and K Nearest Neighbor (KNN) classifiers produced the lowest overall error rates in the final testing phase of classifying RB as a function of the derived Wx parameters.

LNKnet feature selection has revealed that in modeling RB as a function of each Wx parameter separately, parameters associated with Wx vertical extent in an ATC sector (i.e., *etops25+* and *l3andet25*) have the greatest explanatory power over the variability seen in RB followed by the Wx parameter associated with high-intensity Wx (*level3+wx*). While parameters associated with Wx vertical extent and intensity generally provide the highest explanatory power of the variability seen in RB, results show that a combination of Wx parameters provides much lower classification errors than does using parameters associated with intensity and vertical extent by themselves.

As stated in section 1.3, with the exception of CIWS, most current forecast systems used operationally display both probabilistic and deterministic fields of Wx intensity from a 2-D perspective, without information on Wx vertical characteristics or type. This 2-D perspective is simulated in this study by the actual converge of high-intensity VIL within an ATC sector (i.e., *level3+wx).* Below in table 3-1 is an error summary from the previous results sections comparing KNN classifications of RB that utilize the best combination of Wx parameters to RB classifications based solely on 2-D information provided by the *level3+wx* Wx parameter. The comparison illustrates the importance of including a combination of Wx parameters that provide the 3rd dimension of vertical extent as well as some information on regional storm characteristics. In one comparison, a nearly 5:1 reduction in the overall error is realized by utilizing the best combination of Wx parameters (ZDC37).

TABLE 3-1

Comparison of classification errors of a KNN RB model based on the single parameter *level3+wx* (row 2) to that of a KNN RB model based on the best combination of Wx parameters as determined through feature selection (row 3). Row 4 is the *level3+wx* to *best combination* ratio. In all 10 ATC sectors, the best combination of Wx parameters holds the lowest classification error. Bottom row indicates combined number of samples collected for training and testing.

ATC Sector	ZAU24	ZOB28	ZOB46	ZOB48	ZOB77	ZID66	ZID82	ZID83	ZDC12	ZDC37
Level3+wx Error %	14.63	18.33	24.92	12.52	15.81	31.5	31.69	41.07	19.37	23.93
Best Combination Error %	5.67	12.22	9.97	4.72	7.15	10.1	13.22	10.83	13.68	5.04
Improvement Ratio	2.58	1.50	2.50	2.65	2.21	3.12	2.40	3.79	1.42	4.75
Total # of Samples	1682	2468	3089	3027	3383	2960	3566	1992	1764	1992

For each of the ten ATC sectors, the KNN classification routine outperformed all other classifiers made available through the LNKnet software package. With the exception of the RB error results calculated for ZOB28, the decrease in overall error made by using KNN has been determined to be statically significant in comparison to the Gaussian mixture and MLP classifier errors. This determination has been made by examining the 2σ error separation as described in section 2.4.4.

The KNN classification routine is most successful at modeling RB as a function of derived Wx parameters because of its ability to form complex decision regions within the pattern input space. It does not rely on function fitting routines such as the MLP and Gaussian mixture classifiers. At RB intervals where the data is sparse, distributions are ill-fitted by MLP sigmoid functions and the probability density functions created by the Gaussian mixture classifier. These ill-fitting functions lead to the larger errors seen in MLP and Gaussian mixture classifier. KNN classification is able to include populations of patterns within an RB interval that would otherwise be considered outliers by other classification routines.

Examination of the KNN feature selection results shows that for ATC sectors ZAU24, ZOB46, ZID83, and ZDC37 a reduced combination of Wx parameters decreases training errors with statistical significance. Theses excluded Wx parameters, while different for each sector, consist of *level1+wx, line, orientation, small, large, embedded,* and *wx-type.* Mutually excluded Wx parameters for the above-listed sectors are *wx-type* and *small.* The remaining six sectors utilized the full ordered combination of Wx parameters.

Statistics on the KNN classification results have been compiled for each ATC sector of the study. Confusion matrices and error statistics show that for the heavily sampled RB interval of [0–20%), errors in classification were held to less than five percent for all ten sectors. While far less sampled, the [80–100%] RB interval was perfectly classified for sectors ZOB28 and ZOB48. The most egregious error rate for this interval occurred within sector ZOB24, misclassifying two of three test patterns. Middle-range RB intervals of [20–40%), [40–60%), and [60–80%) consistently exhibited the largest errors throughout the ten sectors.

Voluminous sampling of the patterns associated with a RB of [0–20%) allowed for the high success rate of its classification. As revealed by figure 2-8 of section 2.5, roughly between 70% and 90% of the patterns collected, depending on the ATC sector, are attributed to this RB interval. Table 3-2 lists the per ATC sector classification errors for the [0–20%) RB interval as realized by the KNN routine. As stated previously, for [0–20%), near perfect classifications have been made for ZAU24, ZOB48, ZID66, and ZDC37. Very low but elevated errors for the [0–20%) RB interval (above 4%) has been calculated for ZOB28, ZOB46, and ZDC12 and are the result of a slightly more complex input space. High data density is the main contributor to these low classification errors for this interval.

TABLE 3-2
Per ATC sector classification errors for the RB interval of [0–20%). Bottom row indicates combined number of samples collected for training and testing.

ATC Sector	ZAU24	ZOB28	ZOB46	ZOB48	ZOB77	ZID66	ZIB82	ZID83	ZDC12	ZDC37
[0–20%) Error %	1.01	4.96	4.63	1.50	3.25	1.78	3.30	2.62	4.27	1.42
# of samples	1493	2016	2164	2672	2480	2530	2277	2487	1404	1764

Classification errors are highest for the middle-range RB intervals of [20–40%), [40–60%), and [60–80%) in comparison to the errors calculated for the tail RB intervals of [0–20%) and [80–100%]. Input spaces attributed to these mid-intervals overlap one another. This overlap is most evident in figures of the limited Wx parameter transfer functions in each ATC sector subsection. Here, the input spaces of the three middle-range RB intervals are heavily mixed, contributing to the higher calculated error rates of the function fitting classifiers (MLP and Gaussian Mixture) as well as KNN classifiers. For MLP and Gaussian mixture classifiers, ill-fitted mixed distributions cause incorrect RB classifications. For KNN, RB intervals are less distinguishable from their neighbors of a different class. As seen in table 3-3, the combined errors calculated for these middle intervals are above or equal to 25% for all 10 ATC sectors.

TABLE 3-3
Per ATC sector combined classification errors for the RB intervals [20–40%), [40–60%), and [60–80%). Bottom row indicates combined number of samples collected for training and testing.

ATC Sector	ZAU24	ZOB28	ZOB46	ZOB48	ZOB77	ZID66	ZIB82	ZID83	ZDC12	ZDC37
[20–80%) Error %	41.18	50.63	25.16	27.63	25.00	37.09	54.13	30.50	54.84	34.09
Combined # of samples	172	403	783	388	546	764	550	1004	317	317

These results are also evident in the confusion matrix results of each ATC sector subsection. Incorrectly classified patterns spread out over all RB intervals and are most evident in tables A.2-3, A.3-3, A.6-3, and A.8-3 of the appendix (for ATC sectors ZOB28, ZOB46, ZID66, and ZID82, respectively). Largest improvements need to be made at these mid-intervals.

While sparse, patterns associated with the high RB interval of [80–100%] exhibit good classification success when even a small number of patterns are made available for training and testing. These patterns reside in an input space that allows them to be distinguished well, and these patterns are separable from the lower RB intervals. Table 3-4 indicates that that only a single ATC sector ZAU24 had a poor classification at this RB interval, with an error of 66.67%.

Comparing ZAU24 to those sectors with perfect classification at the [80–100%] RB interval shows the input space for ZAU24 at this interval is highly scattered in comparison to those sectors that exhibit perfect classification at these RB intervals. This is noticeable when comparing scattered points associated with [80–100%] RB interval along the top row of appendix figure A.1-4 of ZAU24 to the clustered points of that RB interval along the top row of appendix figures A.2-4 and A.4-4 (ZOB28 and ZOB48, respectively). Sparseness of input patterns also reveals that for ZOB77 and ZDC37, no patterns associated with the [80–100%] RB interval were available for testing.

TABLE 3-4

Per ATC sector classification errors for the RB interval of [80–100%]. Bottom row indicates number of samples collected for training and testing.

ATC Sector	ZAU24	ZOB28	ZOB46	ZOB48	ZOB77	ZID66	ZIB82	ZID83	ZDC12	ZDC37
[80–100%] Error %	66.67	0.00	6.67	0.00	NAN	17.65	15.38	20.00	25.00	NAN
# of samples	17	49	77	29	1	89	133	75	2	43

Total classification errors summarized in table 3-5 show that KNN classification is best achieved for the ATC enroute sector of ZOB48. Near perfect and perfect classifications have been made at the highest and lowest RB intervals (1.52% for [0–20%) and 0.0% for [80–100%], see tables 3-2 and 3-4).

TABLE 3-5

Total classification errors for the RB of each ATC sector. Bottom row indicates combined number of samples collected for training and testing.

ATC Sector	ZAU24	ZOB28	ZOB46	ZOB48	ZOB77	ZID66	ZIB82	ZID83	ZDC12	ZDC37
Total Error %	5.67	12.22	9.97	4.72	7.15	10.10	13.22	10.83	13.68	5.04
Total # of Samples	1682	2468	3089	3027	3383	2960	3566	1992	1764	1992

The confusion matrix for ZOB48 in table A.4-3 of the appendix can be compared to those in tables A.2-3, A.3-3, A.6-3, and A.8-3. Notice that the misclassifications for ZOB48 are confined to one RB interval—either side of the correct classification diagonal—while misclassifications for ZOB28, ZOB46, ZID66, and ZID82 spread across all RB intervals. Not only does the classification of RB for ZOB48 yield a low error (4.72%), but the tightly bound confusion matrix indicates that the variability of the RB classification is also low. While patterns at the RB intervals at [80–100%] are absent, this pattern is repeated in the classification results for ZOB77 and ZDC37.

Table 3-6 shows the classification errors for each ATC sector comparing errors for RB interval of [0–20%) to the combined errors of RB intervals equal to and above 20%. Here, large errors are realized at the higher RB intervals, which are directly related to the lack of data density associated with these intervals.

TABLE 3-6

Summary comparing classification errors of RB intervals equal to and above 20% (bottom row) to those of the single RB interval below 20% (middle row). Comparison shows that classification errors dramatically increase above the well-sampled [0–20%) RB interval.

ATC Sector	ZAU24	ZOB28	ZOB46	ZOB48	ZOB77	ZID66	ZIB82	ZID83	ZDC12	ZDC37
Error % for RB < 20%	1.01	4.96	4.63	1.50	3.25	1.78	3.30	2.62	4.27	1.42
Error % for RB ≥ 20%	43.24	45.45	23.53	25.93	25.00	35.12	46.67	29.77	51.43	34.09

While the KNN routine classifies RB with the lowest error rates, as with the other PPC algorithms examined in this study, its effectiveness is significantly limited by the number and diversity of input data presented during training. This is evident in the figures of each ATC sector subsection that represent the limited Wx parameter transfer functions. Note that there were a number of cases where the full range of sector blockages did not occur in the test data set, such as for ZOB77 and ZDC37 (figures A.5-4 and A.10-4 of the appendix).

The computed transfer functions of RB based on fractional coverage by high-reflectivity weather and high echo tops differed significantly from what is expected from the viewpoint of conceptual arguments of function dependency. The route blockage is expected to exhibit a monotonic increase as *etops25*+ and *level3*+wx increases as is illustrated in appendix figure A.0-1. The transfer functions constructed for each ATC en route sector show that this expected functional dependency is not apparent in the KNN-derived prediction models. Moreover, unrealistic decision regions are constructed by the models beyond the limits of the input data. Additionally, the disjoint and complex decision regions that fall within the limits of the input data clearly appear very odd.

While the decision regions constructed by the KNN routine effectively reduce classification errors based on the data that has been collected, the results cannot be considered fully realistic, statistically meaningful representations of RB decision surfaces that should occur if one were able to base the model development on a more complete population from the ensemble of expected Wx events. Providing a major (e.g., factor of at least 10 and preferably 25) increase in the number of experimental data points should result in more reasonable functions for estimating RB from the weather parameters. Also, with a significant increase in the number of experimental data points with higher RB values, more robust classification algorithms can be used, allowing model functions to better represent the underlying data (improving MLP and Gaussian Mixture results). Such an increase in the number of data points is certainly feasible since typically there are about 100 days per year in which a CIWS ARTCC encounters Wx in a year [see Robinson et al. (2004)] and there are now several years of CIWS archives available.

4. CONCLUSIONS

This exploratory Wx-RB modeling study is the first published attempt to relate an operational measure of RB within an ATC sector to actual Wx parameters. This was accomplished by first selecting data from a number of active Wx events in the ATC sectors considered. Wx parameters have been derived to account for Wx intensity, organizational type, and vertical extent.

The ATC sectors used were chosen due to their geographical differences, differences in their spatial size, route complexity, and route orientation. This ATC sector-specific data was combined with the Wx data mentioned above to derive percentage of RB for each ATC sector for each time sample of actual Wx.

Calculation of RB considering vertical extent as represented by echo tops as well as storm reflectivity reduces the estimated loss of capacity due to Wx by roughly a factor of two. Our findings suggest that the estimated sector capacity loss due to Wx can be significantly reduced by considering echo tops as well as storm reflectivity in assessing the operational impact of Wx.

Statistics have been compiled matching each instance of RB with the spatial distribution of Wx within a sector at that time. This data set is then ingested into a series of practical pattern classification algorithms to model RB of each ATC sector as a function of the derived Wx parameters.

Results show that, based on the data collected from 20 active Wx days across the NAS, modeling of ATC sector impact has been accomplished reasonably well for the relatively low (less than 20%) route blockage events. Apparent success for these events is due to the relatively large number of Wx events with low route blockage. The number of experimental low blockage Wx events (RB less than 20%) is an order of magnitude larger than the combined number of sampled higher blockage Wx events (RB greater and equal to 20%).

The statistical pattern recognition models developed for the higher route blockage events in many cases are clearly inadequate[6]. Additionally, the relatively coarse intervals (20%) for route blockage that were dictated by the relatively limited number of weather cases used would not be desirable operationally (e.g., there is a very significant operational difference in TMU challenge between 23% route blockage and 39% route blockage for a number of these highly congested sectors).

These obvious model deficiencies do not, in our opinion, reflect problems with the methodology used, but rather, are a reflection of the limited amount of data that could be processed given the very limited scope of this study.

[6] E.g., the functional dependency on fractional coverage by high-reflectivity weather and high echo tops is inconsistent with what logically must be the functional dependence (e.g., the route blockage should increase monotonically as the fractional coverage of high-reflectivity cells and high echo tops cells increases).

5. RECOMMENDATIONS

1. Automate a data collection process for all ATC sectors within CIWS domain. Given that the CIWS architecture is in place, an algorithm can be developed to collect data whenever active Wx is present within an ATC sector. This will increase the data made available at the now poorly sampled higher RB values and significantly increase the number of “unorganized” weather type events. Also, as the number of Wx-route blockage data points increases, the quantization of the route blockage intervals could be decreased. With proper sampling of higher RB intervals, more complex pattern classification routines such as MLP and Gaussian mixture that fit distribution functions to the underlying data can be applied, at the same time achieving lower classification errors.

2. Experimental verification of the impact metric RB using actual flight track data. It would be desirable to experimentally validate the individual route blockage scores and the ATC sector blockage scores as a measure of the sector capacity. The individual route blockage computations are being validated to a degree by the ongoing RAPT validation activity although it should be noted that the region of time during which departures are at cruise altitude in the RAPT domain is relatively short.

3. Consideration of the time-varying usage of the various routes in an ATC sector.

Figure 5-1 shows that the daily demand on the various routes within the ATC sectors considered in this study varies considerably. Based on feedback from airline participants in the CDM program (Russ Gold, Air Transport Association, personal communication), it would be desirable to <u>not</u> weight the various routes shown in figure 2-4 identically in the calculation of route blockage for the ATC sector. Rather, one should consider the fair-weather demand in determining an ATC sector route blockage score:

$$\text{Sector RB (time of day)} = \Sigma \text{ Route blockage for } k^{th} \text{ route (for that time of day)} \times \text{fraction of demand which uses route k at that time of day in fair weather} \quad (5\text{-}1)$$

where the summation is over the route index k. Figure 5-2 shows a typical time variation in the usage of various routes within the ZID83 sector while figure 5-3 shows the time variation in route usage within ZAU 24.

However, given the limited scope of this study, there clearly were far too few (Wx, RB) data points to develop a model for each hour during the day.

If one were willing to instead use the daily average relative route usage for the various routes during a day, it would be relatively straightforward to recompute the ATC sector route blockage for each time sample using equation (5-1) with the average fractional demand on a route for a given day. However, this would also necessitate rerunning all of the statistical pattern classification modeling and verification steps since now both the training and verification input data had changed.

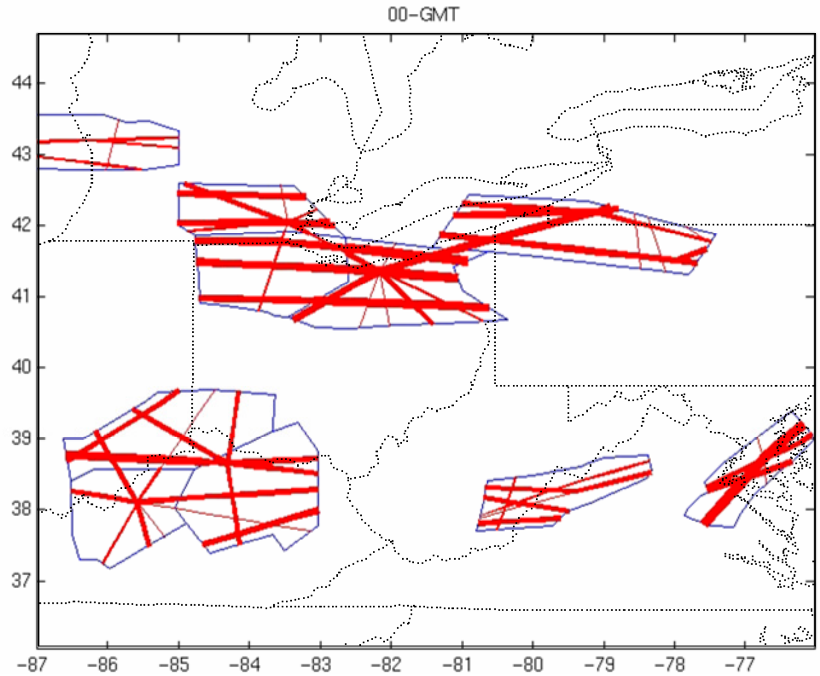

Figure 5-1. Fair-weather traffic usage of the various routes over a day. The width of the routes is proportional to the number of aircraft that were found on that route on a fair-weather day. Note that some of the routes are relatively rarely used in various sectors. Blockage of those particular routes will have a lesser influence on the overall route blockage score for the sector than does blockage of a high-usage route.

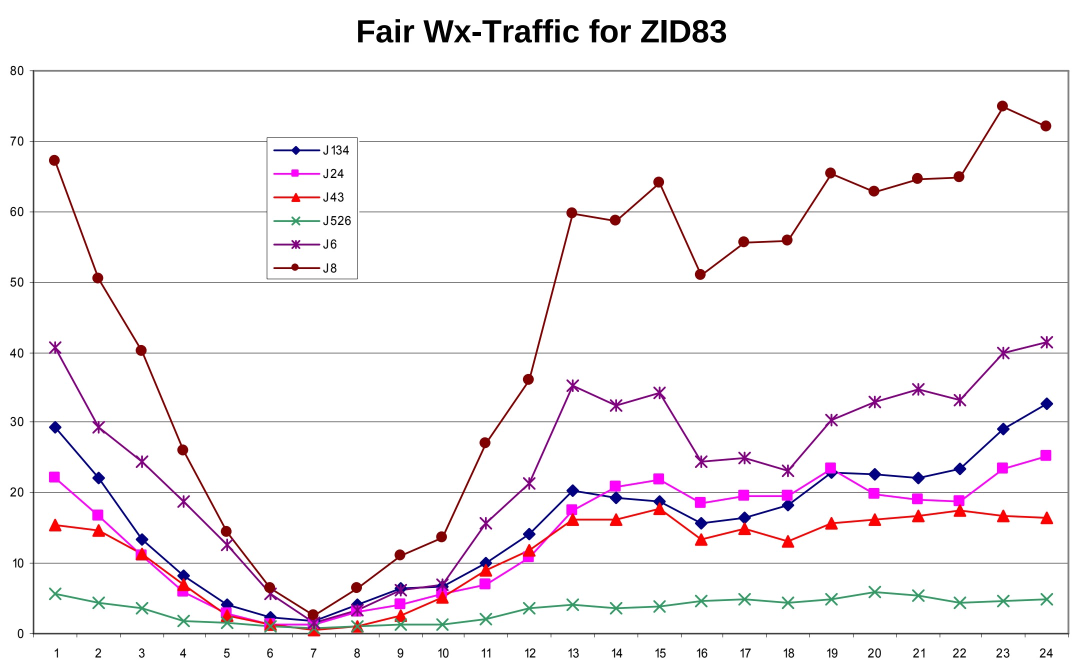

Figure 5-2. Typical changes in demand for various routes within en route sector ZID83.

ZAU24 Daily Traffic

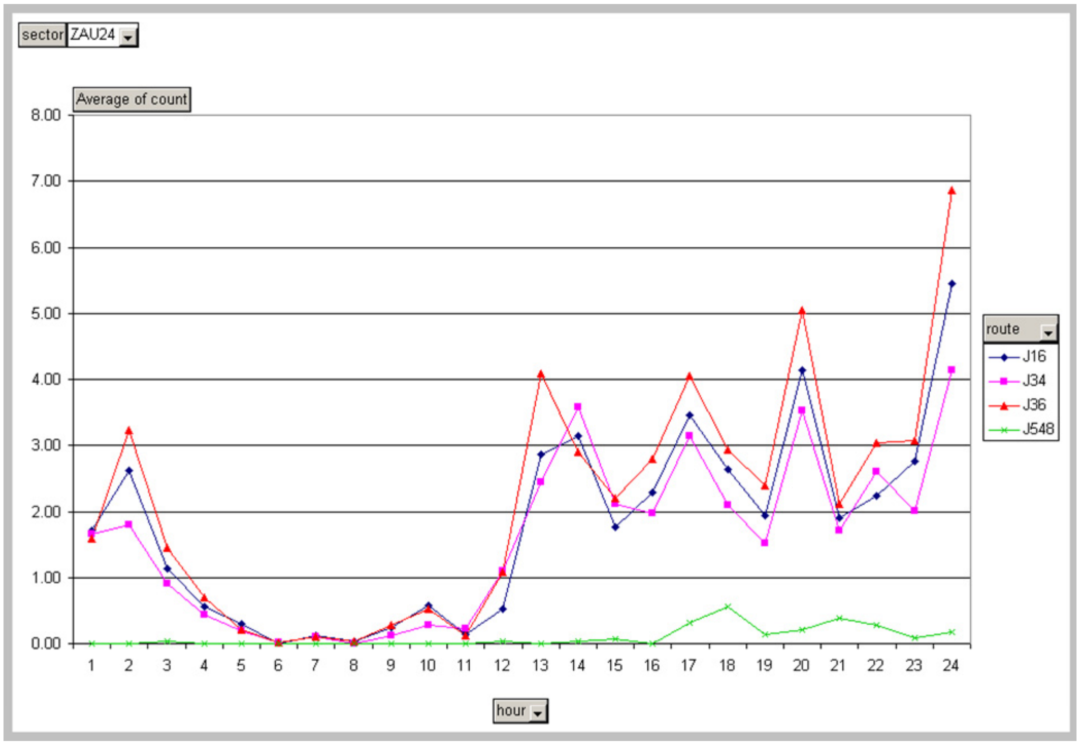

Figure 5-3. Daily traffic on various routes within en route sector ZAU24 on a fair-weather day.

APPENDIX A
MODELING RESULTS FOR INDIVIDUAL SECTORS

The following supplemental material details the pattern classification results for each ATC sector of the Wx-RB modeling study. For the three best classification routines, the explanatory power of the Wx parameters over the variability in RB have been examined and listed in a comparison table. Given a classification routine, explanatory power is revealed by modeling RB as a function of each Wx parameter separately and examining the resultant classification performance. The examination of each Wx parameter is performed during the training phase of classification. The explanatory power has been expressed as a percentage of the RB variability correctly classified solely by that Wx parameter. Low percentages indicate low explanatory power; high percentages indicate high explanatory power of a Wx parameter.

Wx parameters are presented to the classification routines in the order that produces the lowest classification training error as determined by feature selection. As defined in section 2.2.4, if feature selection produces a smaller set of Wx parameters that provides a lower, statistically significant training error, this reduced set of Wx parameters will be presented for final classification. Otherwise, the full-ordered set of Wx parameters will be used.

Within the following subsections of the results, a brief description of each ATC sector is provided. The comparison table of classifiers for that sector follows, showing the explanatory power of each Wx parameter and the overall error rates produced by Gaussian, MLP, and KNN classifiers.

To give a better sense of the variability seen in the data used to train classifiers, distributions of RB as they relate to a single Wx parameter of high explanatory power are then presented. These include the distribution of RB to parameters *etops25+* and *level3+wx*. Median values, and the upper and lower quartile ranges of the continuous raw data RB are compared to the discrete intervals presented to the classifier.

Given that the KNN classifier has been most successful at modeling RB as a function of the derived Wx parameters, discussion of feature selection results and expanded test results for KNN classification have been included.

Finally, in order to better examine the response of modeling RB as a function of Wx parameters, a synthetic data set made up of three Wx parameters has been presented to the KNN routine for classification. The synthetic data consist of the full possible range of *etops25+* percentages, *level3+wx* percentages, and the categorical parameter *wx-type*. The resulting transfer functions of RB are first based on the single parameter *etop25+*, then on both *etops25+* and *level3+wx*.

One expects the following functional behavior:

(1) Single-parameter function dependence
As the fractional coverage of high echo tops (*etops25+*) or high VIL (*level3+wx*) increases in an ATC en route sector, there should be a monotonic increase in RB. This conceptual model is illustrated on the left side of figure A.0-1 as it relates to the RB intervals of this study. Here, as the coverage of *etops25+* or *level3+wx* increases, the discrete RB interval monotonically increases to higher values.

(2) Two-parameter functional dependence

RB should increase as a function of high echo tops coverage within an ATC en route sector at a fixed coverage percentage of VIL or as a function of VIL at a fixed coverage percentage of echo tops. This would translate into the concave decision regions illustrated in the right side image of figure A.0-1. Here, the monotonic increase in RB maps to the increase in coverage of both *etops25+* and *level3+wx.*

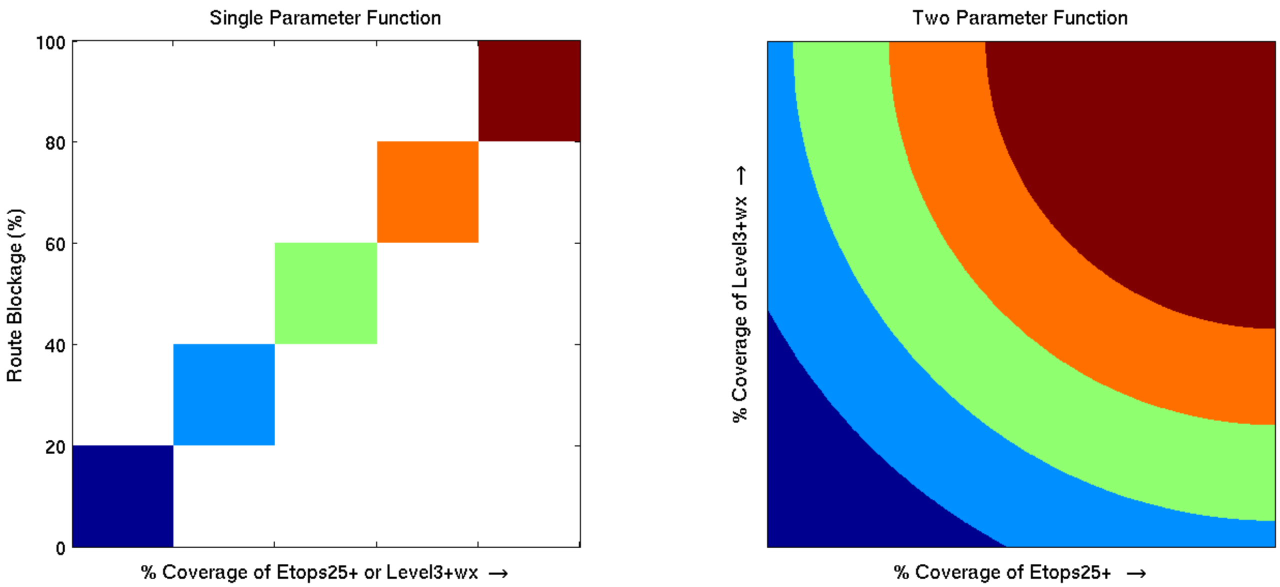

Figure A.0-1. Conceptual illustration of the expected functional dependence of RB to the single-parameter model based on either etops25+ *or* level3+wx *(left image) and the expected functional dependence of RB to a two-parameter model based on both* etops25+ *and* levelA+wx *(right image). Colors are meant to help differentiate between discrete RB intervals. Discrete RB of blue = [0–20%), light blue = [20–40%), green = [40–60%), orange = [60–80%), and garnet = [80–100%]. This color designation is maintained throughout section A. Axes of coverage % have not been given values purposely because of variability in coverage % seen between ATC sectors.*

A three-parameter transfer function based on *etops25+*, *level3+wx*, and *wx-type* is also examined (not shown in above figure). Differences indicate the response of the KNN routines to newly added Wx parameters associated with well-sampled line storm and stratiform events. For simplicity, the poorly sampled *wx-types* associated with small, large, and embedded events are not shown (refer to the last distribution on the bottom row of figure 2-7 for reference to *wx-type* sampling).

A.1 ZAU24

ZAU24 is the single ATC sector from Chicago center included in this study (figure A.1-1). J545 is the single north-south crossing route. The remaining three high jet routes are oriented east to west with J16 and J36 converging at the sector's midpoint.

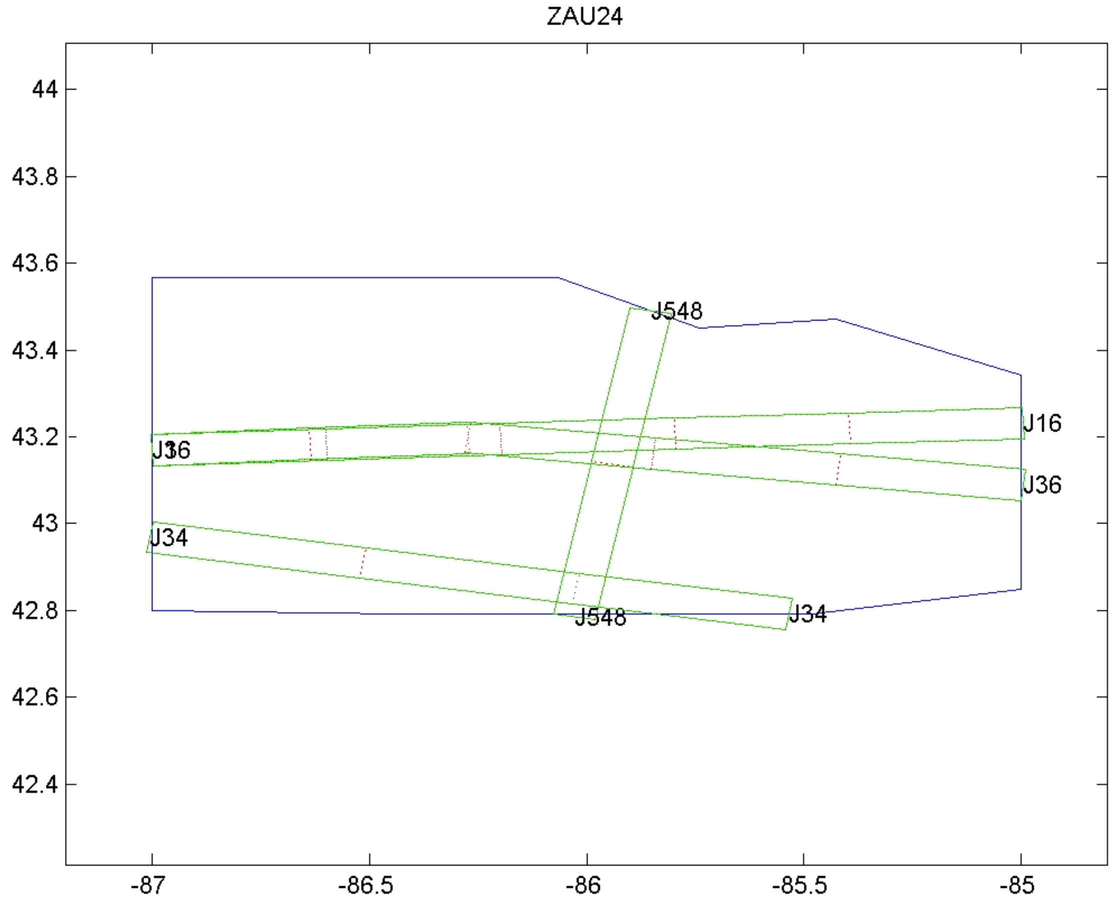

Figure A.1-1. Feature selection processing as performed by the KNN classifier. Utilizes a K=3, ZAU24 is the single ATC sector from Chicago center included in this study (figure A.1-1). J548 is the single north-south crossing route. The remaining three high jet routes are oriented east to west with J16 and J36 converging at the sector's midpoint.

For ZAU24, feature selection reveals that of the three best classifiers listed in table A.1-1, Wx parameters associated with vertical extent demonstrate the most explanatory power for RB. The best performing classifier is KNN, with an overall testing error of 5.67%. For KNN, echo tops parameters exhibited the highest explanatory percentages. When classifying RB with a single Wx parameter, *etops25+* was able to account for 88% of the RB variability and *l3andet25* was able to account for 87%. Parameters associated with reflectivity are almost as effective. Four Wx parameters have low explanatory power (less than 50%). Those include *small, line, orientation,* and *embedded.*

TABLE A.1-1

A comparison table of Gaussian, MLP, and KNN classifiers for ATC sector ZAU24. First column indicates classification routine. Second column indicates the overall error rate produced at the final testing phase of each classifier. Final column lists the Wx parameters in order of Explanatory Power over the variability seen in RB. Explanatory Power is expressed as a percentage in the parentheses to the right of each Wx parameter. The KNN classifier, as in all ATC sector results, produces the lowest testing error and is highlighted in red.

Classifier	Error	Explanatory Power of Individual Features
Gaussian	8.36%	l3andet25 (90), level3+wx (90), wx-type (89), embedded (89), small (89), large (88), orientation (87), etops25+ (87), level1+wx (86), line (84), stratiform (79)
MLP	13.1%	l3andet25 (83), level3+wx (80), line (79), etops25+ (76), orientation (70), level1+wx (66), wx-type (64), stratiform (51), large (25), small (24), embedded (6)
KNN	5.67%	etops25+ (88), l3andet25 (87), level3+wx (87), level1+wx (86), stratiform (79), large (79), wx-type (74), small (41), line (37), orientation (35), embedded (29)

Probability, box, and scatter plots along the top row of figure A.1-2 indicate that RB for ZAU24 is distributed over a wide dynamic range of *etops25+*. This, coupled with the strong weighting of echo tops in the RB calculation, explains why the echo tops terms have such high explanatory power. For a range of *etops25+* spanning 0–25%, the combination of box plot and probability distributions indicate that RB is densely centered near zero, with many non-zero RB values lying outside 1.5 times the inner quartile range (IQR). Outliers fall beyond the whiskers (1.5*IQR) and are displayed as '+' in the center figure. No box plots are displayed for the 0–5% and 5–10% bins of *etops25+* because medians and quartiles for these bins are essentially zero. Beyond a 25% coverage of *etops25+*, RB trends toward larger RB intervals. Examining the spread of the quartiles and the probability distribution shows that data density becomes sparse past *etops25+* of 25% and is widely distributed over most of the continuous range of RB.

In comparison to *etops25+*, RB for ZAU24 is distributed over a shallow range of *level3+wx* with the spread of RB being limited to a maximum of 45% fractional Wx coverage (bottom row, left image of figure A.1-2). While VIL is a major contributor to the RB calculation, this shorter dynamic range decreases the explanatory power of *level3+wx* relative to the echo tops related terms. As with *etops25+*, the combination of box plot and probability distributions indicates that RB is densely centered near zero for low fractional coverage with no IQR being displayed for the 5% discrete bin of RB.

Median slopes in the right column of figure A.1-2 indicate a positive trend in the relationship of RB to increasing fractional Wx coverage. Variability of the medians around the least squares fit is indicated by the r^2 values. RB varies much more as a function of fractional Wx coverage for ZAU24 than is the case for the other ATC en route sector RB. Here, r^2 suggests a higher variance with values for both RB vs. *etops25+* and RB vs. *level3+wx* being near 0.70. As with all ATC sector RB, the positive least squares slope for *level3+wx* vs. RB is steeper than that of *etops25+* vs. RB.

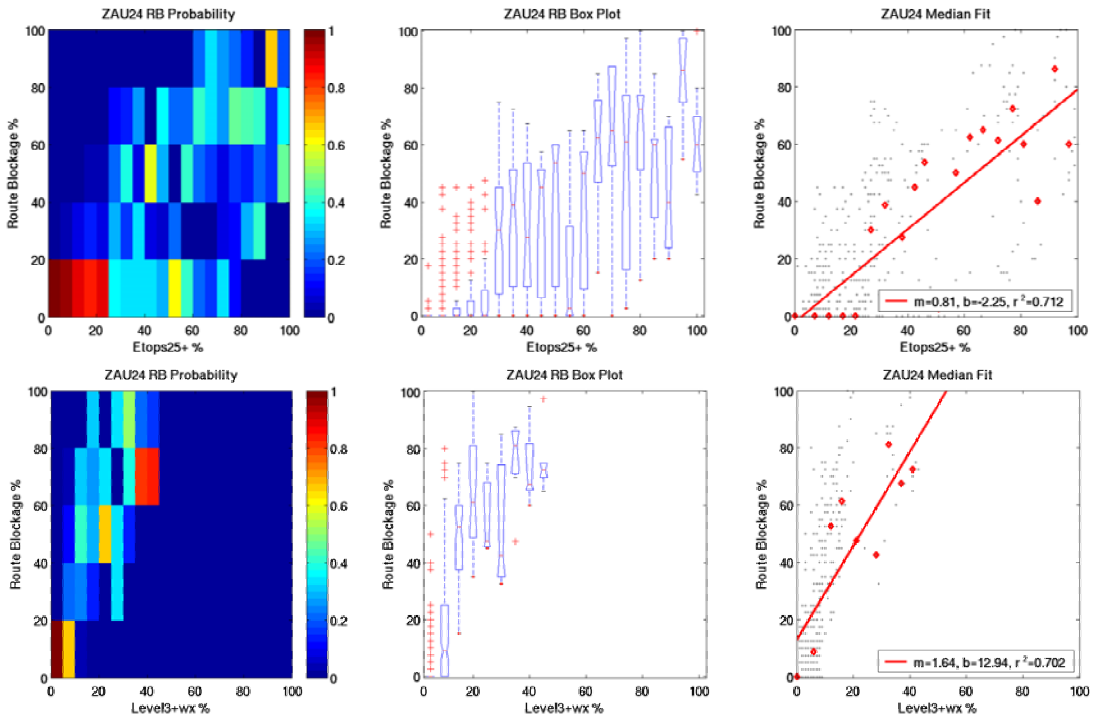

Figure A.1-2. ZAU24 distribution of RB as related to the Wx parameter etops25+ *(top row) and* level3+wx *(bottom row). (Left) Probability distribution of discrete RB (discrete RB as defined in section 2.4.5) along a 5% bin interval of* etops25+ *(top) and* level3+wx *(bottom). (Center) Median value, upper quartile and lower quartile range of RB expressed as a box plot for the 5% bin interval of* etops25+ *(top) and* level3+wx *(bottom). (Right) Least squares fit of median RB values as related to the* etops25+ *(top) and* level3+wx *(bottom) Wx parameters. Background scatter (gray) represents data points making up the two distributions.*

Of the Wx parameters, figure A.1-3 shows that nine ordered parameters excluding *wx-type* and *small* minimize the training error to 6.0% with statistical significance. These nine parameters have been presented to the KNN classifier for the final training and testing phase of RB classification.

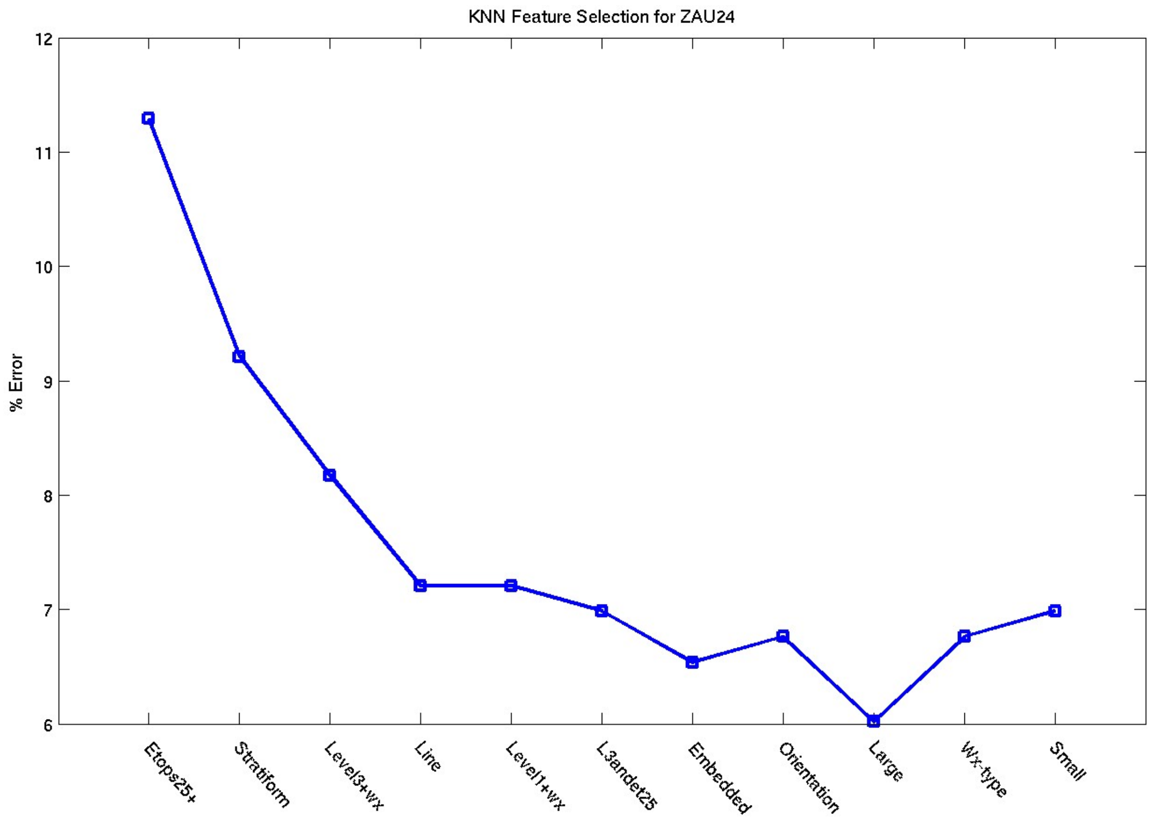

Figure A.1-3. Feature selection processing as performed by the KNN classifier. Utilizes a K = 3, leave-one-out, cross-validation scheme. Error expressed as a percentage along the ordinate axis. Wx parameters are ordered in a combination that minimizes the training error rate. Wx parameters that fall to the right of the minimum increase the combined training error. In this case, all Wx parameters are included in the best combination *set.*

Parameters associated with Wx intensity and vertical extent typically demonstrate high explanatory power for RB. Table A.1-2 compares the per RB interval errors of 3 single Wx parameter KNN models to a KNN model that utilizes all Wx parameters except *large*, *small*, and *wx-type*. Results show that the best combination of Wx parameters determined through feature selection significantly reduces the classification error. While a significant reduction in the errors is apparent, given the small number of cases reflecting RB vales beyond the [0–20%) interval, results summarized in table A.1-2 cannot be regarded as statistically meaningful for RB $\geq$ 20%.

TABLE A.1-2.
ZAU24 comparison table of four different KNN models brought through both training and testing phases of classification. Each column to the right of the "number of samples" column represents the error percentages produced by modeling RB as a function of the single explanatory parameters *level3+wx*, *l3andet25*, and *etops25+* as compared to the best combination of Wx parameters as determined through the feature selection process (left to right, respectively). Values down each column are per RB interval error expressed as a percentage. The best combination of Wx parameters consistently yields the lowest error rates.

RB interval	# samples	*Level3+wx*	*L3andet25*	*Etops25+*	*Best Combination*
[0–20%)	1493	6.04	5.37	2.68	1.01
[20–40%)	66	100.00	100.00	92.31	53.85
[40–60%)	60	91.67	33.33	83.33	16.67
[60–80%)	46	55.56	77.78	88.89	55.56
[80-100%]	17	66.67	100.00	66.67	66.67
Total Error	----	14.63	12.84	11.94	5.67

Additional insights into KNN classification performance are provided by table A.1-3, which shows the "confusion matrix" (left side of the table) and the per class error summaries (right side of the table).

Rows of the confusion matrix contain totals for the number of times a sampled Wx input pattern was associated with an RB interval. Columns of the confusion matrix contain the number of times classification was computed by the KNN routine for an RB interval. RB interval class labels are in the first column of the table. An error-free classification of the test data would consist of a confusion matrix with all patterns falling along the red diagonal and all off-diagonal bins would thus be empty.

The error summaries to the right contain the number of patterns made available for testing split by associated RB interval, the number of errors and the error percentage (highlighted in red) for each RB interval, the estimated binomial standard deviation of the error estimate, and the root mean-square-error difference between the desired RB classification and the computed RB classification [for more information see Lippmann et al. (1993) and Kukolich and Lippmann (2004)].

Results in table A.1-3 show that for ZAU24, RB of [0–20%) has a near perfect classification with only a 1.01% testing error. The overall error rate for the ZAU24 KNN classification is low at 5.67%. Classification results for RB ≥ 20% show the poorly sampled interval of [80–100%] has the largest calculated error exceeding 60%. Middle values of RB show mixed results. While the [40–60%) RB interval has an lower classification error of 16.67%, it is bounded by errors exceeding 50% for both the [20–40%) and [60–80%) RB ranges. Again, small sampling indicates that results for RB ≥ 20% cannot be regarded as statistically meaningful.

TABLE A.1-3.

KNN (K = 3) test results for ZAU24 consisting of the classification confusion matrix to the left and per class statistics to the right. Red highlighted numbers along the diagonal of the confusion matrix indicate correctly classified instances of RB. Numbers that fall to either side of the diagonal are incorrectly classified RB. Red highlighted column to the right indicates the per class error. The number at the bottom of this column is the overall error rate of the classification (5.67%).

TEST:ZAU24.test   Time: 0.07 secs RMS Err: 0.151 Err: 5.67%

K-Nearest Neighbor (K=3) classifier: 20 cases - trained on 80% of data tested on 20% ECHO-BSD

Desired	Computed Class												
Class	0	1	2	3	4	Total	Class	Patterns	#Errors	%Errors	StdDev	RMSE	Label
0_20	295	3				298	0	298	3	1.01	(0.6)	0.063	0_20
20_40	2	6	5			13	1	13	7	53.85	(13.8)	0.464	20_40
40_60	1	1	10			12	2	12	2	16.67	(10.8)	0.258	40_60
60_80			4	4	1	9	3	9	5	55.56	(16.6)	0.471	60_80
80_100			1	1	1	3	4	3	2	66.67	(27.2)	0.516	80_100
Total	298	10	20	5	2	335	Overall	335	19	5.67%	(1.3)	0.151	

Interesting insights into the functional dependence of RB to the Wx parameters can be obtained by plotting the KNN model classification results as a function of synthetic test data (figure A.1-4). The training phase was performed using the three Wx parameters of *etops25+*, *level3+wx*, and *wx-type*. Once again, because of under sampling, *wx-type* dominated by small, large, and embedded events have been omitted from the figure.

KNN training and test results modeling RB as a function of the single Wx parameter *etops25+* are shown in the first image—bottom row of figure A.1-4. For each value of *etops25+* ranging from 0–100%, a single interval of RB is estimated by the KNN routine. This transfer function can be compared to the training data set (image directly above) in which a range of RB intervals can be related to each unique value of *etops25+*. Because much of the data that makes up the training set is associated with RB values in the [0–20%) interval, this RB interval dominates the KNN model estimation. Only in the instances where *etops25+* exceeds roughly 75% does KNN model estimate an RB greater than or equal to 20%.

Adding *level3+wx* as the second Wx parameter reveals the complex decision region within the synthetic *etops25+* vs. *level3+wx* plane (second image, bottom row). Decision regions have been colored by their respective RB interval. Training data influencing the creation of this 2-D transfer function is shown in the scatter plot directly above. These points are also colored by associated RB interval (second image, top row). Points of scatter plot indicate how far the training data extends into the *etops25+* vs. *level3+wx* input space (0–100% and 0–43%, respectively). Portions of the KNN decision regions that fall beyond the outlying points in the scatter are influenced mainly by those points and their associated RB values. This accounts for the large, broadly colored regions lying above the *level3+wx* data extent that may be determined unrealistic as the number of input patterns increases.

Most compact of the decision regions is the heavily sampled [0–20%) RB interval. Complexity develops along the interface between [0–20%) RB and the intervals of [20–40%), [40–60%), and [60–80%). Disjoint regions of the higher RB intervals scatter throughout the input space and are the result of small clustering of similar events as well as possible under sampling.

The addition of the third parameter, *wx-type*, shifts decision regions generated by using only two Wx parameters of *etops25+* and *level3+wx*. For ZAU24, a *wx-type* associated with line storm events (plots in the third column of figure A.1-4) shift decision regions toward the larger RB intervals. This is most evident in the area bounded by 20–40% of *etops25+* and 0–15% of *level3+wx*. Here, the RB interval of [0–20%) recedes and the larger RB intervals of [20–40%) and [40–60%) expand in its place. This is the result of *wx-type* associated with line being attributed to patterns of both higher intensity and large vertical extent (represented by *level3+wx* and *etops25+* parameters, respectively), which can effectively increase RB within an ATC sector.

By contrast, given the same possible values of *etops25+* and *level3+wx,* the *wx-type* associated with stratiform events increases the size of decision regions made by lower RB intervals. In the case of ZAU24 (bottom row, last plot), higher RB intervals recede while lower RB intervals expand. While occurring at all RB intervals, this is most evident at the [0–20%) RB interval. This is the result of *wx-type* associated with stratiform being attributed to more benign Wx events that result in lower calculated RB percentages within an ATC sector.

Figure A.1-4 indicates that the KNN RB transfer function applied to the synthetic data set does not fit the expected functional dependence defined by the conceptual model in figure A.0-1. Decision regions of the KNN transfer function are disjoint, and RB does not monotonically increase with increasing *etops25+* and/or *level3+wx*. Concavity is only vaguely suggested by the transfer function but undersampling keeps the model from being a fully realistic, statistically meaningful representation of RB based on the chosen Wx parameters. We would expect that providing a much greater number of Wx events to the classifier algorithms will remove anomalies seen in the decision regions.

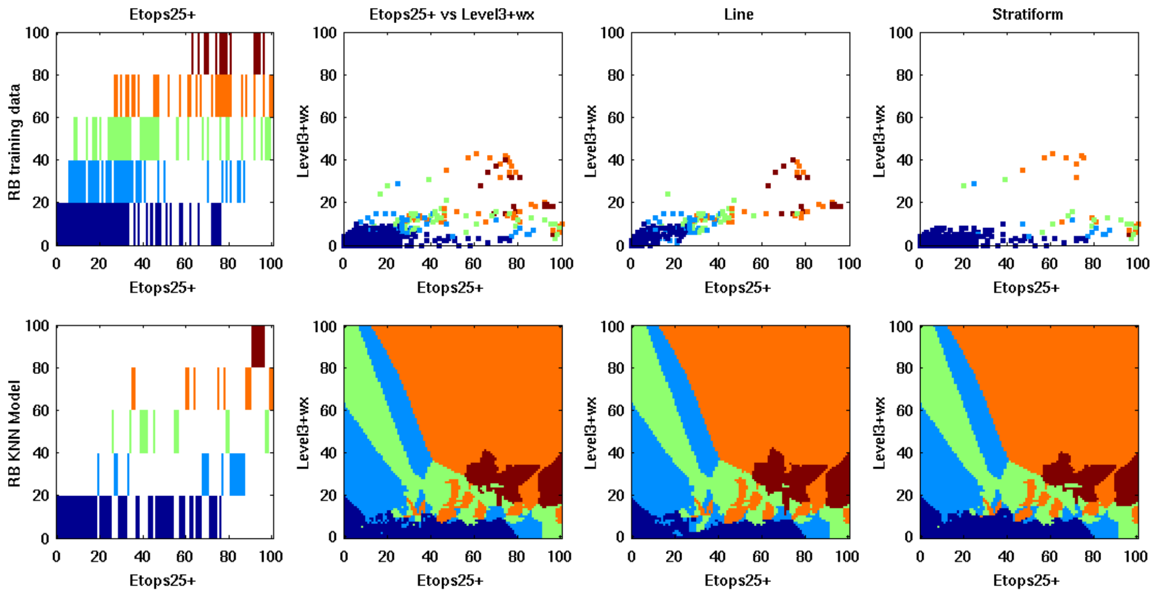

Figure A.1-4. (Top Row) ZAU24 training data distribution of discrete RB intervals as a function of etops25+, etops25+ *and* level3+wx, etops25+ *and* level3+wx *separated by* wx-type *line*, etops25+ *and* level3+wx *separated by* wx-type *stratiform (left to right, respectively). Colors differentiate between the five discrete RB intervals and are consistent throughout the figure. (Bottom Row) KNN transfer function of RB based on synthetic data covering full possible range of* etops25+, level3+wx, *and* wx-type*. For simplicity, poorly sampled* wx-types *small, large, and embedded are not shown. Complex decision regions in the last three images of the bottom row are colored by their respective RB interval.*

A.2 ZOB28

Figure A.2-1 shows that ZOB28 consists of six high jet routes, five of which converge at the Carleton VORTAC of Cleveland center. J70 is the single nonconverging route in the sector and is oriented east-west. ZOB28 shares its southern border with ZOB46.

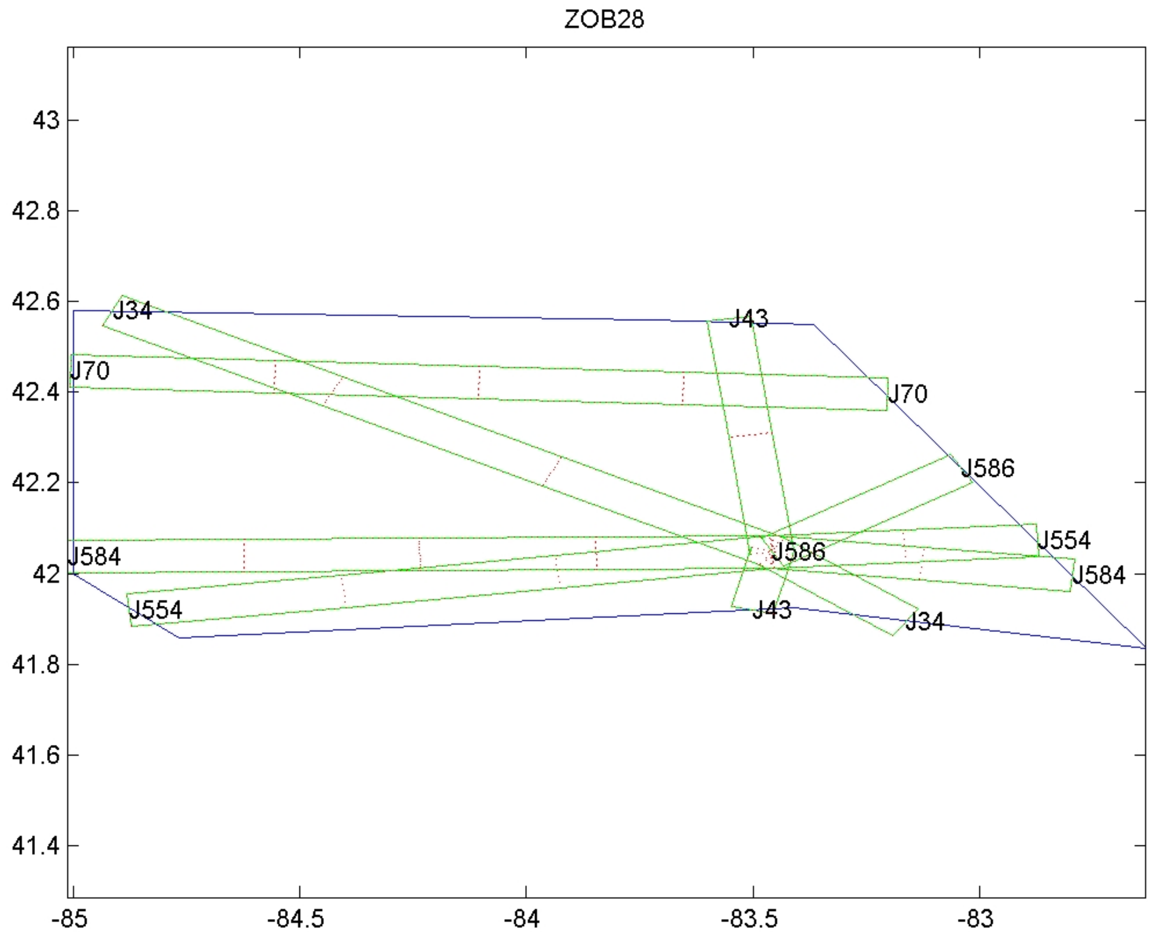

Figure A.2-1. ATC sector ZOB28 showing route orientation. Six high jet routes are in total.

Feature selection for ZOB28 found that parameters associated with echo tops demonstrate the most explanatory power over RB variability. KNN shows that both echo tops-related parameters have the highest explanatory percentages. *Etops25+* and *l3andet25* are able to account for 83% of the variation seen in RB when calculated as the single Wx parameter. For ZOB28, explanatory powers of each parameter for RB are relatively flat for the KNN classification routine, none having an explanatory percentage of less than 70% (table A.2-1).

TABLE A.2-1.
A comparison table of Gaussian, MLP, and KNN classifiers for ATC sector ZOB28. First column indicates classification routine. Second column indicates the overall error rate produced at the final testing phase of each classifier. Final column lists the Wx parameters in order of explanatory power over the variability seen in RB. Explanatory power is expressed as a percentage in the parentheses to the right of each Wx parameter. The KNN classifier, as in all ATC sector results, produces the lowest error rate and is highlighted in red.

Classifier	Error	Explanatory Power of Individual Features
Gaussian	12.8%	l3andet25 (79), etops25+ (79), level3+wx (75), embedded (72), stratiform (72), large (72), small (72), orientation (71), level1+wx (71), wx-type (70), line (70)
MLP	12.6%	etops25+ (81), l3andet25 (80), level3+wx (78), line (73), wx-type (72), embedded (72), stratiform (72), large (72), small (72), orientation (72), level1+wx (72)
KNN	12.2%	etops25+ (77), l3andet25 (76), level3+wx (74), embedded (72), line (72), orientation (68), wx-type (67), small (62), level1+wx (61), stratiform (58), large (35)

In contrast to ZAU24, median values of RB for ZOB28 trend along a better defined upward slope with a more compact IQR per bin, indicating greater data density around those median values (top row, center of figure A.2-2).

The RB for ZOB28 is distributed over a wide dynamic range of *etops25+* and is evident in the discrete probability distribution of RB for each 5% bin of the Wx parameter *etops25+* (top row, left images, figure A.2-2). This, coupled with the strong weighting of echo tops in the RB calculation, explains why the echo tops terms have such high explanatory power. In comparison to *etops25+*, RB for ZOB28 is distributed over a more shallow range of *level3+wx* with the spread of RB being limited to a 55% fractional Wx coverage (bottom row, left image of figure A.2-2). This limited spread decreases the explanatory power of *level3+wx* relative only to the echo tops-related terms. As with *etops25+*, the combination of box plot and probability distributions indicates that RB is densely centered near zero for low fractional coverage with no IQR being displayed for the 5% discrete bin of RB.

Median slopes in the right column of figure A.2-2 indicate a positive trend in the relationship of RB to increasing fractional Wx coverage. Variability of the medians around the least squares fits are indicated by the r^2 values. As with all ATC sector RBs, the positive least squares slope of median values for *level3+wx* vs. RB is steeper than that of *etops25+* vs. RB. Lower variability is seen in the RB-Wx coverage relationship for ZOB28 and is reflected in the r^2 values of 0.95 and 0.863 (for *etops25+* and *level3+wx*, respectively).

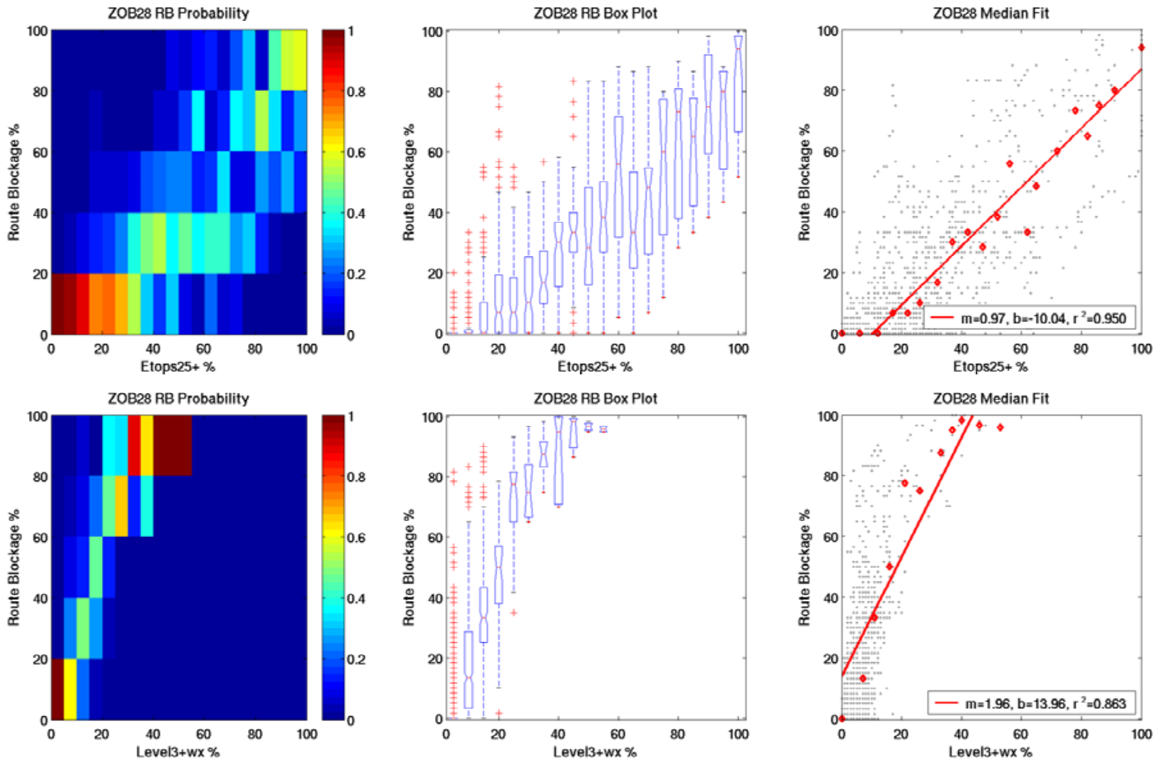

Figure A.2-2. ZOB28 distribution of RB as related to the Wx parameter etops25+ *(top row) and* level3+wx *(bottom row). (Left) Probability distribution of discrete RB (discrete RB as defined in section 2.4.5) along a 5% bin interval of* etops25+ *(top) and* level3+wx *(bottom). (Center) Median value, upper quartile and lower quartile range of RB expressed as a box plot for the 5% bin interval of* etops25+ *(top) and* level3+wx *(bottom). (Right) Least squares fit of median RB values as related to the* etops25+ *(top) and* level3+wx *(bottom) Wx parameters. Background scatter (gray) represents data points of the two distributions.*

As with ZAU24, KNN feature selection for ZOB28 shows that nine parameters once again minimize the training error for RB classification (figure A.2-3). While, in this case, the exclusion of *large* and *small* leads to a reduction in the training error of 0.4%, the calculation of standard deviation shows the decrease to a 7.2% error is not statistically insignificant. Therefore, 11 Wx parameters are presented to the KNN classifier for testing.

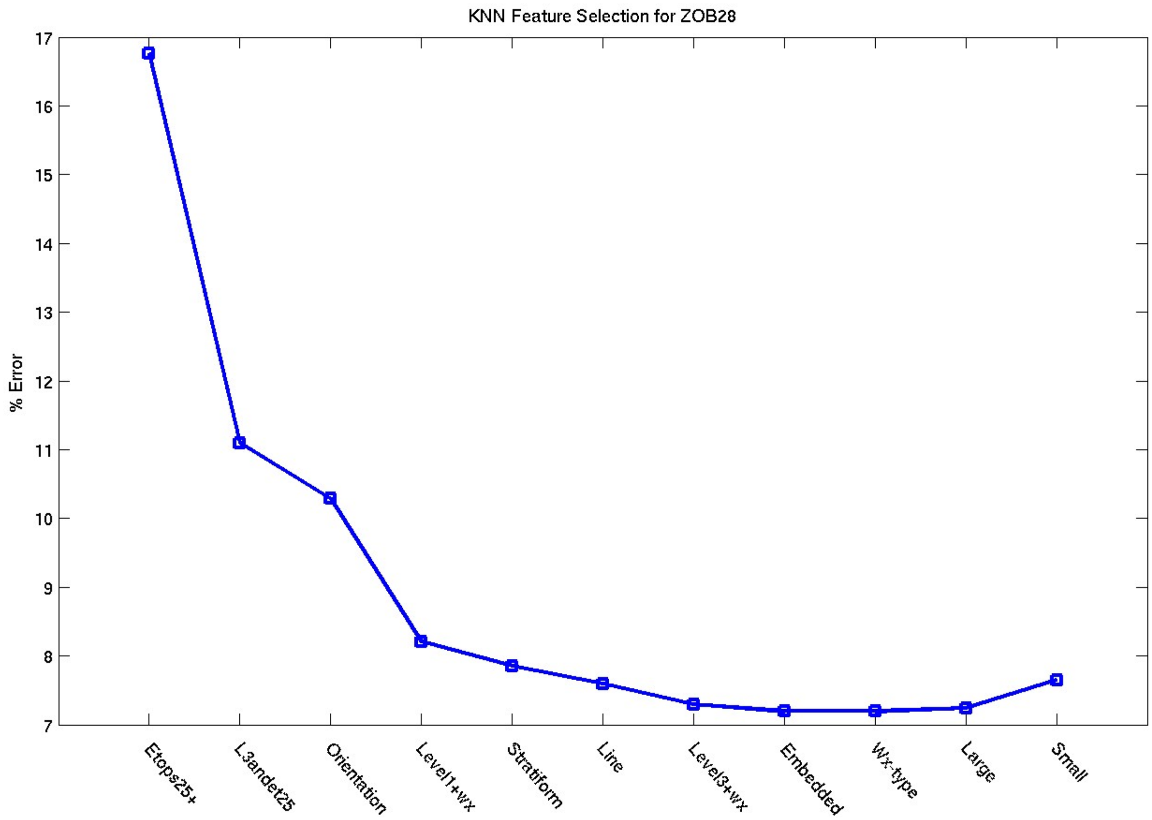

Figure A.2-3. Feature selection processing as performed by the KNN classifier. Utilizes a K=3, leave-one-out, cross-validation scheme. Error expressed as a percentage along the ordinate axis. Wx parameters are ordered in a combination that minimizes the training error rate. Wx parameters that fall to the right of the minimum increase the combined training error. In this case, all Wx parameters are included in the best combination *set.*

Table A.2-2 compares the per RB interval errors of three single Wx parameter KNN models to a KNN model that utilizes the ordered combination of all Wx parameters. Results show that the *best combination* of Wx parameters determined through feature selection significantly reduces the classification error. For the modeling RB of ZOB28, only the [0–20%) RB interval based solely *level3+wx* holds a lower classification error than the *best combination* of Wx parameters. Model results for the undersampled RB intervals (from 60–100%) again cannot be considered fully representative.

TABLE A.2-2

ZOB28 comparison table of four different KNN models brought through both training and testing phases of classification. Each column to the right of the "number of samples" column represents the error percentages produced by modeling RB as a function of the single explanatory parameters *level3+wx*, *l3andet25*, and *etops25+* as compared to the best combination of Wx parameters as determined through the feature selection process (left to right, respectively). Values down each column are per RB interval error expressed as a percentage. The best combination of Wx parameters consistently yields the lowest error rates.

RB interval	# of samples	*level3+wx*	*l3andet25*	*etops25+*	*Best Combination*
[0–20%)	2016	3.47	7.2	6.45	4.96
[20–40%)	240	93.75	72.92	68.75	58.33
[40–60%)	104	80	90	85	40
[60–80%)	59	81.82	81.82	72.73	36.36
[80–100%]	49	66.67	66.67	66.67	0
Total Errors	---	18.33	19.76	18.33	12.22

Table A.2-3 shows that for ZOB28, the overall error rate is 12.22%. A low error (4.96%) and perfect classifications have been made for RB intervals of [0–20%) and [80–100%] respectively. Mid-range RB classification results are poor with the largest error 58.33% occurring at the [20–40%) RB interval. While a perfect classification has been made at the [80–100%] RB interval, the small number of events with a RB $\geq$ 60% indicates that the results may not be a good estimate of the performance for the ensemble of convective Wx events that impact ZOB28.

TABLE A.2-3

KNN (K = 3) test results for ZOB28 consisting of the classification confusion matrix to the left and per class statistics to the right. Red highlighted numbers along the diagonal of the confusion matrix indicate correctly classified instances of RB. Numbers that fall to either side of the diagonal are incorrectly classified RB. Red highlighted column to the right indicates the per class error. The number at the bottom of this column is the overall error rate of the classification (12.22%).

```
TEST:ZOB28.test    Time: 0.14 secs  RMS Err: 0.185  Err: 12.22%
K-Nearest Neighbor (K=3) classifier: 20 cases - trained on 80% of data tested on 20% ECHO-BSD
-----------------------------------------------------------------------------------------------
Desired|   Computed Class
Class  |   0   1   2   3   4  Total  Class  Patterns  #Errors  %Errors  StdDev   RMSE  Label
-----------------------------------------------------------------------------------------------
  0_20 | 383  12   7       1  403     0       403       20       4.96   ( 1.1)  0.122   0_20
 20_40 |  17  20   9   2       48     1        48       28      58.33   ( 7.1)  0.390  20_40
 40_60 |   2   5  12   1       20     2        20        8      40.00   (11.0)  0.320  40_60
 60_80 |       1   2   7   1   11     3        11        4      36.36   (14.5)  0.324  60_80
80_100 |                   9    9     4         9        0       0.00   ( 0.0)  0.157  80_100
-----------------------------------------------------------------------------------------------
 Total | 402  38  30  10  11  491  Overall   491       60      12.22%   ( 1.5)  0.185
-----------------------------------------------------------------------------------------------
```

The single Wx parameter transfer function (bottom row, first image, figure A.2-4) of RB to *etop25+* shows that for low percentages of *etops25+* the input space is dominated by observations that are associated with low RB. This is seen in a range of 0–33% for *etops25+* where the KNN transfer function translates these percentages into a RB interval of [0–20%) alone.

Increasing the percentage of *etops25+* beyond a Wx coverage of 33% results in the somewhat erratic increase of RB to higher intervals. This erratic trend of the 1-D transfer function pattern is evident throughout each sector of the Wx-RB study. Because the KNN routine uses a Euclidian distance formula to determine an input's K nearest neighbors, in this study K = 3 instances do occur where three different classes are determined nearest. This is the result of raw data providing a range of RB for a given percentage of *etops25+* (top row, first image of figure A.2-4). If distances are equal for all three nearest neighbors with different RB, the KNN routine chooses one of the three randomly (refer to section 2.4.3). This is the reason that the single Wx parameter transfer functions jump between RB intervals as *etops25+* increases.

For ZOB28, below *etops25+* of 33%, raw data is dominated by observations associated with RB of [0–20%). This results in the consistency seen at this *etop25+* range during classification. Here, the transfer function continuously classifies RB at the [0–20%) interval (bottom row, first column).

Adding *level3+wx* as a second Wx parameter again reveals a complex decision region of the 2-D transfer function for ZOB28 (bottom row, second image of figure A.2-4). Inputs for training of the KNN routine are shown in the scatter plot directly above. Small, isolated clusters with the same calculated RB are mixed within the input space and increase the complexity of the *etops25+* vs. *level3+wx* plane.

Training data used to generate this two-Wx-parameter KNN model are shown in the scatter plot directly above and the data points have been colored by their respective RB interval (second image, top row). Points of scatter plot indicate how far the training data extends into the *etops25+* vs. *level3+wx* input space (from 0–100% and from 0–54%, respectively). Portions of the KNN decision regions that fall beyond the outlying points in the scatter are influenced mainly by those points and their associated RB values. This accounts for the large, broadly colored regions lying above the *level3+wx* data extent. These regions may be determined unrealistic as the number of input patterns increases.

When the synthetic data includes the full possible range *etops25+*, *level3+wx*, and *wx-type* associated with line type events, lower RB intervals of the transfer function contract while higher RB intervals expand (bottom row, third image). This is most prevalent at the interface between RB interval of [60–80%) and [80–100%]. Here, the RB interval of [60–80%) deteriorates to roughly half of what it was without considering *wx-type* of line; the majority of this region is classified by the [80–100%] RB interval.

When considering the full possible range *etops25+*, *level3+wx*, and *wx-type* associated with stratiform type events, as with ZAU24, decision regions associated with higher RB intervals contract while lower RB intervals expand. In the case of ZOB28, the inclusion of *wx-type* stratiform also generalizes decision regions, making them less disjoint.

Figure A.2-4 shows that the KNN RB model for ZOB28 does not fit the expected functional dependence defined by the conceptual model in figure A.0-1. Decision regions of the KNN transfer function are disjoint and RB does not monotonically increase with increasing *etops25+* and/or *level3+wx*. No concavity is apparent in the decision regions and as stated in the previous section, undersampling of the distribution of Wx events affecting ZOB28 keeps the model from being a fully realistic representation of RB based on the chosen Wx parameters.

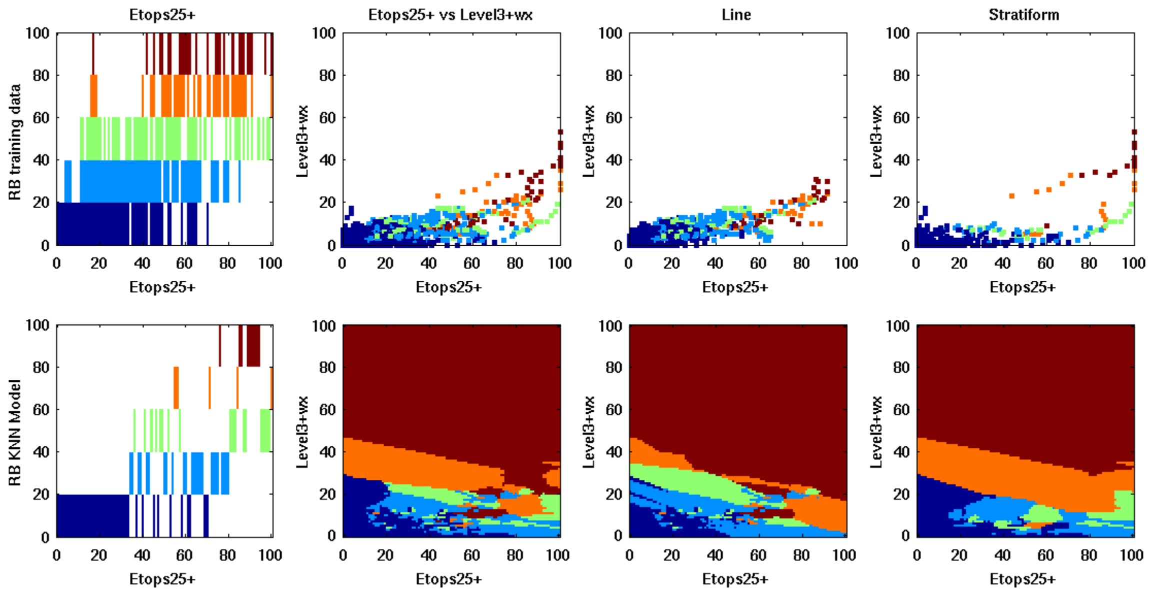

Figure A.2-4. (Top Row) ZOB28 training data distribution of discrete RB intervals as a function of etops25+, etops25+ *and* level3+wx, etops25+ *and* level3+wx *separated by* wx-type line, etops25+ *and* level3+wx *separated by* wx-type stratiform *(left to right, respectively). Colors differentiate between the five discrete RB intervals and are consistent throughout the figure. (Bottom Row) KNN transfer function of RB based on synthetic data covering full possible range of* etops25+, level3+wx, *and* wx-type. *For simplicity, poorly sampled* wx-types *small, large, and embedded are not shown. Complex decision regions in the last three images of the bottom row are colored by their respective RB interval.*

A.3 ZOB46

ZOB46 has the simplest high jet route structure of the ZOB sectors included in this study (see figure A.3-1). Three east-west routes run in parallel across the sector with the single J43 crossing route spanning from north to south. A small portion of J34 is under the responsibility of ZOB46 managers and is located in the northeast corner of the sector. ZOB46 is bounded to the east by ZOB48 and shares its northern border with ZOB28.

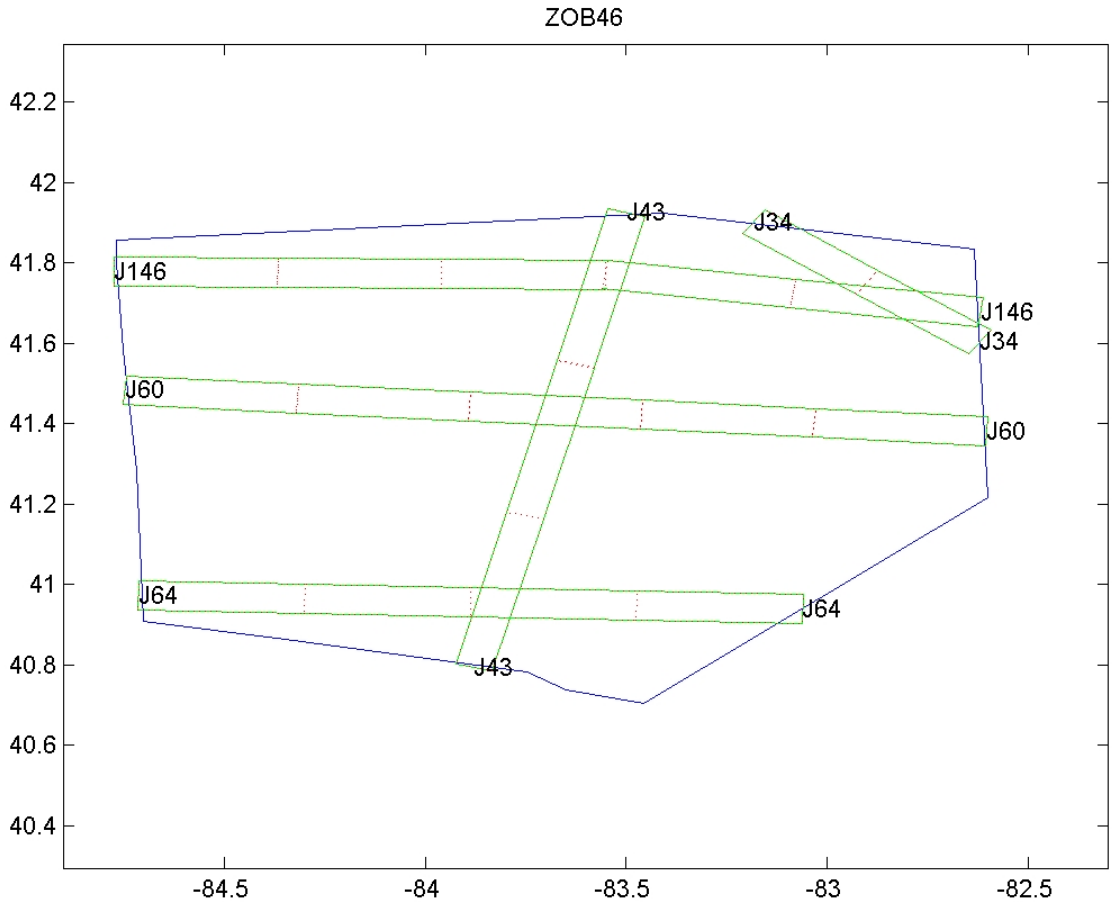

Figure A.3-1. ATC sector ZOB46 showing route orientation. Five high jet routes are in total.

For ZOB46, the Gaussian, MLP, and KNN classifiers listed in table A.3-1 all show that Wx parameters associated with vertical extent and high-intensity Wx display the most explanatory power for RB. These variables include *etops25+*, *l3andet25*, and *level3wx+*. For the KNN classifier (with the lowest test error of 9.97%), only the Wx parameter *large* held an explanatory percentage of less than 50%.

TABLE A.3-1

A comparison table of Gaussian, MLP, and KNN classifiers for ATC sector ZOB46. First column indicates classification routine. Second column indicates the overall error rate produced at the final testing phase of each classifier. Final column lists the Wx parameters in order of explanatory power over the variability seen in RB. Explanatory power is expressed as a percentage in the parentheses to the right of each Wx parameter. The KNN classifier, as in all ATC sector results, produces the lowest error rate and is highlighted in red.

Classifier	Error	Explanatory Power of Individual Features
Gaussian	17.9%	l3andet25 (79), etops25+ (79), level3+wx (75), embedded (72), stratiform (72), large (72), small (72), orientation (71), level1+wx (71), wx-type (70), line (70)
MLP	15.0%	etops25+ (81), l3andet25 (80), level3+wx (78), line (73), wx-type (72), embedded (72), stratiform (72), large (72), small (72), orientation (72), level1+wx (72)
KNN	9.97%	etops25+ (77), l3andet25 (76), level3+wx (74), embedded (72), line (72), orientation (68), wx-type (67), small (62), level1+wx (61), stratiform (58), large (35)

For ZOB46, RB spans the full dynamic range of *etops25+* in the raw data used for both training and testing of classifiers. A near-linear response can be observed in both the maxes of the discrete probability distribution and the median values of the box plots in figure A.3-2. This, coupled with the strong weighting of echo tops in the RB calculation, explains why the echo tops terms have such high explanatory power. As is common to all distributions of this Wx-RB study, for the lower bins of *etops25+*, RB is highly dense around zero. For fractional coverage of *etops25+* greater than 20%, the RB increases roughly linearly with increasing *etops25+* fractional coverage (see top row, figure A.2-2).

In comparison to *etops25+*, RB for ZOB46 is distributed over a more shallow range of *level3+wx*. The spread of RB is limited to a maximum of 60% fractional Wx coverage (bottom row, left image of figure A.3-2). While VIL is a major contributor to the RB calculation, this shallow dynamic range decreases the explanatory power of *level3+wx* relative only to the echo tops-related terms. As with *etops25+*, the combination of box plot and probability distributions indicates that RB is densely centered near zero for low fractional coverage with no IQR being displayed for the 5% and 10% discrete bins of RB.

In comparison to both ZAU24 and ZOB28, the IQRs of the discrete *etops25+* and *level3+wx* bins are more compact for ZOB46, indicating that the data distribution is more centered near the median values (center images, figure A.3-2).

Compactness is also evident in the background scatter of data in the far right images of figure A.3-2. Median slopes in the right column of figure A.1-2 indicate a positive trend in the relationship of RB to increasing fractional Wx coverage. Variability of the medians around the least squares fit is indicated by the r^2 values. As with all ATC sector RBs, the positive least squares slope of median values for *level3+wx* vs. RB is steeper than that of *etops25+* vs. RB. Lower variability is seen in the RB-Wx coverage relationship for ZOB46 and is reflected in the r^2 values of 0.96 and 0.86 (for *etops25+* and *level3+wx*, respectively).

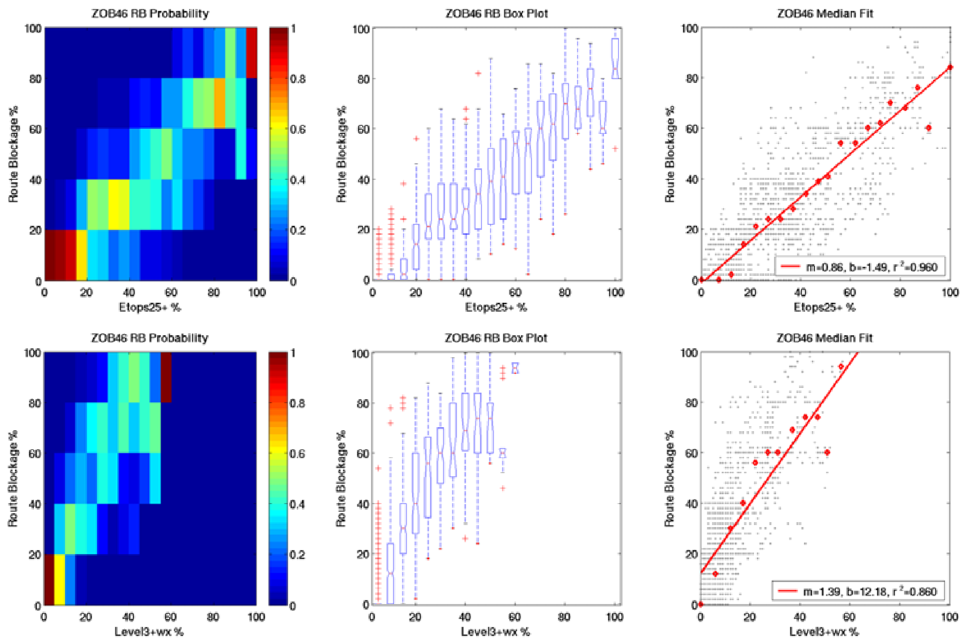

Figure A.3-2. ZOB46 distribution of RB as related to the Wx parameter etops25+ *(top row) and* level3+wx *(bottom row). (Left) Probability distribution of discrete RB (discrete RB as defined in section 2.4.5) along a 5% bin interval of* etops25+ *(top) and* level3+wx *(bottom). (Center) Median value, upper quartile and lower quartile range of RB expressed as a box plot for the 5% bin interval of* etops25+ *(top) and* level3+wx *(bottom). (Right) Least squares fit of median RB values as related to the* etops25+ *(top) and* level3+wx *(bottom) Wx parameters. Background scatter (gray) represents data points of the two distributions.*

For ZOB46, feature selection reveals that a combination of eight Wx parameters yields the lowest training error of 12.6%. Wx parameters that, in combination, increase this error include *wx-type*, *large*, and *small*. This error is separated by two standard deviations of the error produced using the full Wx parameter combination (14.0%) and is thus statistically significant. The reduced Wx parameter set has been presented to the KNN classifier for testing (figure A.3-3).

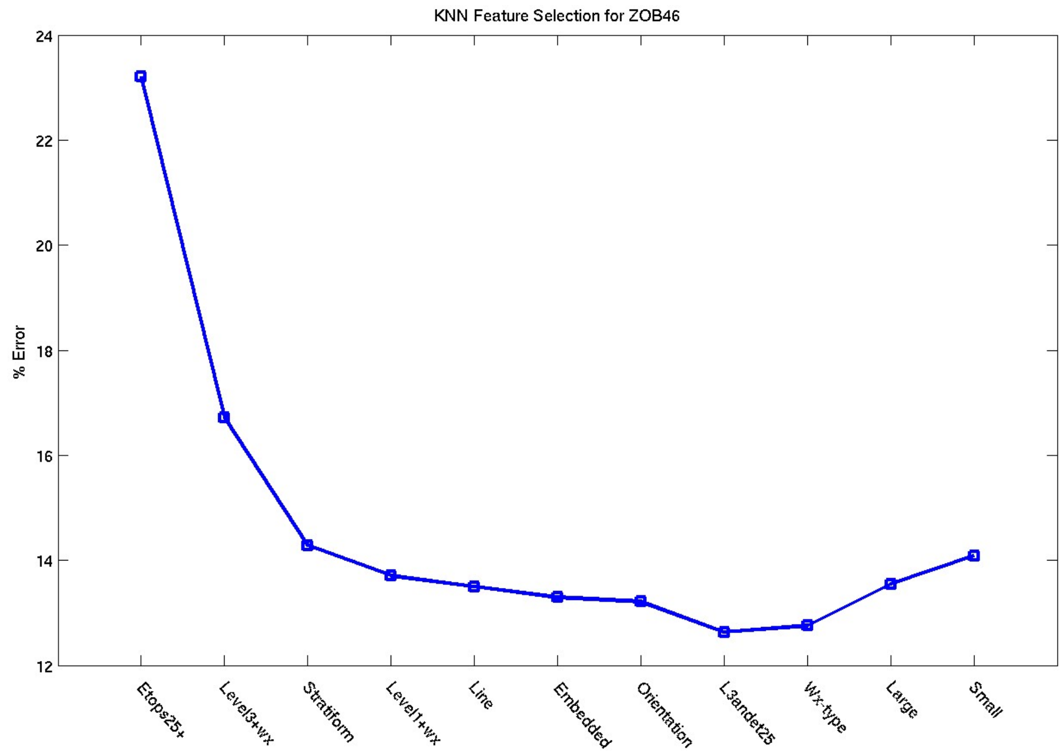

Figure A.3-3. Feature selection processing as performed by the KNN classifier. Utilizes a K=3, leave-one-out, cross-validation scheme. Error expressed as a percentage along the ordinate axis. Wx parameters are ordered in a combination that minimizes the training error rate. Wx parameters that fall to the right of the minimum increase the combined training error and were not used in the best combination *parameter selection.*

Table A.3-2 compares the per RB interval errors of three single Wx parameter KNN models to a KNN model that utilizes all Wx parameters except *wx-type*, *large*, and *small*. Results show that the best combination of Wx parameters determined through feature selection significantly reduces the classification error. In predicting RB for ZOB46, all RB intervals show reduced classification errors when the best combination of Wx parameters is used.

TABLE A.3-2

ZOB46 comparison table of four different KNN models brought through both training and testing phases of classification. Each column to the right of the number of samples represents the error percentages produced by modeling RB as a function of the single explanatory parameters *level3+wx*, *l3andet25*, and *etops25+* as compared to the best combination of Wx parameters as determined through the feature selection process (left to right, respectively). Values down each column are per the RB interval error expressed as a percentage. The best combination of Wx parameters consistently yields the lowest error rates.

RB interval	# of samples	*level3+wx*	*l3andet25*	*etops25+*	*Best Combination*
[0–20%)	2164	7.87	3.47	10.19	4.63
[20–40%)	435	58.82	48.24	49.41	27.06
[40–60%)	204	72.5	80	90	22.5
[60–80%)	154	80	73.33	56.67	23.33
[80–100%]	77	86.67	80	66.67	6.67
Total Errors	---	24.92	20.27	24.75	9.97

Table A.3-3 shows the results of KNN classification for ZOB46. The overall error rate for the KNN classification of ZOB46 RB is 9.97%. Low error rates have been achieved for both low and high RB intervals. In comparison to the previously examined ATC sector RB classification results, the middle intervals of RB spanning 20% to 80% have lower classification errors. The largest error of 27.06% occurs at the [20–40%) RB interval.

TABLE A.3-3

KNN (K = 3) test results for ZOB46 consisting of the classification confusion matrix to the left and per class statistics to the right. Red highlighted numbers along the diagonal of the confusion matrix indicate correctly classified instances of RB. Numbers that fall to either side of the diagonal are incorrectly classified RB. Red highlighted column to the right indicates the per class error. The number at the bottom of this column is the overall error rate of the classification (9.97%).

```
TEST:ZOB46.test    Time: 0.17 secs  RMS Err: 0.2  Err: 9.97%
K-Nearest Neighbor (K=3) classifier: 20 cases - trained on 80% of data tested on 20% ECHO-BSD
---------------------------------------------------------------------------------------------
Desired|   Computed Class
Class  |   0   1   2   3   4  Total  Class  Patterns  #Errors  %Errors  StdDev   RMSE  Label
---------------------------------------------------------------------------------------------
  0_20 | 412  19   1          432     0      432       20        4.63  ( 1.0)  0.136   0_20
 20_40 |  13  62   9   1       85     1       85       23       27.06  ( 4.8)  0.329  20_40
 40_60 |   1   3  31   4   1   40     2       40        9       22.50  ( 6.6)  0.300  40_60
 60_80 |       1   3  23   3   30     3       30        7       23.33  ( 7.7)  0.306  60_80
80_100 |               1  14   15     4       15        1        6.67  ( 6.4)  0.163  80_100
---------------------------------------------------------------------------------------------
 Total | 426  85  44  29  18  602  Overall   602       60         9.97%  ( 1.2)  0.200
---------------------------------------------------------------------------------------------
```

The scatter plots along the top row of figure A.3-4 show that a better sampled range of fractional Wx coverage has been made for ZOB46 in comparison to ATC sectors ZAU24 and ZOB28. This better sampling may account for the lower per class error rates calculated during the testing phase of the KNN routine (red column of table A.3-3). Comparing ZOB46 to all sectors, error rates of the middle range RB intervals [20–40%), [40–60%), and [60–80%) are relatively low and stay consistent.

As with the other ATC sectors, the single Wx parameter transfer function erratically trends toward larger RB intervals with increasing *etops25+* (bottom row, first column, figure A.3-4).

Of all sectors, ZOB46 contains the smallest decision region attributed to the [0–20%) RB interval. This can be seen in both the single- and multidimensional transfer functions along the bottom row of figure A.3-4. A complex decision region is revealed with the addition of *level3+wx*. Isolated clusters of Wx coverage associated with a similar RB interval mix with the input space, adding noise to the decision regions of the *etops25+* vs. *level3+wx* plane (bottom row, second image).

As in the previous sections, training data used to generate the two-Wx-parameter KNN model is shown in the scatter plot directly above. Data points have been colored by their respective RB interval (second image, top row). Points of scatter plot indicate how far the training data extends into the *etops25+* vs. *level3+wx* input space (0–100% and 0–58%, respectively). Portions of the KNN decision regions that fall beyond the outlying points in the scatter are influenced mainly by those points and their associated RB values. This accounts for the large, broadly colored regions lying above the *level3+wx* data extent. These regions may be determined unrealistic as the number of input patterns increases.

The addition of *wx-type* line generally shifts decision regions toward higher RB intervals where *wx-type* associated with stratiform shifts decision regions toward lower RB intervals (third and fourth column of figure A.3-4). Side-by-side model comparisons indicate that events associated with *wx-type* stratiform contribute to the generalization of classification decision regions, *wx-types* associated with line maintain complexity similar to that of modeling RB as a function of *etops25+* and *level3+wx* alone. Most noticeable differences are the shift between RB intervals of [40–60%) and [60–80%) with the addition of *wx-type* and the smoothing of the regions between [0–20%) and [20–40%) when *wx-type* is stratiform.

Figure A.3-4 indicates that the KNN RB transfer function applied to the synthetic data set does not fit the expected functional dependence defined by the conceptual model in figure A.0-1. Decision regions of the KNN transfer function are disjoint and RB does not monotonically increase with increasing *etops25+* and/or *level3+wx*. While the concave nature of the conceptual model is also vaguely evident in the RB [0–20%) decision region, the region is not continuous. To get a realistic representation of the ensemble relationship of RB to Wx, a significant increase in the number of sampled RB/Wx data is needed.

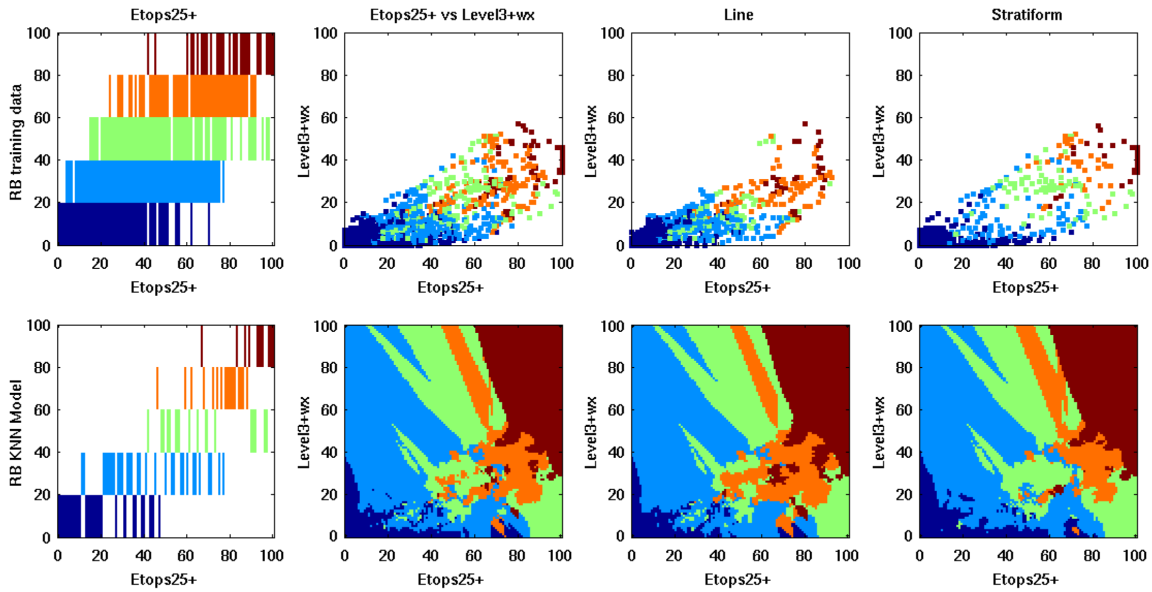

Figure A.3-4. (Top Row) ZOB46 training data distribution of discrete RB intervals as a function of etops25+, etops25+ *and* level3+wx, etops25+ *and* level3+wx *separated by* wx-type line, etops25+ *and* level3+wx *separated by* wx-type stratiform *(left to right, respectively). Colors differentiate between the five discrete RB intervals and are consistent throughout the figure. (Bottom Row) KNN transfer function of RB based on synthetic data covering full possible range of* etops25+, level3+wx, *and* wx-type. *For simplicity, poorly sampled* wx-types *small, large, and embedded are not shown. Complex decision regions in the last three images of the bottom row are colored by their respective RB interval.*

A.4 ZOB48

ZOB48 seen in figure A.4-1 contains a highly complex route structure that receives a major portion of the air traffic within the NAS. Of the nine high jet routes contained within the sector, all but two converge over Cleveland-Hopkins International Airport. Those nonconverging east-west routes include J146 and J64. ZOB48 shares a portion of its northern border with ZOB77 and is bounded from the west by ZOB46.

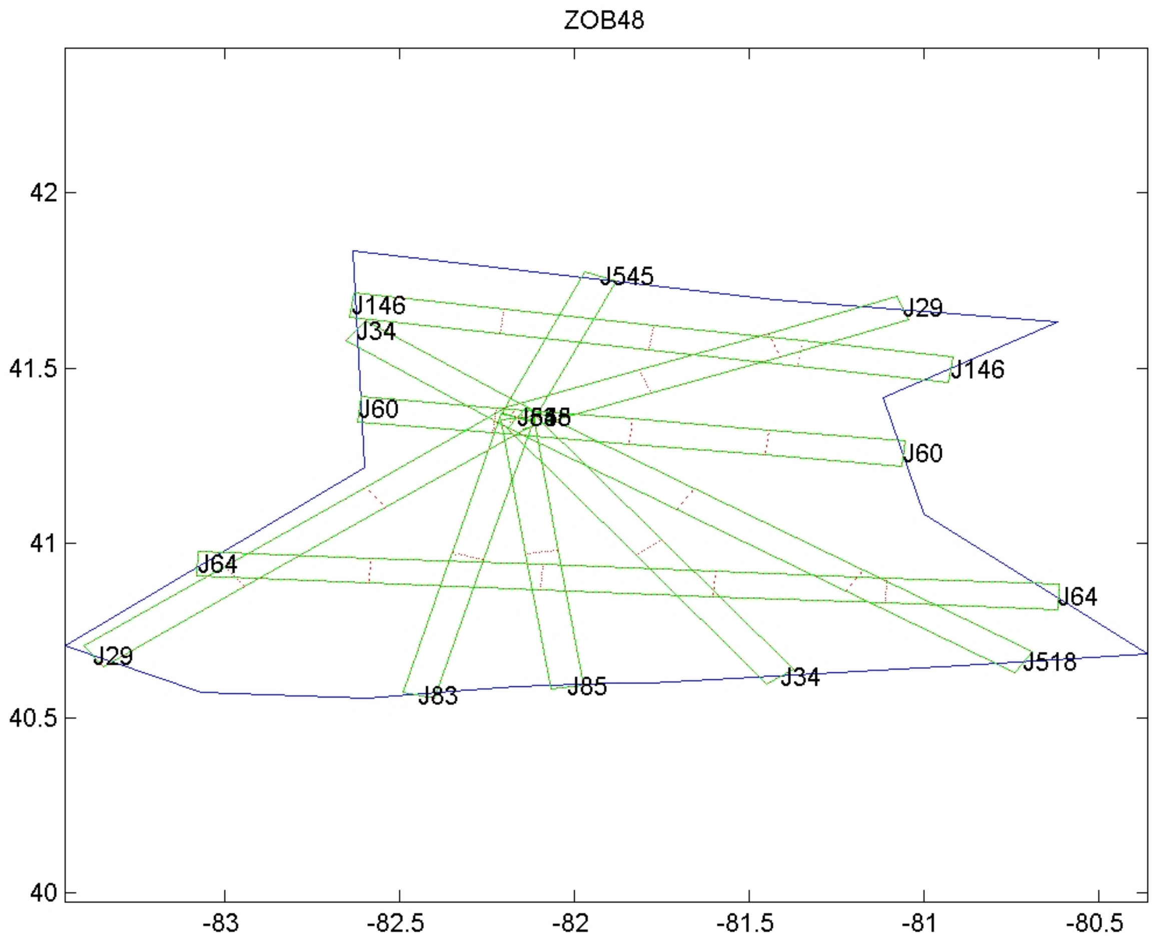

Figure A.4-1. ATC sector ZOB48 showing route orientation. Nine high jet routes are in total.

For ZOB48, Wx parameters associated with echo tops have the greatest explanatory power over the variability seen in the RB data. In Table A.4-1, one of the echo tops-related parameters is listed first with an explanatory percentage of no less than 90% in each of the classification routines. For KNN, with a low test error of 4.27%, all Wx parameters have explanatory percentages greater than 50%.

TABLE A.4-1.
A comparison table of Gaussian, MLP, and KNN classifiers for ATC sector ZOB48. First column indicates classification routine. Second column indicates the overall error rate produced at the final testing phase of each classifier. Final column lists the Wx parameters in order of explanatory power over the variability seen in RB. Explanatory power is expressed as a percentage in the parentheses to the right of each Wx parameter. The KNN classifier, as in all ATC sector results, produces the lowest error rate and is highlighted in red.

Classifier	Error	Explanatory Power of Individual Features
Gaussian	9.76%	l3andet25 (90), wx-type (87), large (87), small (87), etops25+ (87), level3+wx (87), embedded (86), level1+wx (86), orientation (85), stratiform (84), line (84)
MLP	6.18%	l3andet25 (91), etops25+ (90), line (88), level3+wx (88), wx-type (87), embedded (87), stratiform (87), large (87), small (87), orientation (87), level1+wx (87)
KNN	4.27%	etops25+ (90), l3andet25 (88), level3+wx (88), embedded (87), large (87), line (87), level1+wx (81), orientation (80), small (73), stratiform (68), wx-type (52)

Figure A.4-2 shows that RB is distributed over the full range of *etops25+* for ZOB48 (top left image). Box plots in the top-center image indicate that for the range *etops25+* below 50%, the distribution of raw data inputs falls close to median RB values, resulting in compact IQRs per 5% incremental bin of *etops25+*. For *etops25+* greater than 50%, sampling becomes less dense and irregular, resulting in a jagged upward trend of median RB values with increasing *etops25+*. The spread of the quartiles through this range become less consistent and maxes in the discrete probabilities (left, figure A.4-2) lose their linear trend.

In comparison to *etops25+*, RB for ZOB48 is distributed over a more shallow range of *level3+wx*. The spread of RB is limited to a maximum of 40% fractional Wx coverage (bottom row, left image of figure A.4-2). As with *etops25+*, the combination of box plot and probability distributions indicates that RB is densely centered near zero for low fractional coverage with no IQR being displayed for the 5% discrete bin of RB.

Median slopes in the right column of figure A.4-2 indicate a positive trend in the relationship of RB to increasing fractional Wx coverage. Variability of the medians around the least squares fits are indicated by the r^2 values. As with all ATC sector RB, the positive least squares slope of median values for *level3+wx* vs. RB is steeper than that of *etops25+* vs. RB. Variability is low but slightly elevated by the increased scatter seen at higher Wx fractional coverage and is reflected in the r^2 values (right column of figure A.4-2).

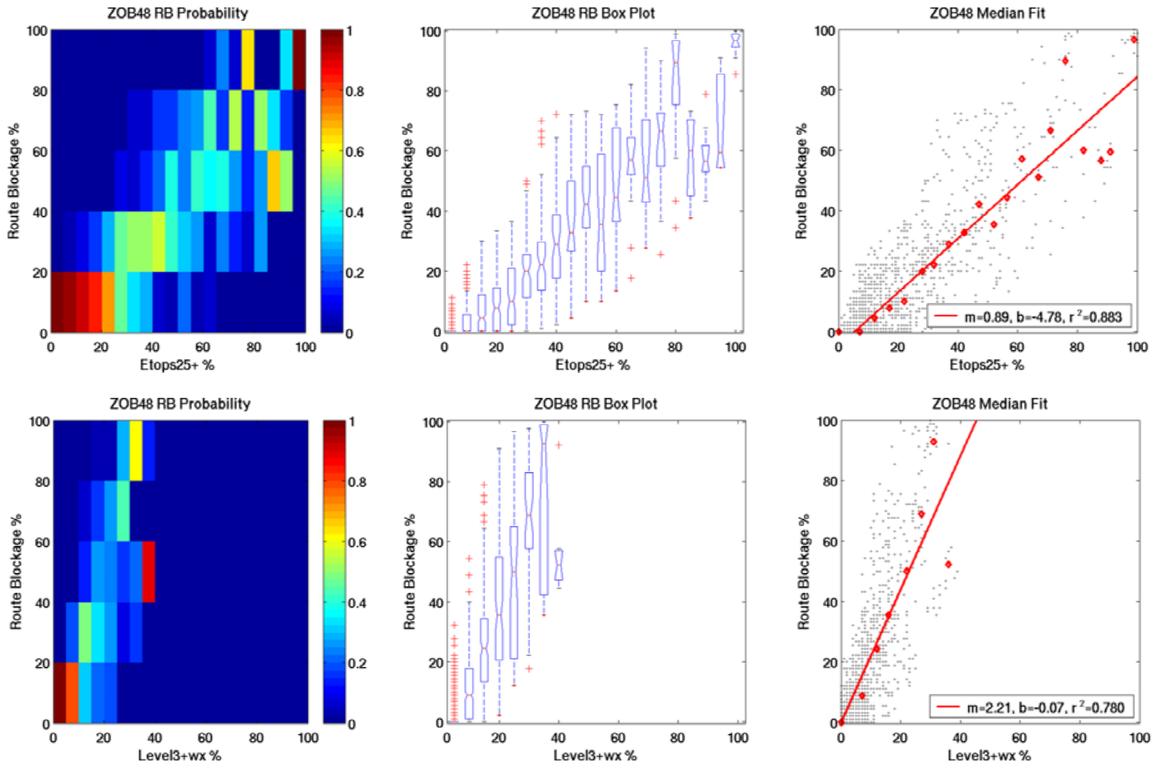

Figure A.4-2. ZOB48 distribution of RB as related to the Wx parameter etops25+ *(top row) and* level3+wx *(bottom row). (Left) Probability distribution of discrete RB (discrete RB as defined in section 2.4.5) along a 5% bin interval of* etops25+ *(top) and* level3+wx *(bottom). (Center) Median value, upper quartile and lower quartile range of RB expressed as a box plot for the 5% bin interval of* etops25+ *(top) and* level3+wx *(bottom). (Right) Least squares fit of median RB values as related to the* etops25+ *(top) and* level3+wx *(bottom) Wx parameters. Background scatter (gray) represents data points of the two distributions.*

Figure A.4-3 shows that the use of all Wx parameters produces a training error of 5.1%. Excluding the last four Wx parameters decreases this error by only 0.2%, which has been calculated to be a statistically insignificant difference. Therefore, all Wx parameters have been presented to the KNN classification routine for the modeling of ZOB48 RB.

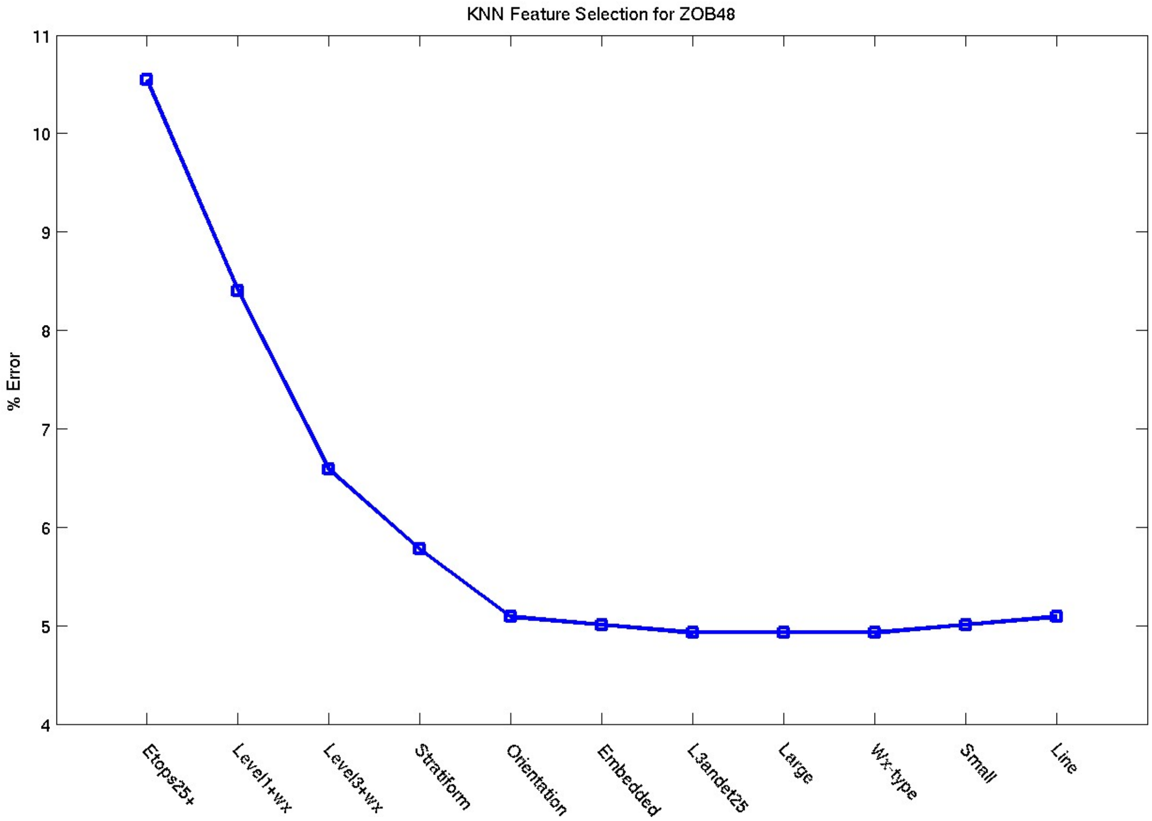

Figure A.4-3. Feature selection processing as performed by the KNN classifier. Utilizes a K=3, leave-one-out, cross-validation scheme. Error expressed as a percentage along the ordinate axis. Wx parameters are ordered in a combination that minimizes the training error rate. Wx parameters that fall to the right of the minimum increase the combined error. In this case, all Wx parameters are included in the best combination *set.*

Table A.4-2 compares the per RB interval errors of three single-Wx-parameter KNN models to a KNN model that utilizes all Wx parameters. Results show that the best combination of Wx parameters determined through feature selection significantly reduces the classification error. For the modeling RB of ZOB48, all RB intervals show improved classification errors when the best combination of Wx parameters is used.

TABLE A.4-2

ZOB48 comparison table of four different KNN models brought through both training and testing phases of classification. Each column to the right of the "number of samples" column represents the error percentages produced by modeling RB as a function of the single explanatory parameters *level3+wx*, *l3andet25*, and *etops25+* as compared to the best combination of Wx parameters as determined through the feature selection process (left to right, respectively). Values down each column are per the RB interval error expressed as a percentage. The best combination of Wx parameters consistently yields the lowest error rates.

RB interval	# of samples	level3+wx	l3andet25	etops25+	Best Combination
[0–20%)	2672	3.93	6.37	3	1.5
[20–40%)	247	65.31	38.78	65.31	20.41
[40–60%)	84	68.75	62.5	68.75	43.75
[60–80%)	57	90.91	72.73	100	36.36
[80–100%]	29	60	60	20	0
Total Errors	---	12.52	12.03	11.54	4.72

Table A.4-3 shows that near-perfect and perfect classifications have been made for RB intervals of [0–20%) and [80–100%], respectively. The largest error of 43.75% has been produced at the [40–60%) RB interval. A low overall testing error of 4.72% has been produced by the KNN classification for ZOB48. Small sampling of RB ≥ 60% indicates that results at these intervals may not be a statistically meaningful representation of all Wx events that can affect the RB of ZOB48.

TABLE A.4-3

KNN (K = 3) test results for ZOB48 consisting of the classification confusion matrix to the left and per class statistics to the right. Red highlighted numbers along the diagonal of the confusion matrix indicate correctly classified instances of RB. Numbers that fall to either side of the diagonal are incorrectly classified RB. Red highlighted column to the right indicates the per class error. The number at the bottom of this column is the overall error rate of the classification (4.72%).

```
TEST:ZOB48.test    Time: 0.19 secs  RMS Err: 0.125  Err: 4.72%
K-Nearest Neighbor (K=3) classifier: 20 cases - trained on 80% of data tested on 20% ECHO-BSD
----------------------------------------------------------------------------------------------
Desired|   Computed Class
Class  |   0   1   2   3   4  Total  Class  Patterns  #Errors  %Errors  StdDev   RMSE  Label
----------------------------------------------------------------------------------------------
  0_20 | 526   8                534      0       534        8     1.50  ( 0.5)  0.068   0_20
 20_40 |   7  39   3               49      1        49       10    20.41  ( 5.8)  0.259  20_40
 40_60 |       4   9   3           16      2        16        7    43.75  (12.4)  0.365  40_60
 60_80 |           4   7           11      3        11        4    36.36  (14.5)  0.376  60_80
80_100 |                   5        5      4         5        0     0.00  ( 0.0)  0.133 80_100
----------------------------------------------------------------------------------------------
 Total | 533  51  16  10   5  615  Overall   615       29        4.72%  ( 0.9)  0.125
----------------------------------------------------------------------------------------------
```

A comparison of images in column one of figure A.4-4 shows that the positive trend of RB as a function of the single Wx parameter *etops25+* (bottom) mimics the distribution seen in the input data distribution (top). Tails of the *etops25+* range are classified into two distinct RB intervals. For low values of *etops25+* ranging from 0–21%, the KNN transfer function classifies the synthetic data continuously as a RB interval of [0–20%). For possible high values of 92–100%, the KNN routine predicts that the RB interval will be [80–100%].

Addition of *level3+wx* as the second Wx parameter shows complex decision regions are constructed for all intervals except for the RB of [80–100%]. For this interval alone, a continuous decision region has been formed (bottom row, second column). Other RB intervals are made disjoint as a result of isolated clusters associated with similar RB mixing within the input space.

Again, training data used to generate the two-Wx-parameter KNN model is shown in the scatter plot directly above. Data points have been colored by their respective RB interval (second image, top row). Points of scatter plot indicate how far the training data extends into the *etops25+* vs. *level3+wx* input space (0–100% and 0–39%, respectively). Portions of the KNN decision regions that fall beyond the outlying points in the scatter are influenced mainly by those points and their associated RB values. This accounts for the large, broadly colored regions lying above the *level3+wx* data extent. These regions may be determined unrealistic as the number of input patterns increases.

As with previously discussed ATC sectors, the addition of *wx-type* line generally shifts decision regions toward higher RB intervals where *wx-type* associated with stratiform shifts regions toward lower intervals. Events associated with *wx-type* stratiform contribute to the generalization of decision regions; *wx-types* associated with line contribute to complexity (columns three and four of figure A.4-4).

A comparison of decision regions shows that RB of [80–100%] remains continuous with the addition of Wx parameters *level3+wx* and *wx-type*. The distinct and continuous separation of the [80–100%] RB interval from the others may be the reason a perfect classification for this interval has been made (see the error statistics of table A.4-3).

Figure A.4-4 shows that the KNN RB model for ZOB48 does not fit the expected functional dependence defined by the conceptual model in figure A.0-1. Decision regions of the KNN transfer function are disjoint and RB does not monotonically increase with increasing *etops25+* and/or *level3+wx*. The expected concave nature of the two-parameter model is implied by the [0–20%) decision region, but anomalies in the surface are the result of mixing of the input space which breaks down the continuity of the region. Proper sampling of Wx events will bring these disjoint regions closer to the conceptual model.

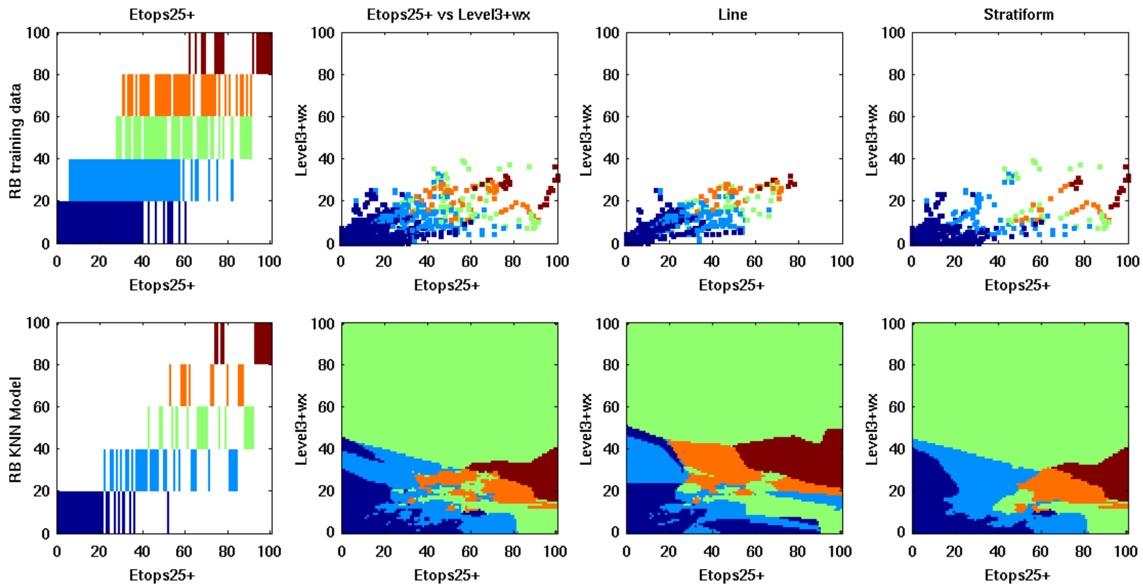

Figure A.4-4. (Top Row) ZOB48 training data distribution of discrete RB intervals as a function of etops25+, etops25+ *and* level3+wx, etops25+ *and* level3+wx *separated by* wx-type line, etops25+ *and* level3+wx *separated by* wx-type stratiform *(left to right, respectively). Colors differentiate between the five discrete RB intervals and are consistent throughout the figure. (Bottom Row) KNN transfer function of RB based on synthetic data covering full possible range of* etops25+, level3+wx, *and* wx-type*. For simplicity, poorly sampled* wx-types *small, large, and embedded are not shown. Complex decision regions in the last three images of the bottom row are colored by their respective RB interval.*

A.5 ZOB77

ZOB77 is the easternmost ATC sector of the Cleveland center cluster (figure A.5-1). ZOB77 has a total of nine high jet routes. Routes crossing northern and southern borders include J82, J29, J109, and J61. The remainders consist of east-west oriented routes. ZOB77 managers are responsible for a small segment of J220, located in the sector's northeast corner.

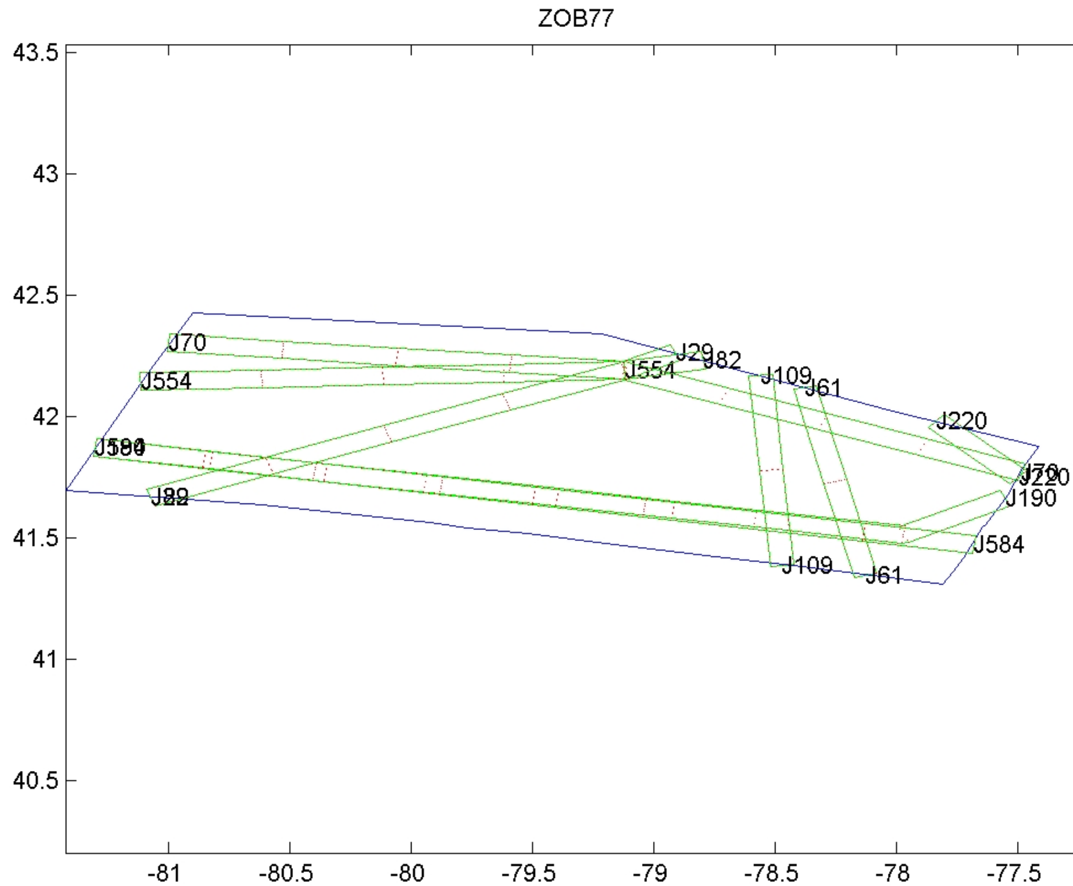

Figure A.5-1. ATC sector ZOB77 showing route orientation. Nine high jet routes are in total.

For ZOB77, the Gaussian, MLP, and KNN classifiers listed in table A.5-1 all show that Wx parameters associated with vertical extent and high-intensity Wx display the highest explanatory power over RB variability. These variables include *etops25+*, *l3andet25*, and *level3wx+*. For the KNN classifier (with the lowest test error of 7.57%), *l3andet25* of 87% displays the highest explanatory power over the RB variability. The KNN feature selection reveals that all Wx parameters yield an explanatory percentage of at least 75%.

TABLE A.5-1

A comparison table of Gaussian, MLP, and KNN classifiers for ATC sector ZOB77. First column indicates classification routine. Second column indicates the overall error rate produced at the final testing phase of each classifier. Final column lists the Wx parameters in order of explanatory power over the variability seen in RB. Explanatory power is expressed as a percentage in the parentheses to the right of each Wx parameter. The KNN classifier, as in all ATC sector results, produces the lowest error rate and is highlighted in red.

Classifier	Error	Explanatory Power of Individual Features
Gaussian	15.5%	l3andet25 (89), level3+wx (86), etops25+ (84), wx-type (82), embedded (82), large (82), small (82), orientation (81), level1+wx (81), stratiform (77), line (77)
MLP	9.25%	l3andet25 (89), etops25+ (86), level3+wx (86), line (83), wx-type (82), embedded (82), stratiform (82), large (82), small (82), orientation (82), level1+wx (82)
KNN	7.15%	l3andet25 (87), etops25+ (85), level3+wx (85), wx-type (82), embedded (82), small (82), orientation (82), line (82), large (79), stratiform (77), level1+wx (75)

Figure A.5-2 shows that for ZOB77, the data collection effort has not sampled RB to the full dynamic range of the *etops25+* Wx parameter. In fact, examination of the probability plot (far left) and histogram for ZOB77 in figure 2-8 reveals that sampling captured only a single Wx occurrence associated with the [80–100%] RB interval.

Although the range of data is limited, the quartiles of the box plot (center of figure A.5-2) show limited spread. This indicates the data distribution for ZOB77 is centered near median values. Maxes in the probability distribution for RB and medians of the box plots exhibit a linear trend.

RB for ZOB77 is also distributed over a shallow range of *level3+wx*. The spread of RB is limited to a maximum of 0% fractional Wx coverage (bottom row, left image of figure A.5-2). As with *etops25+*, the combination of box plot and probability distributions indicates that RB is densely centered near zero for low fractional coverage with no IQR being displayed for the 5% discrete bin of RB.

Median slopes in the right column of figure A.5-2 indicate a positive trend in the relationship of RB to increasing fractional Wx coverage. Variability of the medians around the least squares fit is indicated by the r^2 values. As with all ATC sector RB, the positive least squares slope of median values for *level3+wx* vs. RB is steeper than that of *etops25+* vs. RB although the slope for *etop25+* is comparatively steeper for ZOB77. A low variance is revealed by the r^2 values 0.966 and 0.962 (for *etops25+* and *level3+wx* to RB, respectively).

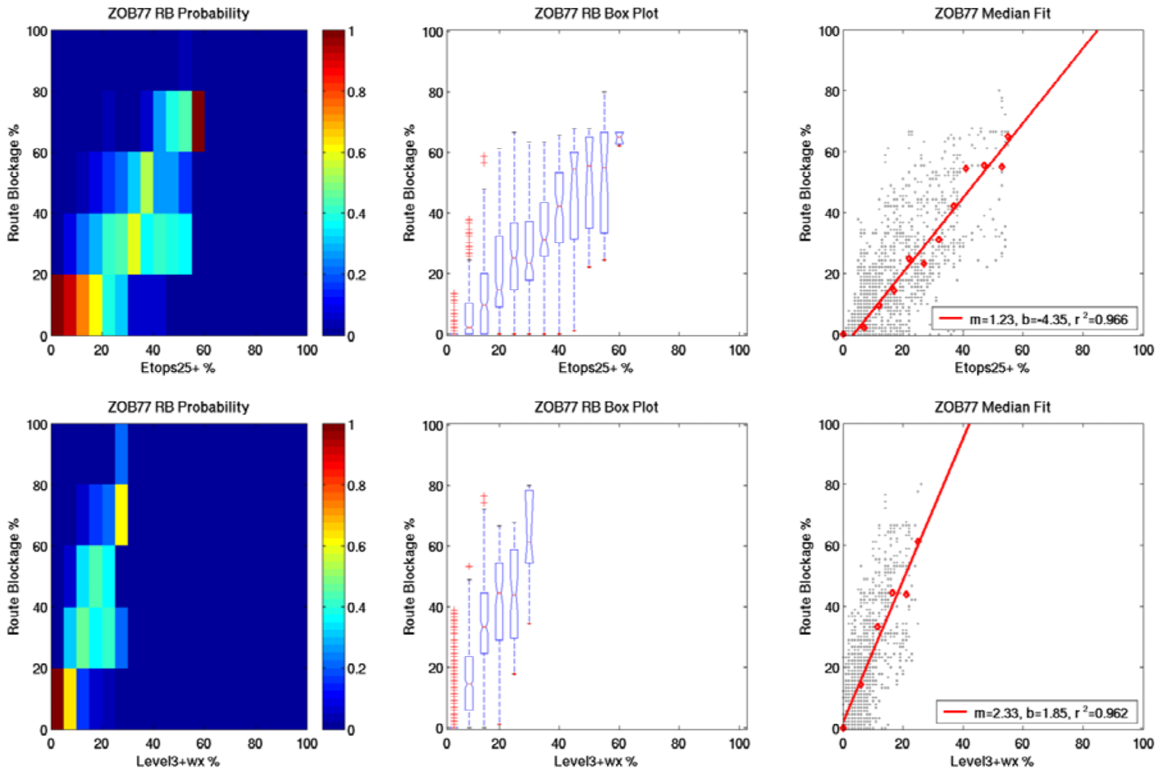

Figure A.5-2. ZOB77 distribution of RB as related to the Wx parameter etops25+ *(top row) and* level3+wx *(bottom row). (Left) Probability distribution of discrete RB (discrete RB as defined in section 2.4.5) along a 5% bin interval of* etops25+ *(top) and* level3+wx *(bottom). (Center) Median value, upper quartile and lower quartile range of RB expressed as a box plot for the 5% bin interval of* etops25+ *(top) and* level3+wx *(bottom). (Right) Least squares fit of median RB values as related to the* etops25+ *(top) and* level3+wx *(bottom) Wx parameters. Background scatter (gray) represents data points of the two distributions.*

In figure A.5-3, the KNN feature selection for ZOB77 shows that an ordered combination of all Wx parameters produces the lowest training error rate of 5.8%. Through selection, the number of parameters presented to the KNN classifier can be reduced to the first six for testing, but would make no statistically significant difference in the error rate.

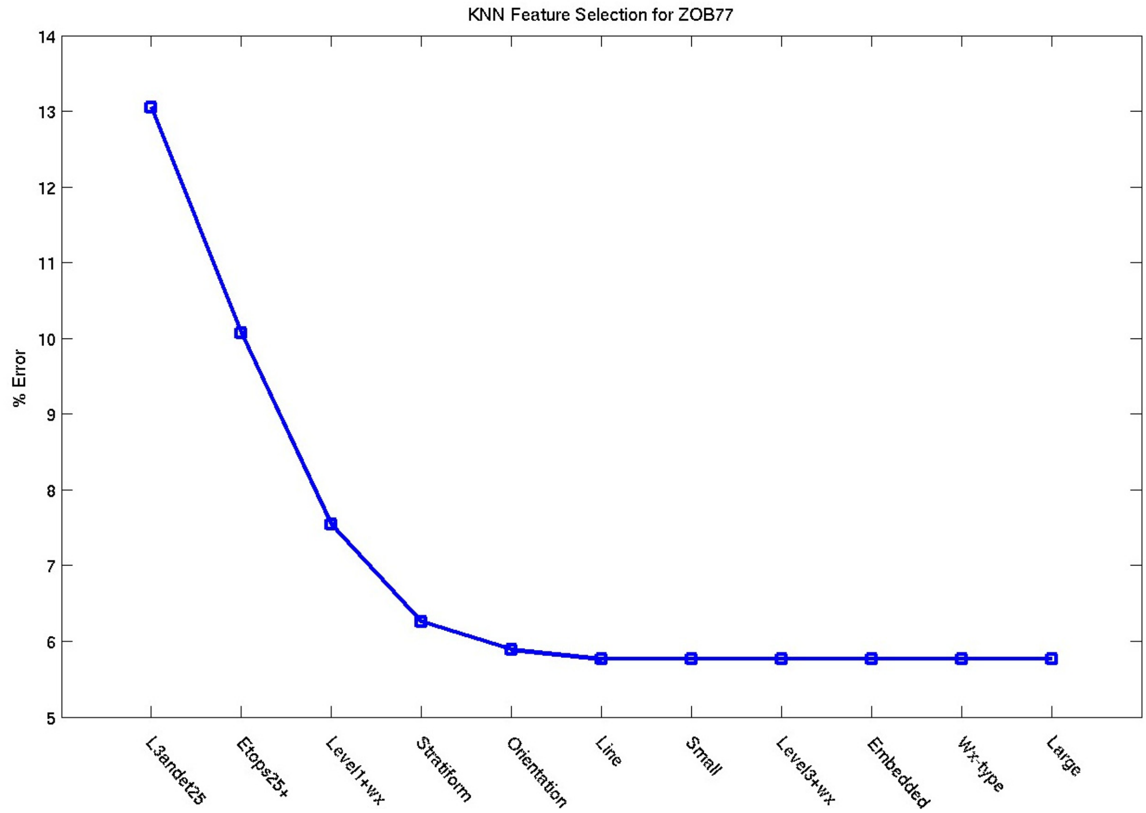

Figure A.5-3. Feature selection processing as performed by the KNN classifier. Utilizes a K=3, leave-one-out, cross-validation scheme. Error expressed as a percentage along the ordinate axis. Wx parameters are ordered in a combination that minimizes the training error rate. Wx parameters that fall to the right of the minimum increase the combined error. In this case, all Wx parameters are included in the best combination *set.*

Table A.5-2 compares the per RB interval errors of three single-Wx-parameter KNN models to a KNN model that utilizes all Wx parameters. Results show that the best combination of Wx parameters determined through feature selection significantly reduces the classification error. For the modeling RB of ZOB77, *level3+wx* and *l3andet25* show better error percentages at the RB interval of [0–20%) than does a model that utilizes the best combination of Wx parameters. Results for RB ≥ 60% have been undersampled and cannot be considered representative of the full population of possible high RB events.

TABLE A.5-2

ZOB77 comparison table of four different KNN models brought through both training and testing phases of classification. Each column to the right of the "number of samples" column represents the error percentages produced by modeling RB as a function of the single explanatory parameters *level3+wx*, *l3andet25*, and *etops25+* as compared to the *best combination* of Wx parameters as determined through the feature selection process (left to right, respectively). Values down each column are per the RB interval error expressed as a percentage. The best combination of Wx parameters consistently yields the lowest error rates.

RB interval	# of samples	*level3+wx*	*l3andet25*	*etops25+*	*Best Combination*
[0–20%)	2480	0.41	0.41	4.26	3.25
[20–40%)	352	90	81.43	57.14	27.14
[40–60%)	152	73.33	86.67	76.67	23.33
[60–80%)	42	100	87.5	87.5	12.5
[80–100%]	1	NaN	NaN	NaN	NaN
Total Errors	---	15.81	15.31	15.14	7.15

Table A.5-3 shows that the overall error rate produced by the KNN classifier for ZOB77 is low at 7.15%. Largest errors occur at the [20–40%) RB interval with 51 of 70 patterns being correctly classified. For the RB interval of [80–100%], only one pattern exists and is included in the training data set. Although 20 active Wx events were sampled for this Wx-RB study, no data for [80–100%] RB interval is available for testing. Both [0–20%) and [60–80%) RB intervals have low classification errors (3.25% and 12.5%, respectively).

TABLE A.5-3

KNN (K = 3) test results for ZOB77 consisting of the classification confusion matrix to the left and per class statistics to the right. Red highlighted numbers along the diagonal of the confusion matrix indicate correctly classified instances of RB. Numbers that fall to either side of the diagonal are incorrectly classified RB. Red highlighted column to the right indicates the per class error. The number at the bottom of this column is the overall error rate of the classification (7.15%).

```
TEST:ZOB77.test    Time: 0.18 secs  RMS Err: 0.169  Err: 7.15%
K-Nearest Neighbor (K=3) classifier: 20 cases - trained on 80% of data tested on 20% ECHO-BSD
--------------------------------------------------------------------------------------------
Desired|   Computed Class
Class  |   0   1   2   3   4  Total  Class  Patterns  #Errors  %Errors  StdDev   RMSE  Label
--------------------------------------------------------------------------------------------
  0_20 | 477  16              493      0      493       16        3.25  ( 0.8)  0.114   0_20
 20_40 |  17  51   2           70      1       70       19       27.14  ( 5.3)  0.330  20_40
 40_60 |       4  23   3       30      2       30        7       23.33  ( 7.7)  0.306  40_60
 60_80 |           1   7        8      3        8        1       12.50  (11.7)  0.224  60_80
80_100 |                  **    0      4        0        *           *       *      *  80_100
--------------------------------------------------------------------------------------------
 Total | 494  71  26  10   0  601  Overall  601       43         7.15%  ( 1.1)  0.169
--------------------------------------------------------------------------------------------
```

Data distributions seen in the top row of figure A.5-4 indicate that collection efforts for ZOB77 did not capture events associated with large fractional coverage of *etops25+* and *level3+wx*. As was revealed in the discussion of figure A.5-2, only a single occurrence of RB [80–100%] shows up in the *etops25+* vs. RB distribution (top row, first column of figure A.5-4). This lack of data at the highest RB interval limits the KNN routine to the construction of four decision regions—[0–20%), [20–40%), [40–60%), [60–80%)—when applied to the full range of possible coverage by Wx parameters *etops25+, level3+wx,* and all possible *wx-types*.

RB as a function of the single Wx parameter *etops25+* shows that low fractional coverage is dominated by the [0–20%) RB classification. Middle-value RB intervals were infrequently predicted with a minimum of classifications being classified at the [40–60%) interval. Beyond 55% of *etops25+*, the KNN routine classifies RB at the [60–80%) interval continuously.

Addition of *level3+wx* as the second Wx parameter reveals a complex decision region within the *etops25+* vs. *level3+wx* plane that is limited to four RB intervals. Noise within these regions is the result of isolated clusters associated with similar RB mixing within the input space. This noise is most evident in the decision region constructed for the [0–20%) RB interval.

Points of scatter plot indicate how far the training data extends into the *etops25+* vs. *level3+wx* input space (0–67% and 0–28%, respectively). Portions of the KNN decision regions that fall beyond the outlying points in the scatter are influenced mainly by those points and their associated RB values. While this complex decision region works to reduce the test errors of the classifier for the test cases used in this study, we feel that the resulting decision regions are probably not representative of the ensemble classifier decision surfaces.

Addition of *wx-type* associated with line events increases complexity while shifting decision regions toward higher RB interval. The *wx-type* associated with stratiform events generalizes decision regions and shifts them toward lower RB intervals.

Comparing figure A.5-4 to figure A.0-1 indicates the ZOB77 KNN RB transfer function applied to the synthetic data set does not fit the expected functional dependence defined by the conceptual model. Decision regions of the KNN transfer function are disjoint and RB does not monotonically increase with increasing *etops25+* and/or *level3+wx*. Concavity is apparent in the [0–20%) and [20–40%) RB intervals, but mixing of the input space makes the surfaces (as well as the surfaces of the other RB intervals, discontinuous. No decision region is resolved for the [80–100%] RB interval and this patent undersampling of high RB cases in the experimental data set keeps the model from being a fully realistic, statistically meaningful representation of RB based on the chosen Wx parameters.

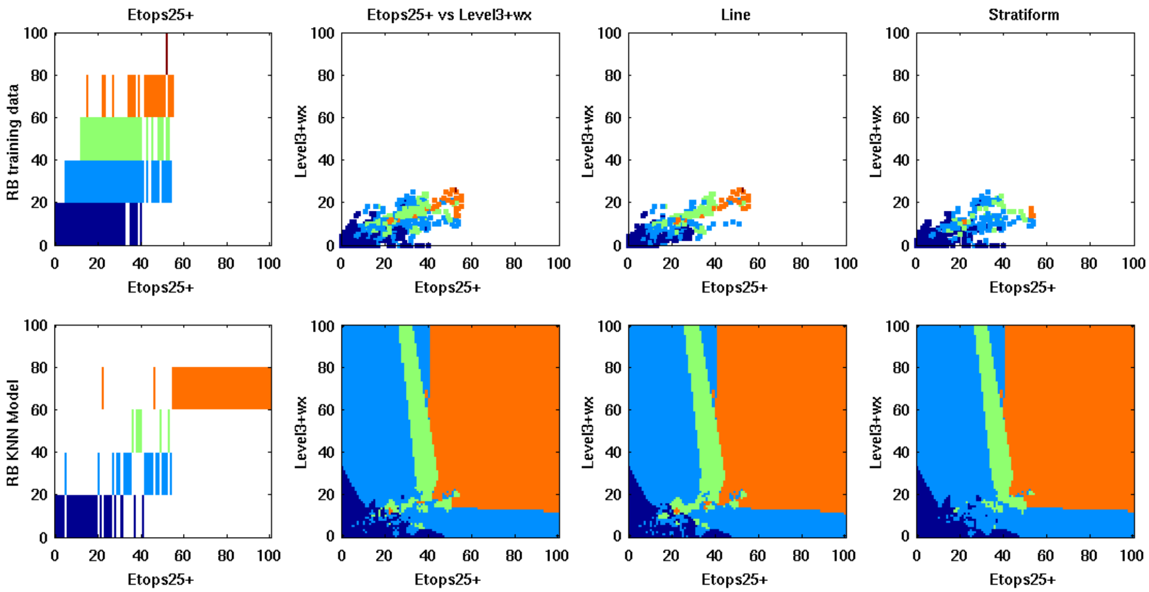

Figure A.5-4. (Top Row) ZOB77 training data distribution of discrete RB intervals as a function of etops25+, etops25+ *and* level3+wx, etops25+ *and* level3+wx *separated by* wx-type line, etops25+ *and* level3+wx *separated by* wx-type stratiform *(left to right, respectively). Colors differentiate between the five discrete RB intervals and are consistent throughout the figure. (Bottom Row) KNN transfer function of RB based on synthetic data covering full possible range of* etops25+, level3+wx, *and* wx-type. *For simplicity, poorly sampled* wx-types *small, large, and embedded are not shown. Complex decision regions in the last three images of the bottom row are colored by their respective RB interval.*

A.6 ZID66

ZID66 is the northernmost ATC sector of the Indianapolis cluster (figure A.6-1). ZID66 shares its southern and southeastern borders with ZID82 and ZID83, respectively. This sector consists of six high jet routes with the majority of routes intersecting both north and south facing borders. Both J134 and J29 are generally oriented east-west, converging at the west end of ZID66.

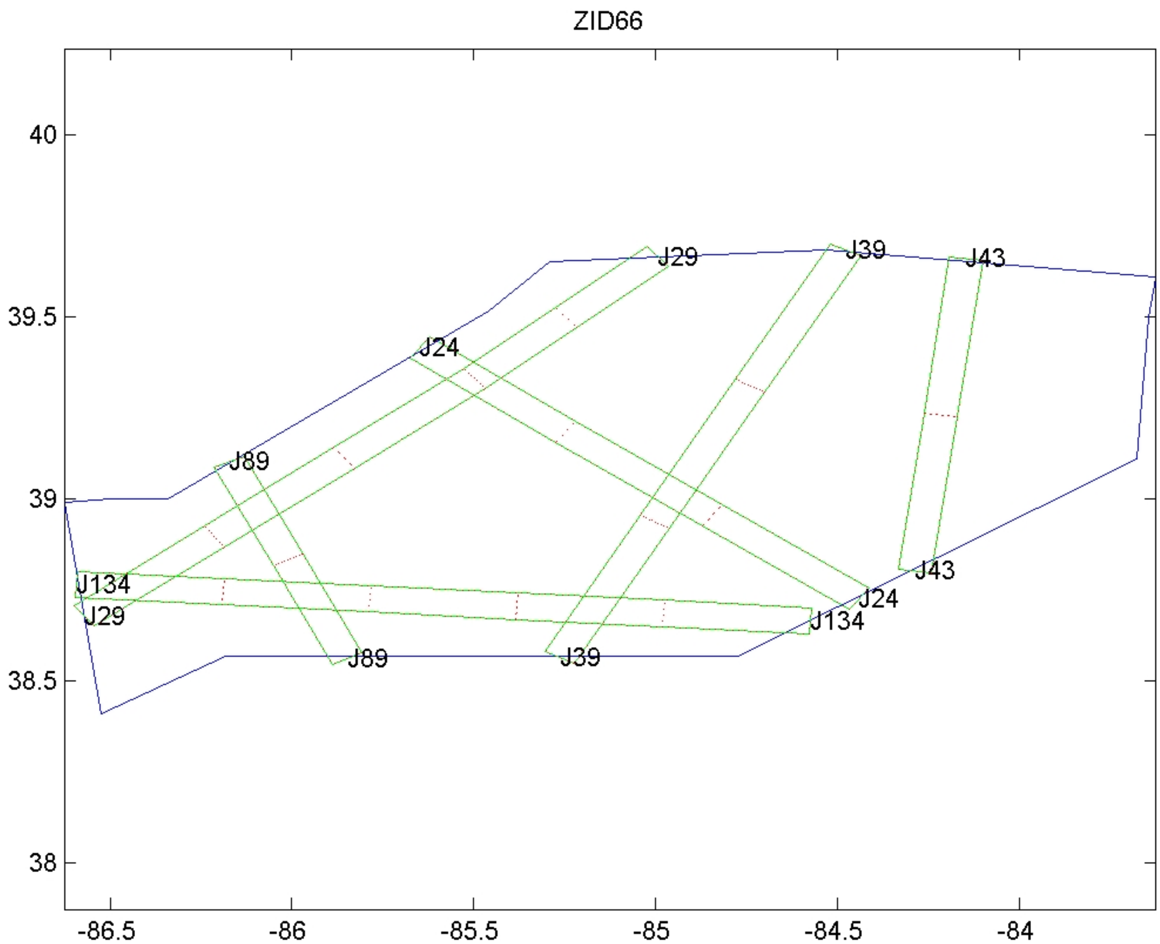

Figure A.6-1. ATC sector ZID66 showing route orientation. Six high jet routes are in total.

The feature selection results seen in table A.6-1 show that echo tops-related parameters provided the greatest explanatory power for RB. The best performing classification routine, KNN, calculates an explanatory percentage of its highest parameter *etops25+* to be 76%. Explanatory power of the Wx parameters for ZID66 are relatively flat, all with KNN calculated percentages between that of the *etops25+* percentage and 62%.

TABLE A.6-1

A comparison of Gaussian, MLP, and KNN classifiers for ATC sector ZID66. First column indicates classification routine. Second column indicates the overall error rate produced at the final testing phase of each classifier. Final column lists the Wx parameters in order of explanatory power over the variability seen in RB. Explanatory power is expressed as a percentage in the parentheses to the right of each Wx parameter. The KNN classifier, as in all ATC sector results, produces the lowest error rate and is highlighted in red.

Classifier	Error	Explanatory Power of Individual Features
Gaussian	21.0%	etops25+ (76), wx-type (75), embedded (75), large (75), small (75), l3andet25 (69), level1+wx (68), stratiform (67), orientation (65), line (63), level3+wx (62)
MLP	16.3%	l3andet25 (80), etops25+ (80), level3+wx (79), level1+wx (77), line (76), wx-type (75), embedded (75), stratiform (75), large (75), small (75), orientation (75)
KNN	10.1%	etops25+ (76), wx-type (75), embedded (75), large (75), small (75), l3andet25 (69), level1+wx (68), stratiform (67), orientation (65), line (63), level3+wx (62)

Unlike the distribution seen in the previous section, RB spans the full dynamic range of *etops25+* for ZID66. This is evident in the probability, box plot, and scatter plot in the top row images that make up figure A.6-2. As seen in sections of previously discussed ATC sectors, for low *etops25+* coverage (0–15%), the combination of box plot and probability distributions indicates that RB is densely centered at zero (top row, left and center images). Past this point, RB responds to increasing *etop25+* values in an increasing near-linear trend. The quartiles of the box plots in the center image become less regular beyond rough 60% of *etops25+*, indicating data distribution at the largest *etops25+* is more scattered and less densely positioned near median values.

In comparison to *etops25+*, RB for ZID66 is distributed over a more shallow range of *level3+wx*. The spread of RB is limited to a maximum of 50% fractional Wx coverage (bottom row, left image of figure A.6-2). As with *etops25+*, the combination of box plot and probability distributions indicates that RB is densely centered near zero for low fractional coverage with no IQR being displayed for the 5% discrete bin of RB.

Compactness is also evident in the background scatter of data in the far right images of figure A.6-2. Median slopes in the right column of figure A.6-2 indicate a positive trend in the relationship of RB to increasing fractional Wx coverage. Variability of the medians around the least squares fit is indicated by the r^2 values. As with all ATC sector RB, the positive least squares slope of median values for *level3+wx* vs. RB is steeper than that of *etops25+* vs. RB. Low variability is seen in the RB-Wx coverage relationship for ZID66 and is reflected in the r^2 values of 0.953 and 0.955 (for *etops25+* and *level3+wx*, respectively).

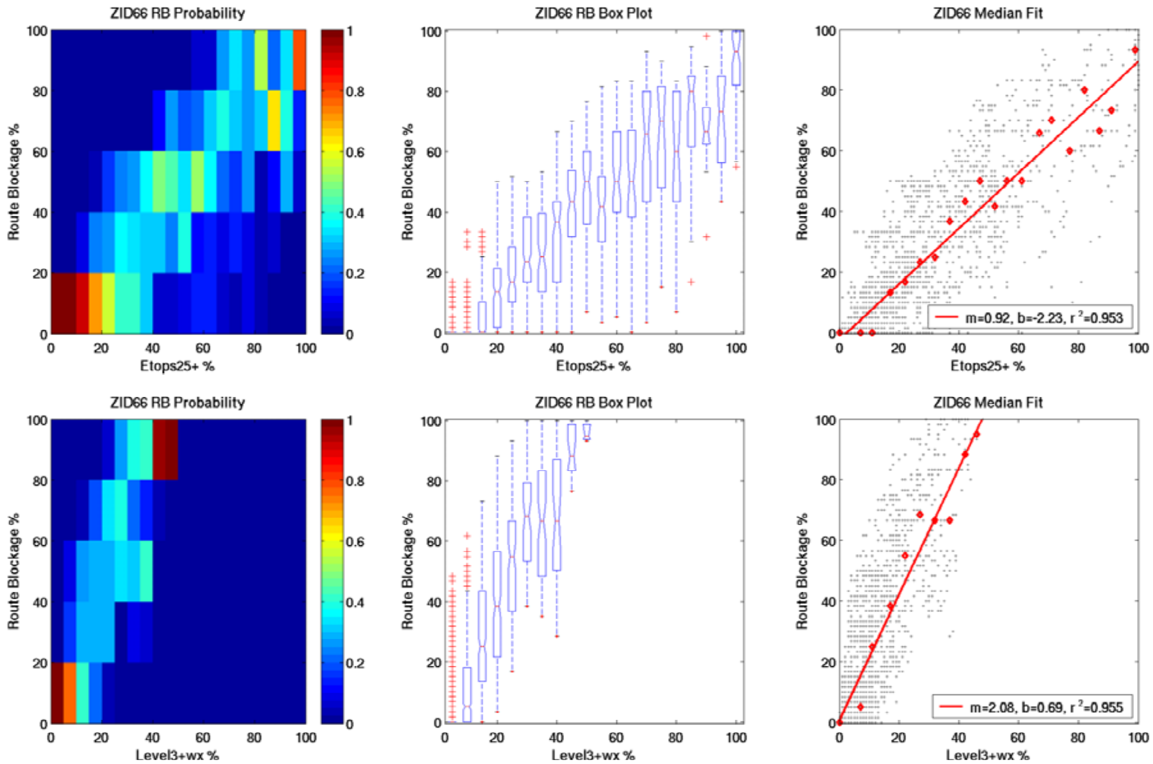

Figure A.6-2. ZID66 distribution of RB as related to the Wx parameter etops25+ *(top row) and* level3+wx *(bottom row). (Left) Probability distribution of discrete RB (discrete RB as defined in section 2.4.5) along a 5% bin interval of* etops25+ *(top) and* level3+wx *(bottom). (Center) Median value, upper quartile and lower quartile range of RB expressed as a box plot for the 5% bin interval of* etops25+ *(top) and* level3+wx *(bottom). (Right) Least squares fit of median RB values as related to the* etops25+ *(top) and* level3+wx *(bottom) Wx parameters. Background scatter (gray) represents data points of the two distributions.*

For ZID66, figure A.6-3 shows that the ordered use of the first 10 Wx parameters produces a 9.3% error while the inclusion of *orientation* increases that error by 0.5%. The increase has been calculated to be statistically insignificant. Therefore, all Wx parameters have been presented to the KNN classification routine for testing.

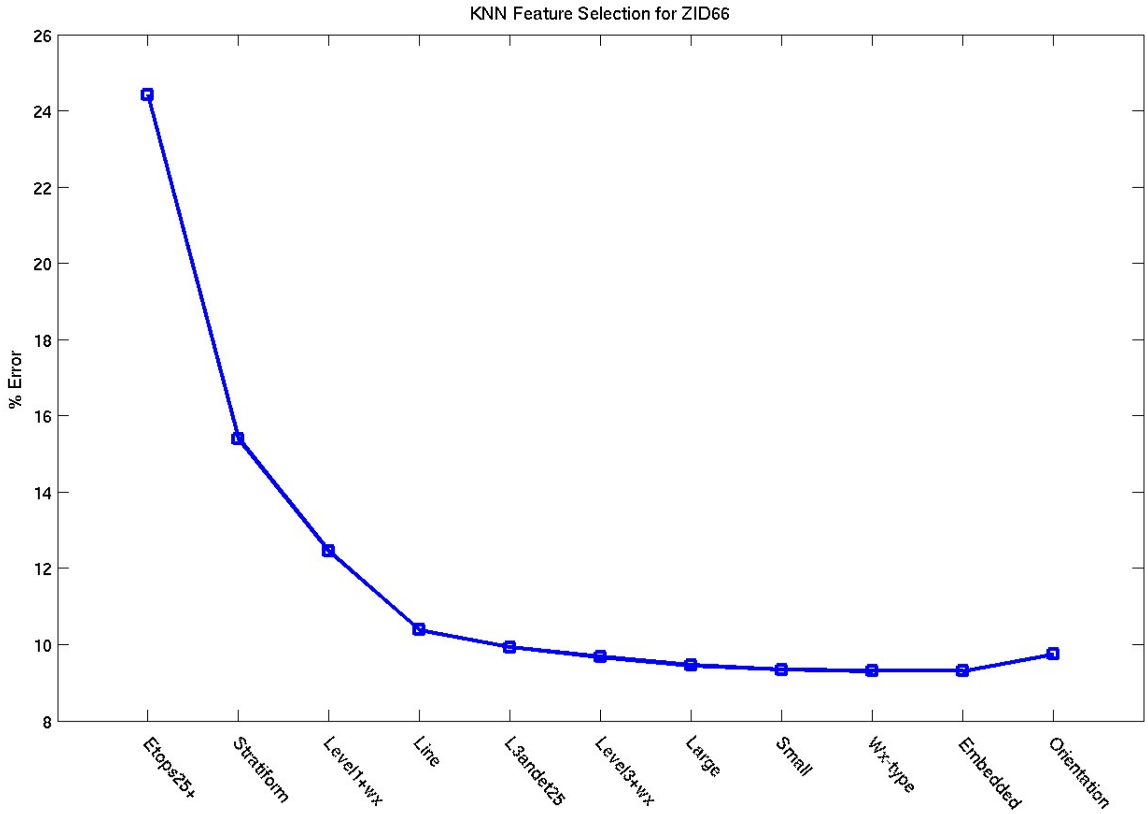

Figure A.6-3. Feature selection processing as performed by the KNN classifier. Utilizes a K=3, leave-one-out, cross-validation scheme. Error expressed as a percentage along the ordinate axis. Wx parameters are ordered in a combination that minimizes the training error rate. Wx parameters that fall to the right of the minimum increase the combined error. In this case, all Wx parameters are included in the best combination *set.*

The exercise summarized in table A.6-2 compares the per RB interval errors of three single-Wx-parameter KNN models to a KNN model that utilizes all Wx parameters. Again, results show that the best combination of Wx parameters determined through feature selection significantly reduces the classification error. For the forecasting of RB for ZID66 all RB intervals show reduced classification errors when the best combination of Wx parameters is used.

TABLE A.6-2

ZID66 comparison table of four different KNN models brought through both training and testing phases of classification. Each column to the right of the "number of samples" column represents the error percentages produced by modeling RB as a function of the single explanatory parameters *level3+wx*, *l3andet25*, and *etops25+* as compared to the best combination of Wx parameters as determined through the feature selection process (left to right, respectively). Values down each column are per the RB interval error expressed as a percentage. The best combination of Wx parameters consistently yields the lowest error rates.

RB interval	# of samples	*level3+wx*	*l3andet25*	*etops25+*	*Best Combination*
[0–20%)	2530	20.4	12.67	20.59	1.78
[20–40%)	339	82.09	77.61	82.09	38.81
[40–60%)	252	53.45	48.28	53.45	34.48
[60–80%)	133	69.23	88.46	73.08	38.46
[80–100%]	89	29.41	23.53	52.94	17.65
Total Errors	---	31.5	25.41	32.39	10.1

Table A.6-3 shows the results for the KNN classification of RB for ATC sector ZID66. For the [0–20%) RB interval a near-perfect classification has been made by the KNN routine. Middle-range RB intervals have similar errors with the maximum of 38.81% occurring at [20–40%). [80–100%] RB classifications have testing errors below 20%. An overall error rate of 10.1% has been achieved for the classification of RB via the KNN routine for ATC sector ZID66.

TABLE A.6-3

KNN (K = 3) test results for ZID66 consisting of the classification confusion matrix to the left and per class statistics to the right. Red highlighted numbers along the diagonal of the confusion matrix indicate correctly classified instances of RB. Numbers that fall to either side of the diagonal are incorrectly classified RB. Red highlighted column to the right indicates the per class error. The number at the bottom of this column is the overall error rate of the classification (10.1%).

```
TEST:ZID66.test    Time: 0.20 secs  RMS Err: 0.201  Err: 10.10%
K-Nearest Neighbor (K=3) classifier: 20 cases - trained on 80% of data tested on 20% ECHO-BSD
--------------------------------------------------------------------------------------------
Desired|   Computed Class
Class  |   0   1   2   3   4  Total  Class  Patterns  #Errors  %Errors  StdDev   RMSE  Label
--------------------------------------------------------------------------------------------
  0_20 | 496   9               505     0      505         9     1.78   ( 0.6)   0.084   0_20
 20_40 |  14  41  12            67     1       67        26    38.81   ( 6.0)   0.394  20_40
 40_60 |   2  12  38   6        58     2       58        20    34.48   ( 6.2)   0.371  40_60
 60_80 |       1   4  16   5    26     3       26        10    38.46   ( 9.5)   0.392  60_80
80_100 |           1   2  14    17     4       17         3    17.65   ( 9.2)   0.266 80_100
--------------------------------------------------------------------------------------------
 Total | 512  63  55  24  19   673  Overall  673        68    10.10%  ( 1.2)   0.201
--------------------------------------------------------------------------------------------
```

Data distributions plotted across the top row of figure A.6-4 indicate a good sampling of the input space that is comparable to the experimental data set for ATC sector ZOB46. Better sampling accounts for the consistency seen in middle RB interval error statistics as well as the relatively low errors made at the tails of the RB interval (red column of table A.6-3).

The single-Wx-parameter transfer function (bottom row, first column) continuously classifies low fractional converge of synthetic *etops25+*, from 0–30%, at the [0–20%) RB interval. As fractional coverage increases from 30%, the KNN routine based on *etops25+* alone classifies RB in the erratic upward trend, as seen in the previously discussed ATC sector results.

A highly complex decision region is revealed through the addition of *level3+wx* as a second synthetic Wx parameter (bottom row, second column). All decision regions within the *etops25+* vs. *level3+wx* plane are disjoint with largest decision regions being constructed for RB intervals of [0–20%) and [80–100%].

The scatter plot in the figure shows that there is relatively little data in the high coverage *etops25+* vs. *level3+wx* input space (0–100% and 0–88%, respectively). Portions of the KNN decision regions that fall beyond the outlying points in the scatter are influenced mainly by those points and their associated RB values. This accounts for the large, broadly colored regions lying above the *level3+wx* data extent. While this complex decision region works to reduce the test errors of the classifier, the regions may not be realistic as the number of input patterns increases.

The addition of *wx-type* line generally shifts decision regions toward higher RB intervals where *wx-type* associated with stratiform shifts decision regions toward lower RB intervals (third and fourth column of figure A.6-4). Side-by-side comparisons indicate events associated with *wx-type* stratiform contribute to the generalization of classification decision regions; *wx-types* associated with line contribute to noise within decision regions.

Figure A.6-4 shows that the KNN RB model for ZID66 does not fit the expected functional dependence defined by the conceptual model in figure A.0-1. Decision regions of the KNN transfer function are disjoint and RB does not monotonically increase with increasing *etops25+* and/or *level3+wx*. The expected concave nature of the two-parameter model is mildly implied by the [0–20%) decision region, but anomalies in the surface that result from the mixing of the input space break down the continuity of the region. Proper sampling of Wx events will reduce the anomalies seen in the RB surfaces, bringing the KNN RB model closer to the conceptual model.

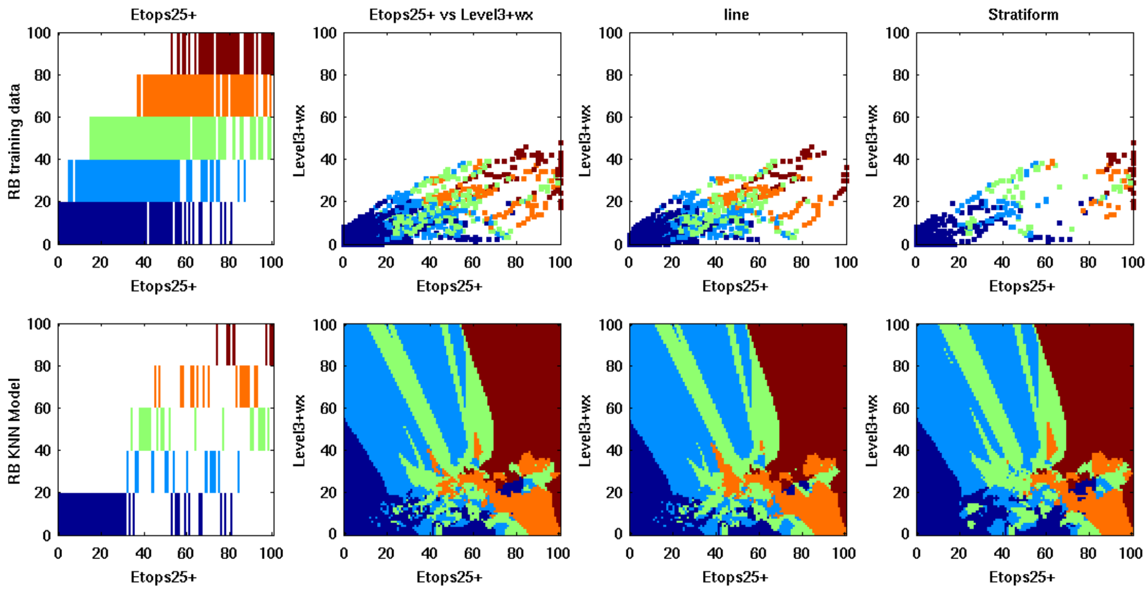

Figure A.6-4. (Top Row) ZID66 training data distribution of discrete RB intervals as a function of etops25+, etops25+ *and* level3+wx, etops25+ *and* level3+wx *separated by* wx-type line, etops25+ *and* level3+wx *separated by* wx-type stratiform *(left to right, respectively). Colors differentiate between the five discrete RB intervals and are consistent throughout the figure. (Bottom Row) KNN transfer function of RB based on synthetic data covering full possible range of* etops25+, level3+wx, *and* wx-type. *For simplicity, poorly sampled* wx-types *small, large, and embedded are not shown. Complex decision regions in the last three images of the bottom row are colored by their respective RB interval.*

A.7 ZID82

Figure A.7-1 shows the route configuration for ZID82. The five high jet routes of ZID82 converge at the Louisville VORTAC (IIU). J89 (north-south), J39 (northeast-southwest), and J8 (east-west) are routes that extend across the sector. Both J99 and J526 merge with these jet routes at IIU. ZID82 shares its eastern border with ZID83 and its northern border with ZID66.

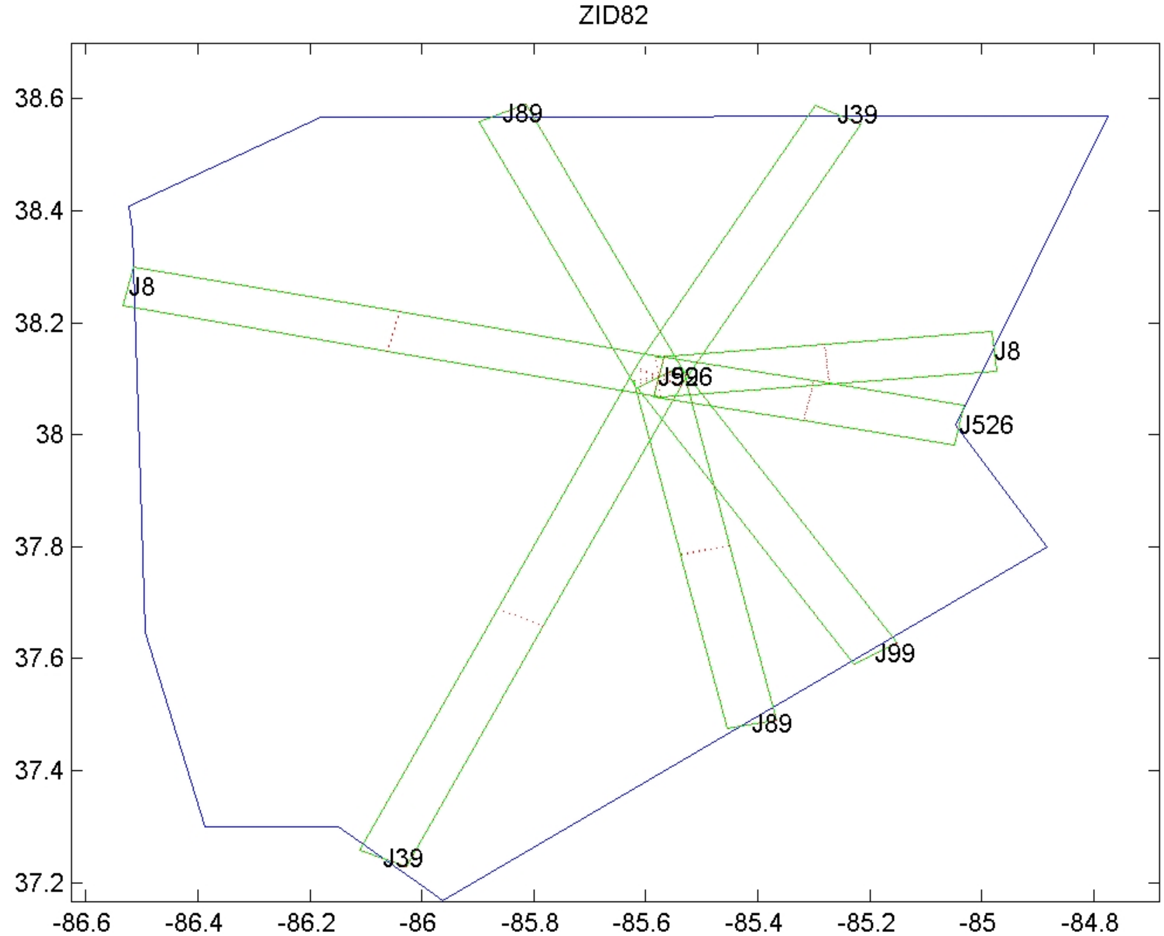

Figure A.7-1. ATC sector ZID82 showing route orientation. Five high jet routes are in total.

As with the other ATC sectors examined previously, feature selection of the routines listed in table A.7-1 show that Wx parameters associated with vertical extent exhibit the highest explanatory power over RB variability. The best performing KNN routine has calculated an explanatory percentage of its lead Wx parameter *l3andet25* to be 77%. Explanatory power is relatively flat for the KNN feature selection with the exception of *orientation*, which yields the lowest percentage of 54%.

TABLE A.7-1

A comparison table of Gaussian, MLP, and KNN classifiers for ATC sector ZID82. First column indicates classification routine. Second column indicates the overall error rate produced at the final testing phase of each classifier. Final column lists the Wx parameters in order of explanatory power over the variability seen in RB. Explanatory power is expressed as a percentage in the parentheses to the right of each Wx parameter. The KNN classifier, as in all ATC sector results, produces the lowest error rate and is highlighted in red.

Classifier	Error	Explanatory Power of Individual Features
Gaussian	25.3%	level1+wx (79), wx-type (77), embedded (77), large (77), small (77), etops25+ (77), orientation (76), stratiform (74), level3+wx (74), line (72), l3andet25 (72)
MLP	17.0%	l3andet25 (80), etops25+ (80), level3+wx (80), line (78), level1+wx (78), wx-type (77), embedded (77), stratiform (77), large (77), small (77), orientation (77)
KNN	13.2%	l3andet25 (77), large (77), small (77), wx-type (77), embedded (77), etops25+ (76), level1+wx (70), stratiform (70), level3+wx (69), line (66), orientation (54)

While figure A.7-2 shows that RB is spread over the full dynamic range of the *etops25+* Wx parameter, RB does not follow the linear upward trend with increasing *etops25+* that has been seen in previously discussed sections. Rather, probabilities indicate that for the range of *etops25+*, the data distribution for ZID82 is skewed more toward the tail RB intervals (left, figure 34). Only in a few instances are mid-range RB probabilities higher than they are for [0–20%) or [80–100%].

This is also evident in the box plots of the center image. Here, box plots indicate that given a 5% bin of *etops25+*, the continuous RB is widely spread over a large range of values. RB outliers of 1.5 times the IQR can be seen in data bins from 0% to 30%, then again at 100%. Box plots for *etops25+* bins between 50% and 80% have whiskers that almost cover the entire range of RB values and have IQRs that span three to four discrete RB intervals.

RB for ZID82 is not distributed over the full dynamic range of *level3+wx*. The spread of RB is limited to a maximum of 55% fractional Wx coverage (bottom row, left image of figure A.7-2). As with *etops25+*, the combination of box plot and probability distributions indicates that RB is densely centered near zero for low fractional coverage with no IQR being displayed for the 5% discrete bin of RB.

Median slopes in the right column of figure A.7-2 indicate a positive trend in the relationship of RB to increasing fractional Wx coverage. Variability of the medians around the least squares fit is indicated by the r^2 values. As with all ATC sector RB, the positive least squares slope of median values for *level3+wx* vs. RB is steeper than that of *etops25+* vs. RB. Low variability is seen in the RB-Wx coverage relationship for ZID82 and is reflected in the r^2 values of 0.903 and 0.865 (for *etops25+* and *level3+wx*, respectively).

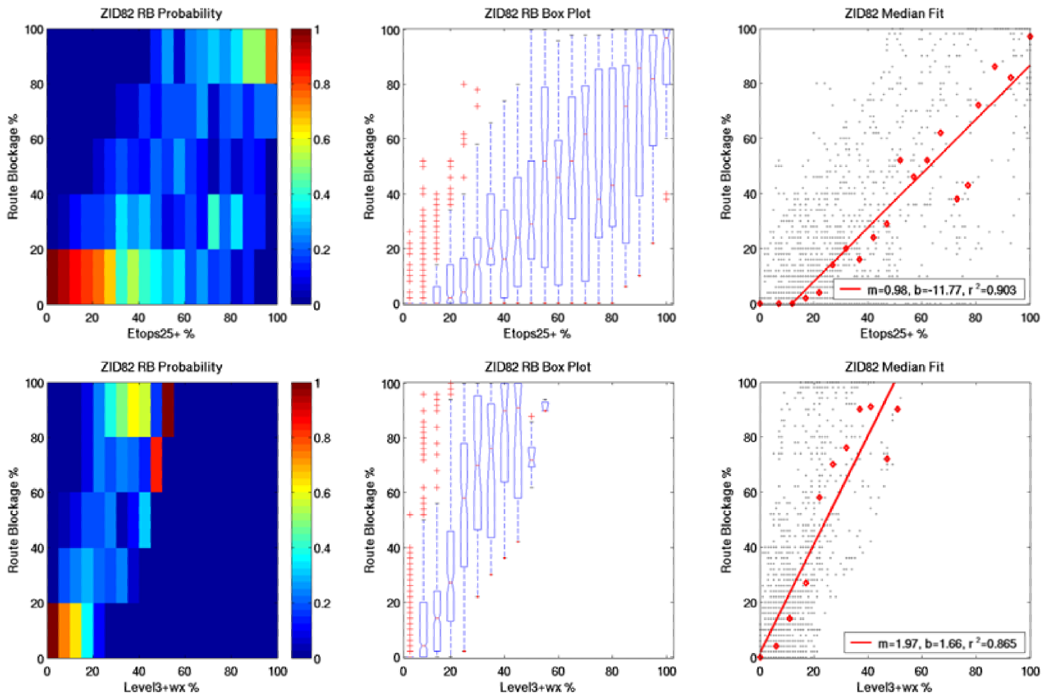

Figure A.7-2. ZID82 distribution of RB as related to the Wx parameter etops25+ *(top row) and* level3+wx *(bottom row). (Left) Probability distribution of discrete RB (discrete RB as defined in section 2.4.5) along a 5% bin interval of* etops25+ *(top) and* level3+wx *(bottom). (Center) Median value, upper quartile and lower quartile range of RB expressed as a box plot for the 5% bin interval of* etops25+ *(top) and* level3+wx *(bottom). (Right) Least squares fit of median RB values as related to the* etops25+ *(top) and* level3+wx *(bottom) Wx parameters. Background scatter (gray) represents data points of the two distributions.*

For ZID82, figure A.7-3 shows that a combination of 10 Wx parameters produces a minimized error during training of 12%. The decrease in error made by excluding *orientation* (a 0.3% difference) is statistically insignificant. All Wx parameters have been presented to the KNN routine for classification of RB.

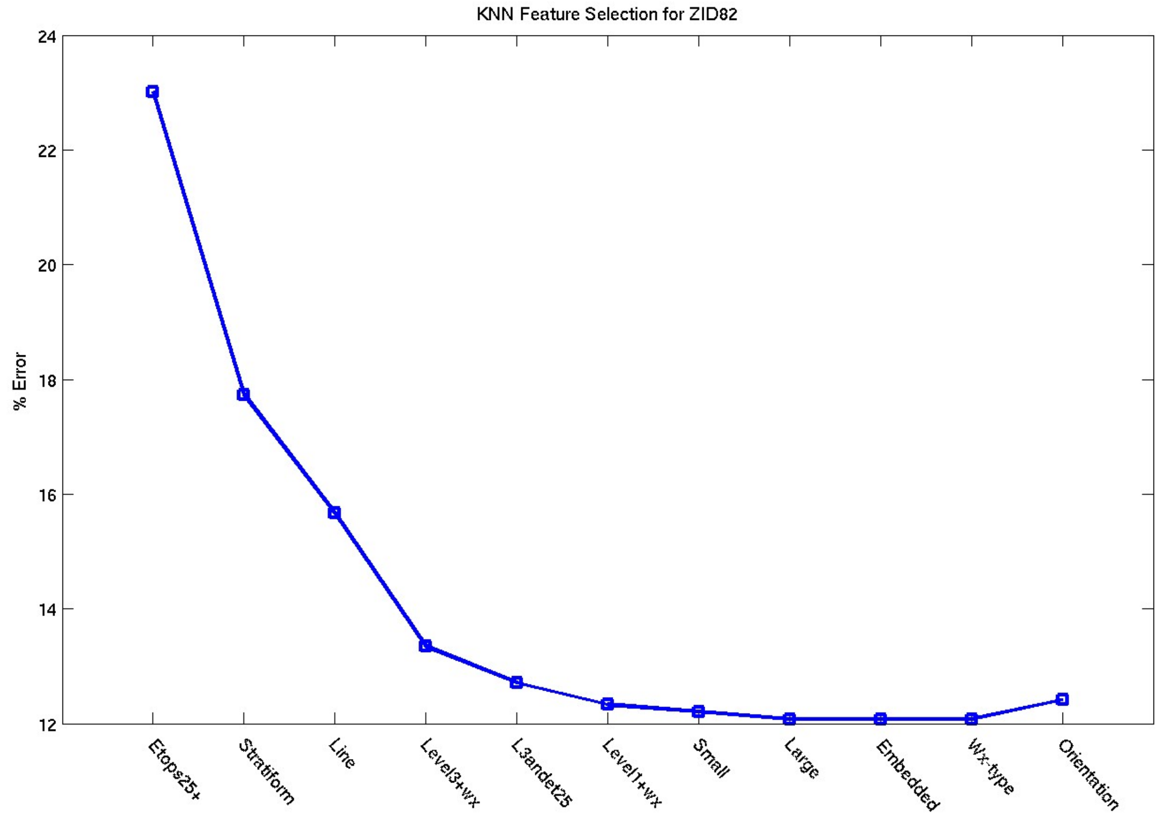

Figure A.7-3. Feature selection processing as performed by the KNN classifier. Utilizes a K=3, leave-one-out, cross-validation scheme. Error expressed as a percentage along the ordinate axis. Wx parameters are ordered in a combination that minimizes the training error rate. Wx parameters that fall to the right of the minimum increase the combined error. In this case, all Wx parameters are included in the best combination *set.*

Table A.7-2 compares the per RB interval errors of three single-Wx-parameter KNN models to a KNN model that utilizes all Wx parameters (label *best combination*). Results show that the *best combination* of Wx parameters significantly reduces the classification error. For the modeling RB of ZID82, all RB intervals show improved classification errors when the *best combination* of Wx parameters is used.

TABLE A.7-2

ZID82 comparison table of four different KNN models brought through both training and testing phases of classification. Each column to the right of the “number of samples” column represents the error percentages produced by modeling RB as a function of the single explanatory parameters *level3+wx*, *l3andet25*, and *etops25+* as compared to the best combination of Wx parameters as determined through the feature selection process (left to right, respectively). Values down each column are per the RB interval error expressed as a percentage. The best combination of Wx parameters consistently yields the lowest error rates.

RB interval	# of samples	*level3+wx*	*l3andet25*	*etops25+*	*Best Combination*
[0–20%)	2277	18.9	11.65	9.67	3.3
[20–40%)	312	80.65	90.32	77.42	50
[40–60%)	140	85.71	85.71	85.71	71.43
[60–80%)	98	78.95	84.21	84.21	42.11
[80–100%]	133	46.15	46.15	88.46	15.38
Total Errors	---	31.69	27.29	26.27	13.22

Table A.7-3 shows the results for the KNN classification of RB for ATC sector ZID82. Here, the [40–60%) RB interval yields the highest error rate seen in the Wx-RB modeling study. Twenty of 28 patterns within this interval have been incorrectly classified. The bounding RB intervals of [20–40%) and [60–80%) have poor error rates of 50% and 42.11%, respectively. As has been typical, the heavily sampled [0–20%) RB interval yields a low classification error. For the RB interval of [80–100%] the routine yields an error rate that falls below 20%. Overall, the error produced by KNN classification of RB for ZID82 is low at 13.22%.

Table A.7-3

KNN (K = 3) test results for ZID82 consisting of the classification confusion matrix to the left and per class statistics to the right. Red highlighted numbers along the diagonal of the confusion matrix indicate correctly classified instances of RB. Numbers that fall to either side of the diagonal are incorrectly classified RB. Red highlighted column to the right indicates the per class error. The number at the bottom of this column is the overall error rate of the classification (13.22%).

```
TEST:ZID82.test    Time: 0.14 secs  RMS Err: 0.23  Err: 13.22%
K-Nearest Neighbor (K=3) classifier: 20 cases - trained on 80% of data tested on 20% ECHO-BSD
---------------------------------------------------------------------------------------------
Desired|   Computed Class
Class  |   0   1   2   3   4  Total  Class  Patterns  #Errors  %Errors  StdDev   RMSE  Label
---------------------------------------------------------------------------------------------
  0_20 | 440  12   2   1       455     0      455        15       3.30  ( 0.8)  0.115   0_20
 20_40 |  25  31   4   2        62     1       62        31      50.00  ( 6.4)  0.447  20_40
 40_60 |   5  10   8   4   1    28     2       28        20      71.43  ( 8.5)  0.535  40_60
 60_80 |       1   1  11   6    19     3       19         8      42.11  (11.3)  0.410  60_80
80_100 |       1       3  22    26     4       26         4      15.38  ( 7.1)  0.248 80_100
---------------------------------------------------------------------------------------------
 Total | 470  55  15  21  29   590 Overall  590        78      13.22%  ( 1.4)  0.230
---------------------------------------------------------------------------------------------
```

For ZID82, the top row of figure A.7-4 shows that the RB intervals are heavily scattered throughout the input space. The plot of *etops25+* vs. RB of the training data (top row, first image) shows that each RB interval is spread over much of the *etops25+* range. Scatter plots show clusters of coverage events with similar RB mixing heavily in amongst those of different intervals.

The transfer function of RB based on the single Wx parameter *etops25+* (bottom row, first image) shows how the mixed input space and data skewness toward the tails of the RB interval affect the output of the KNN routine. Here, there is a less discernible upward trend in RB with increasing *etops25+*. The majority of classifications have been made at the [0–20%) RB interval, with an erratic mix at mid-range intervals that shift toward classification at the [80–100%] RB interval. This pattern resembles the probability distribution of the RB interval, given *etops25+* seen in figure A.7-2 (far-left image).

The addition of *level3+wx* as the second Wx parameter reveals a highly complex decision region within the *etops25+* vs. *level3+wx* plane (bottom row, second image). Disjoint regions have been constructed for all RB intervals and are the result of a heavily scattered training data input space.

With the addition of the third Wx parameter *wx-type*, complexity of the decision regions is reduced only slightly when fractional coverage is associated with *wx-type* stratiform events. This noise reduction is, for the most part, confined to the [0–20%) RB interval space. Generalization of the [0–20%) decision region can be seen in the last image of the bottom row when compared to decision regions constructed for fractional coverage associated with *wx-type* of line (bottom row, third image). The *wx-type* associated with line contributes to complexity within decision regions.

Figure A.7-4 shows that the KNN RB model for ZID82 does not fit the expected functional dependence defined by the conceptual model in figure A.0-1. Decision regions of the KNN transfer function are disjoint and RB does not monotonically increase with increasing *etops25+* and/or *level3+wx*. The expected concave nature of the two-parameter model is implied by the decision regions, but anomalies in the surface are the result of mixing of the input space, thereby breaking down continuity. As presented, the model cannot be considered a fully realistic, statistically meaningful representation of the ensemble decision surfaces for RB as a function of the various Wx parameters. Providing a much greater number of Wx events will bring these disjoint regions closer to the more representative conceptual model seen in figure A.0-1.

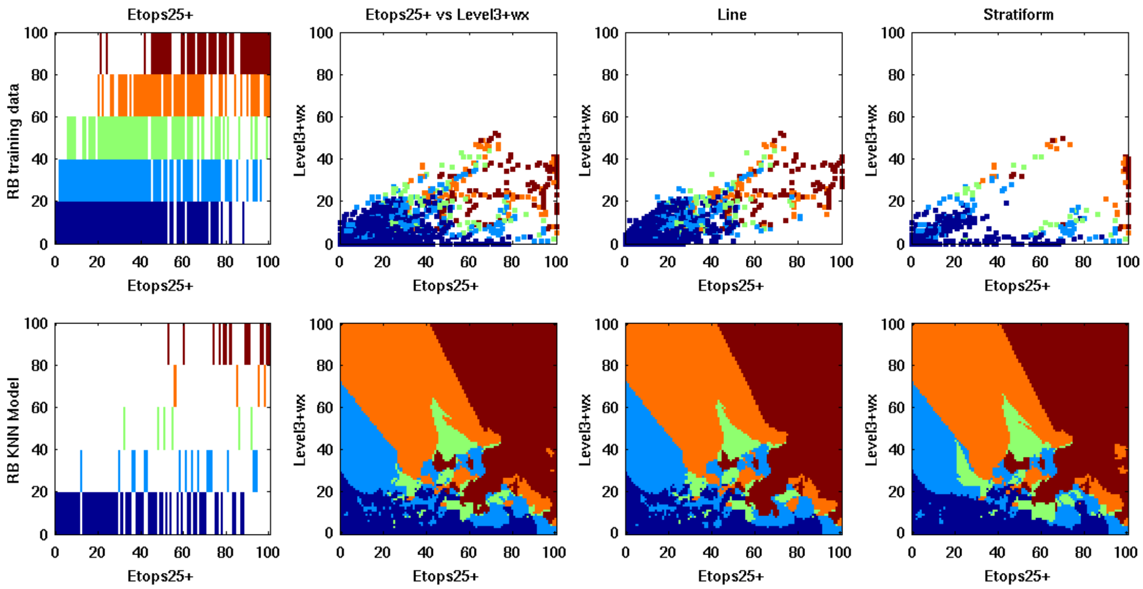

Figure A.7-4. (Top Row) ZID82 training data distribution of discrete RB intervals as a function of etops25+, etops25+ *and* level3+wx, etops25+ *and* level3+wx *separated by* wx-type line, etops25+ *and* level3+wx *separated by* wx-type stratiform *(left to right, respectively). Colors differentiate between the five discrete RB intervals and are consistent throughout the figure. (Bottom Row) KNN transfer function of RB based on synthetic data covering full possible range of* etops25+, level3+wx, *and* wx-type. *For simplicity, poorly sampled* wx-types *small, large, and embedded are not shown. Complex decision regions in the last three images of the bottom row are colored by their respective RB interval.*

A.8 ZID83

Figure A.8-1 shows that ATC sector ZID83 contains six high jet routes within its domain. Five of these routes are oriented for east-west / west-east traffic and the single J43 high jet route is oriented for north-south / south-north air traffic. ZID83 shares its western-facing borders with ZID82 and the two other sectors of the Indianapolis center included in this study, ZID82 and ZID66.

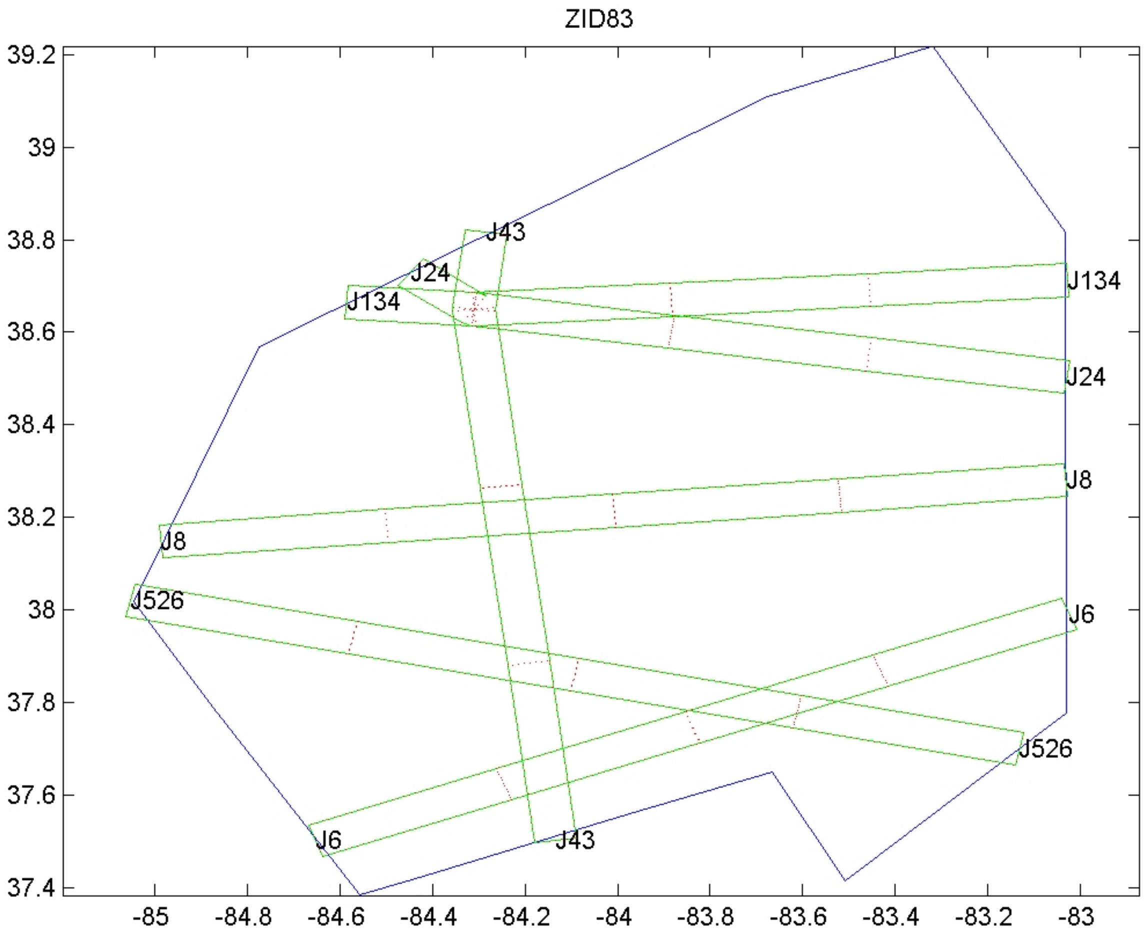

Figure A.8-1. ATC sector ZID83 showing route orientation. Six high jet routes are in total.

Table A.8-1 shows that for feature selection involving Gaussian, MLP, and KNN classifiers, parameters associated with high echo tops exhibit the highest explanatory power over RB variability. The best performing KNN routine has calculated an explanatory percentage for *etops25+* of 73% followed by *l3andet25* of 71%. Wx-type is the sole Wx parameter with a low explanatory percentage below 50%.

TABLE A.8-1

A comparison table of Gaussian, MLP, and KNN classifiers for ATC sector ZID83. First column indicates classification routine. Second column indicates the overall error rate produced at the final testing phase of each classifier. Final column lists the Wx parameters in order of explanatory power over the variability seen in RB. Explanatory power is expressed as a percentage in the parentheses to the right of each Wx parameter. The KNN classifier, as in all ATC sector results, produces the lowest error rate and is highlighted in red.

Classifier	Error	Explanatory Power of Individual Features
Gaussian	27.7%	etops25+ (77), l3andet25 (76), level3+wx (73), line (71), level1+wx (71), embedded (70), large (70), small (70), stratiform (68), orientation (67), wx-type (64)
MLP	16.7%	l3andet25 (77), etops25+ (77), level3+wx (74), line (72), wx-type (70), embedded (70), stratiform (70), large (70), small (70), orientation (70), level1+wx (70)
KNN	10.8%	etops25+ (73), l3andet25 (71), embedded (70), large (70), small (66), level3+wx (66), line (65), level1+wx (64), stratiform (61), orientation (57), wx-type (46)

Figure A.8-2 shows that RB is distributed over the full range of *etops25+* for ZID83. For the range of *etops25+* spanning 0–10%, the combination of box plot and probability distributions indicates that RB is densely centered near zero, with many non-zero RB values lying outside 1.5 times the IQR (outliers fall beyond the whiskers and are displayed as '+' in the center figure). No box plots are displayed for the 0–5% bin of *etops25+* because the median and quartiles for this bin are essentially zero. RB outliers are seen throughout the box plot and are numerous at low *etops25+* values (less than 20%).

Box plots in the center image indicate that for the range *etops25+* from 20–50%, the distribution of raw data inputs falls close to median RB values, resulting in compact IQRs per incremental bin of *etops25+*.

Beyond 50% *etops25+ coverage*, sampling becomes less dense and irregular. This results in a jagged trend of median RB values with increasing *etops25+*. The spread of the quartiles through this range becomes less consistent and the medians lose the linear trend that is evident between 20–50% *etops25+ coverage*. Adding to the complexity of the ZID83 data is the apparent secondary maxima seen in the discrete probability distribution of RB given in figure A.8-2 (far-left image). This accounts for the irregular trend of median and IQR values past 50%.

In comparison to *etops25+*, RB for ZID82 is distributed over a very shallow range of *level3+wx*. The spread of RB is limited to a maximum of just 35% fractional Wx coverage (bottom row, left image of figure A.8-2). As with *etops25+*, the combination of box plot and probability distributions indicates that RB is near zero for low fractional coverage with no IQR being displayed for the 5% discrete bin of RB.

Median slopes in the right column of figure A.8-2 indicate a positive trend in the relationship of RB to increasing fractional Wx coverage. Variability of the medians around the least squares fit is indicated by the r^2 values. As with all ATC sector RB experimental distributions presented previously in this report, the positive least squares slope of median values for *level3+wx* vs. RB is steeper than that of *etops25+* vs. RB. A low variability is seen in the RB-Wx coverage relationship for ZID83 and is reflected in the r^2 values of 0.899 and 0.912 (for *etops25+* and *level3+wx*, respectively).

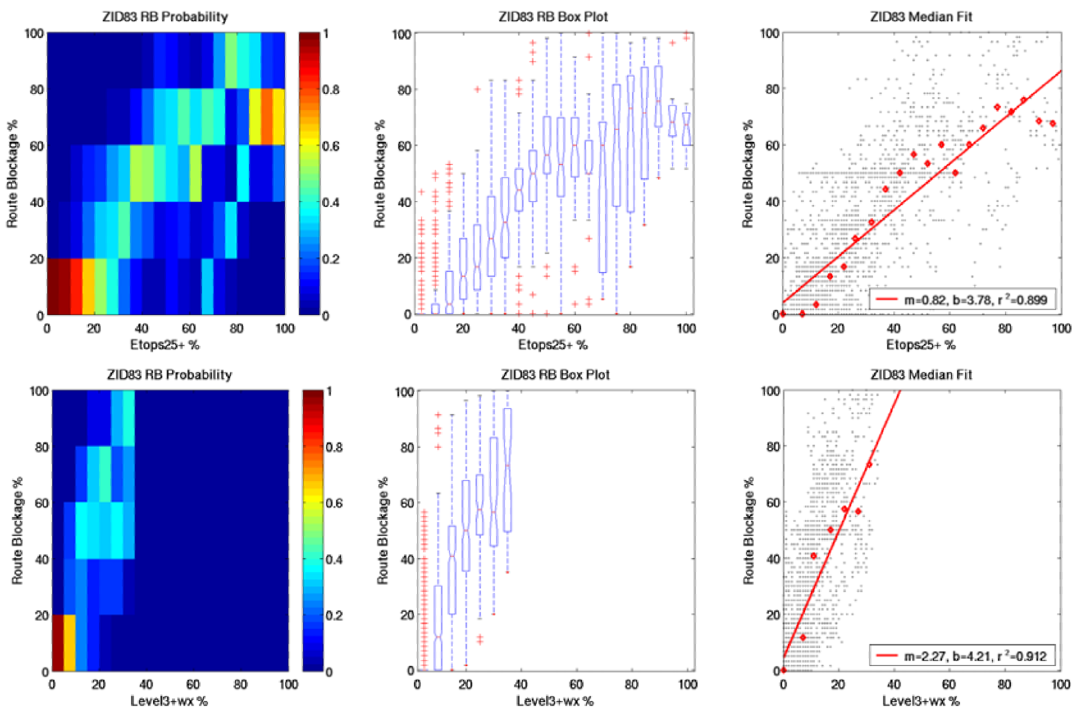

Figure A.8-2. ZID83 distribution of RB as related to the Wx parameter etops25+ *(top row) and* level3+wx *(bottom row). (Left) Probability distribution of discrete RB (discrete RB as defined in section 2.4.5) along a 5% bin interval of* etops25+ *(top) and* level3+wx *(bottom). (Center) Median value, upper quartile and lower quartile range of RB expressed as a box plot for the 5% bin interval of* etops25+ *(top) and* level3+wx *(bottom). (Right) Least squares fit of median RB values as related to the* etops25+ *(top) and* level3+wx *(bottom) Wx parameters. Background scatter (gray) represents data points of the two distributions.*

Figure A.8-3 shows that for ZID83 a combination of the first six parameters produces a training error rate of 12.8%. This error is a statistically significant decrease from the error rate achieved (15%) by using the full ordered combination of Wx parameters. Hence, we did not use *wx-type*, *large*, *small*, *orientation*, and *level1+wx* as inputs to the KNN routine.

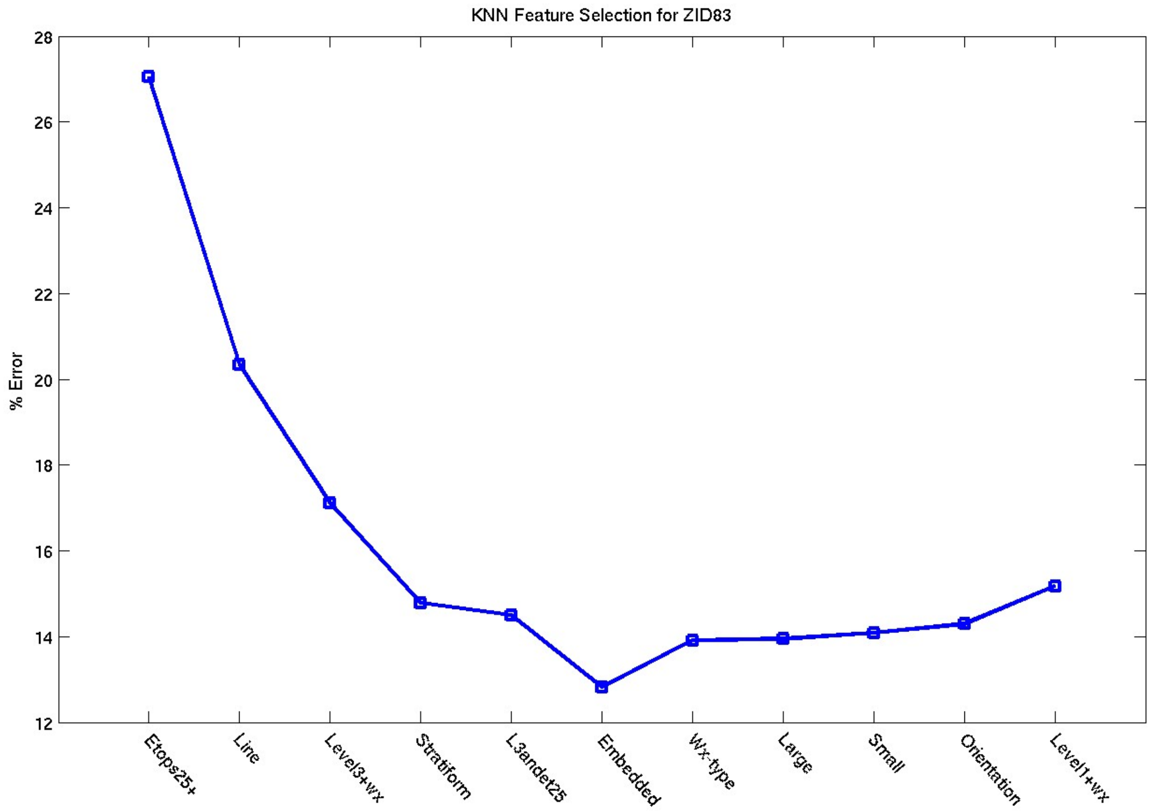

Figure A.8-3. Feature selection processing as performed by the KNN classifier. Utilizes a K=3, leave-one-out, cross-validation scheme. Error expressed as a percentage along the ordinate axis. Wx parameters are ordered in a combination that minimizes the training error rate. Wx parameters that fall to the right of the minimum increase the combined error and were not used in the best combination *parameter selection.*

Table A.8-2 compares the per RB interval errors of 3 single Wx parameter KNN models to a KNN model that utilizes the ordered *best combination* of Wx parameters determined through the feature selection process. The RB models based on the single Wx parameter of *level3+wx, l3andet25,* and *etops25+* developed in both the training and testing phases of pattern classification. Results show that the *best combination* of Wx parameters determined through feature selection significantly reduces the classification error. For the modeling RB of ZID83 all RB intervals show improved classification errors when the *best combination* of Wx parameters is used.

TABLE A.8-2

ZID83 comparison table of four different KNN models brought through both training and testing phases of classification. Each column to the right of the "number of samples" column represents the error percentages produced by modeling RB as a function of the single explanatory parameters *level3+wx*, *l3andet25*, and *etops25+* as compared to the best combination of Wx parameters as determined through the feature selection process (left to right respectively). Values down each column are per the RB interval error expressed as a percentage. The best combination of Wx parameters consistently yields the lowest error rates.

RB interval	# of samples	*level3+wx*	*l3andet25*	*etops25+*	*Best Combination*
[0–20%)	2487	30.85	13.91	14.52	2.62
[20–40%)	368	72.6	71.23	73.97	38.36
[40–60%)	436	73.56	77.01	77.01	28.74
[60–80%)	200	35	30	67.5	20
[80–100%]	75	53.33	73.33	86.67	20
Total Errors	---	41.07	29.68	32.77	10.83

Table A.8-3 shows that a low classification error has been realized for the highly sampled [0–20%) RB interval. The largest error of 38.36% occurs at the [20–40%) RB interval. Remaining RB intervals have calculated error rates that fall below 30%. Overall, the KNN classification routine produced a low error rate of 10.83% for ZID83.

TABLE A.8-3

KNN (K = 3) test results for ZID83 consisting of the classification confusion matrix to the left and per class statistics to the right. Red highlighted numbers along the diagonal of the confusion matrix indicate correctly classified instances of RB. Numbers that fall to either side of the diagonal are incorrectly classified RB. Red highlighted column to the right indicates the per class error. The number at the bottom of this column is the overall error rate of the classification (10.83%).

```
TEST:ZID83.test    Time: 0.07 secs  RMS Err: 0.208  Err: 10.83%
K-Nearest Neighbor (K=3) classifier: 20 cases - trained on 80% of data tested on 20% ECHO-BSD
---------------------------------------------------------------------------------------------
Desired|   Computed Class
Class  |   0   1   2   3   4  Total  Class  Patterns  #Errors  %Errors  StdDev   RMSE  Label
---------------------------------------------------------------------------------------------
  0_20 | 483  10   3          496     0      496       13        2.62  ( 0.7)  0.102   0_20
 20_40 |  17  45   9   2         73     1       73       28       38.36  ( 5.7)  0.392  20_40
 40_60 |   5  12  62   8         87     2       87       25       28.74  ( 4.9)  0.339  40_60
 60_80 |           8  32         40     3       40        8       20.00  ( 6.3)  0.283  60_80
80_100 |               3  12     15     4       15        3       20.00  (10.3)  0.283  80_100
---------------------------------------------------------------------------------------------
 Total | 505  67  82  45  12  711  Overall  711         77       10.83%  ( 1.2)  0.208
---------------------------------------------------------------------------------------------
```

As with ZID82, plots along the top row of figure A.8-4 show that RB intervals are heavily scattered throughout the input space for ZID83. The plot of *etops25+* vs. RB of the training data (top row, first image) shows that each RB interval is spread over much of the *etops25+* range. This is most evident where solid, continuous blocks of an RB interval overlap other solid RB blocks, given a range of *etops25+* values.

The 2-D scatter plots along the top row show clusters of coverage events with similar RB mixing heavily in amongst those of different intervals. While mixed RB regions are seen throughout the range of *etop25+*, this is most prevalent at the 20–70% range of *etops25+*. These factors translate into the erratic trend toward larger RB intervals exhibited when modeling RB as a function of increasing *etops25+* synthetic values (bottom row, first image).

The addition of synthetic *level3+wx* as a second Wx parameter reveals the highly complex decision region of the 2-D transfer function (bottom row, second image). Within the range of *etops25+* spanning 20–70%, complexity is most prevalent and arises from the highly mixed region of the training data input space seen in the image directly above.

Points of scatter plot indicate how far the training data extends into the *etops25+* vs. *level3+wx* input space (0–100% and 0–37%, respectively). Portions of the KNN decision regions that fall beyond the outlying points in the scatter are influenced mainly by those points and their associated RB values. This accounts for the large, broadly colored regions lying above the *level3+wx* data extent. While this complex decision region works to reduce the test errors of the classifier, we view the resulting decision regions as being a poor estimate of the ensemble decision regions.

When the synthetic data includes the full possible range *etops25+*, *level3+wx*, and *wx-type* associated with line type events, lower RB intervals of the transfer function contract while higher RB intervals expand (bottom row, third image). Complexity is maintained with the addition of *wx-type* line.

When the full possible range *etops25+*, *level3+wx*, and *wx-type* associated with stratiform type events is considered, decision regions associated with higher RB intervals contract while lower RB intervals expand. The inclusion of *wx-type* stratiform greatly generalizes decision regions of the ZID83 transfer function.

As seen in the data from other sections, figure A.8-4 shows that the KNN RB model for ZID83 does not fit the expected functional dependence defined by the conceptual model in figure A.0-1. Decision regions of the KNN transfer function are disjoint and RB does not monotonically increase with increasing *etops25+* and/or *level3+wx*. Anomalies in the surfaces are the result of mixing of the input space, thereby breaking down the continuity of the decision regions. A much greater number of experimental Wx events should bring these disjoint regions closer to the conceptual model.

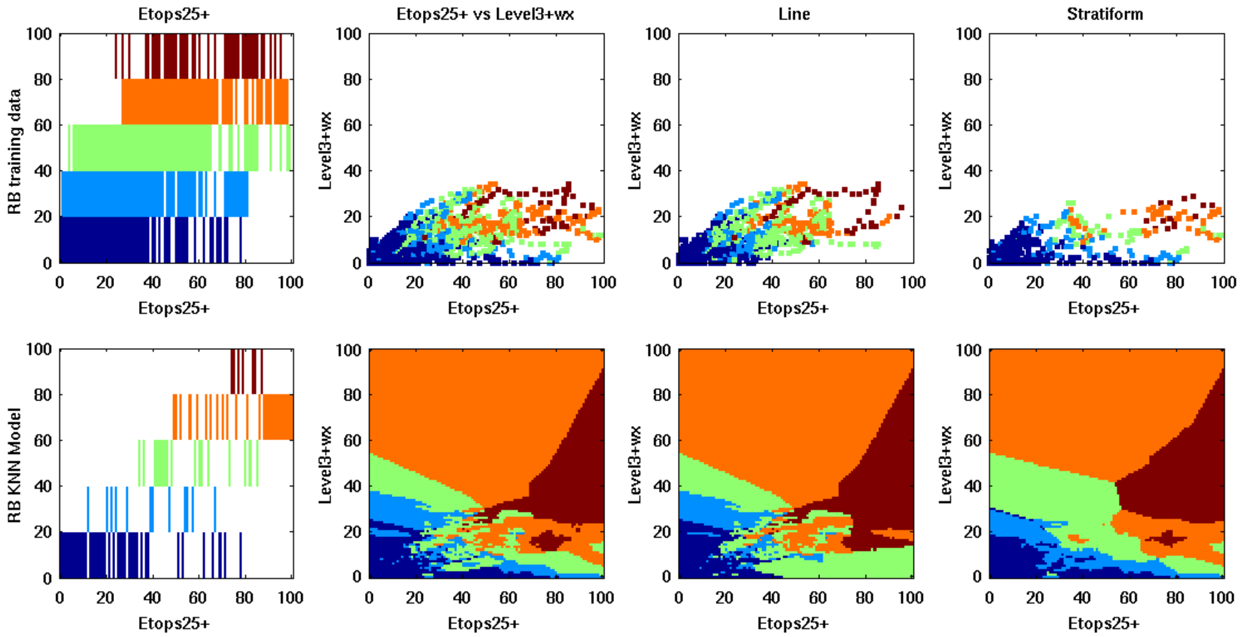

Figure A-.8-4. (Top Row) ZID83 training data distribution of discrete RB intervals as a function of etops25+, etops25+ *and* level3+wx, etops25+ *and* level3+wx *separated by* wx-type line, etops25+ *and* level3+wx *separated by* wx-type stratiform *(left to right, respectively). Colors differentiate between the five discrete RB intervals and are consistent throughout the figure. (Bottom Row) KNN transfer function of RB based on synthetic data covering full possible range of* etops25+, level3+wx, *and* wx-type. *For simplicity, poorly sampled* wx-types *small, large, and embedded are not shown. Complex decision regions in the last three images of the bottom row are colored by their respective RB interval.*

A.9 ZDC12

ZDC12 is the easternmost sector of this study (figure A.9-1). ZDC12 consists of four high jet routes, three of which are oriented northeast to southwest. Crossing all of theses routes is the single north-south oriented route J61.

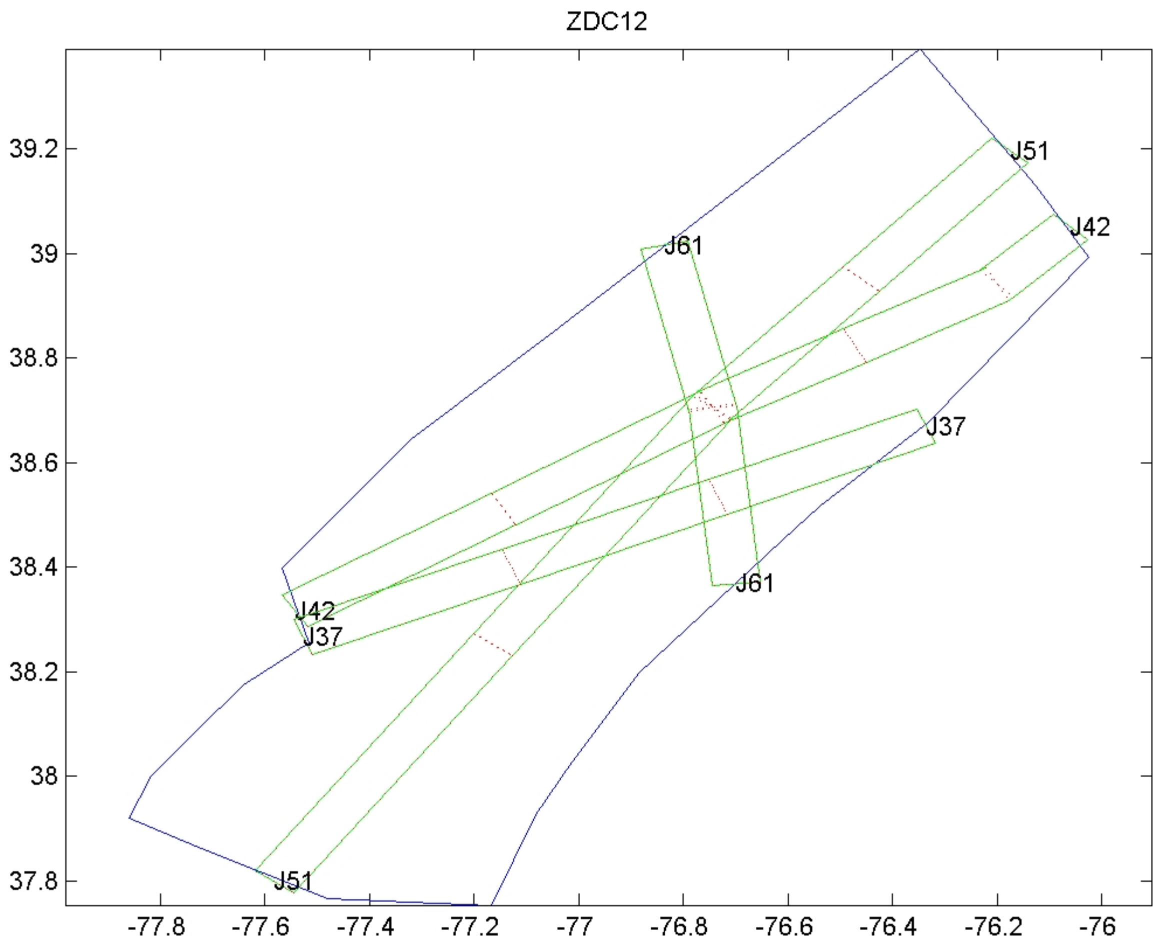

Figure A.9-1. ATC sector ZDC12 showing route orientation. Four high jet routes are in total.

Feature selection of the three routines listed in table A.9-1 indicates that the Wx parameter *l3andet25* ranks highest in explaining the variation seen in the RB-dependent variable. For the best performing KNN classifier, feature selection has calculated the explanatory percentage of *l3andet25* to be 84%. Explanatory percentages for the Wx parameters that follow remain relatively high and flat, not falling below 78%.

TABLE A.9-1

A comparison table of Gaussian, MLP, and KNN classifiers for ATC sector ZDC12. First column indicates classification routine. Second column indicates the overall error rate produced at the final testing phase of each classifier. Final column lists the Wx parameters in order of explanatory power over the variability seen in RB. Explanatory power is expressed as a percentage in the parentheses to the right of each Wx parameter. The KNN classifier, as in all ATC sector results, produces the lowest error rate and is highlighted in red.

Classifier	Error	Explanatory Power of Individual Features
Gaussian	21.4%	l3andet25 (82), wx-type (80), large (80), small (80), level3+wx (80), embedded (79), orientation (76), line (76), etops25+ (76), level1+wx (76), stratiform (69)
MLP	15.1%	l3andet25 (83), line (81), etops25+ (81), level3+wx (81), wx-type (80), embedded (80), stratiform (80), large (80), small (80), orientation (80), level1+wx (80)
KNN	13.68%	etops25+ (84), level3+wx (82), line (81), l3andet25 (81), wx-type (80), embedded (80), large (80), small (80), orientation (79), stratiform (78), level1+wx (78)

RB for ZDC12 is distributed over a wide dynamic range of *etops25+*. This is evident in the probability, box plot, and scatter plot images of figure A.9-2. For a range of *etops25+* spanning 0–20%, the combination of box plot and probability distributions indicates that RB is densely centered near zero with many non-zero RB values lying outside 1.5 times the IQR. No box plots are displayed for the 0–5%, 5–10%, and 10–15% bins of *etops25+* because medians and quartiles for these bins are essentially zero.

Values for RB for ZDC12 do not follow the upward trend with increasing *etops25+* that has been common in most of the previously discussed sections. Rather, probabilities indicate that for the range of *etops25+*, the data distribution for ZDC12 is skewed toward the lowest RB interval (left, figure 42). For a range of *etops25+* spanning 0–50% and 80–90%, higher discrete probabilities for RB have been calculated for [0–20%) than for any other RB interval. This does not make sense intuitively and undoubtedly reflects the limitation of a very limited number of data points corresponding to RB ≥ 20%.

With the exception of only three bins, box plots of RB for *etops25+* ranging from 25% to 100% have whiskers (1.5*IQR) spanning four and five discrete RB intervals indicating that, for the sampled data, RB varies considerably. Also, while the continuous RB is spread over the full dynamic range of *etops25+* fractional coverage, data becomes sparse for *etops25+* greater than 60%.

The RB for ZDC12 increases more rapidly as a function of *level3+wx* than was the case for *etops25+*. The spread of RB is limited to a maximum of 35% fractional Wx coverage (bottom row, left image of figure A.9-2). As with *etops25+*, the combination of box plot and probability distributions indicates that the RB data points are densely centered near zero for low fractional coverage with no IQR being displayed for the 5% discrete bin of RB with low probability density at the middle range RB from 20–80%.

Median slopes in the right column of figure A.9-2 indicate a positive trend in the relationship of RB to increasing fractional Wx coverage. Variability of the medians around the least squares fit is indicated by the r^2 values. As with all ATC sector RB, the positive least squares slope of median values for *level3+wx* vs. RB is steeper than that of *etops25+* vs. RB. A high degree of variability in RB is reflected in the r^2 value for *etops25+* vs. RB calculated at 0.695. This is not the case for *level3+wx* vs. RB where variability is relatively low with a calculated r^2 of 0.988.

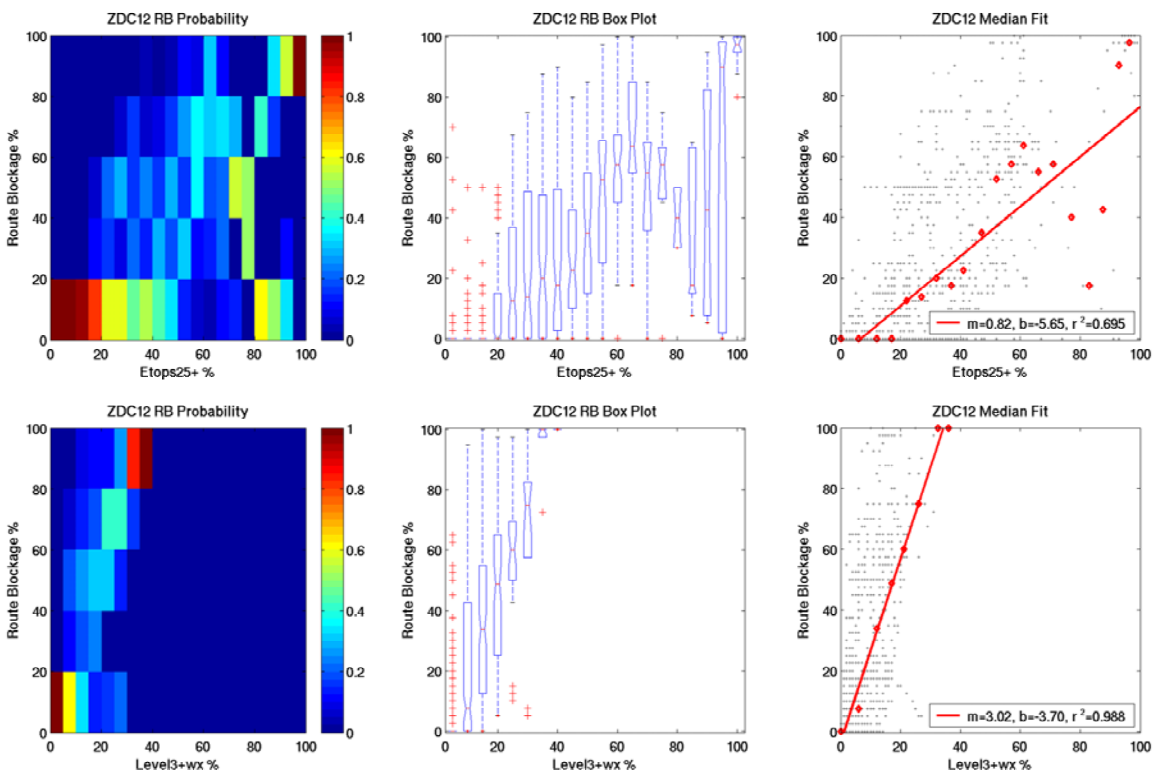

Figure A.9-2. ZDC12 distribution of RB as related to the Wx parameter etops25+ *(top row) and* level3+wx *(bottom row). (Left) Probability distribution of discrete RB (discrete RB as defined in section 2.4.5) along a 5% bin interval of* etops25+ *(top) and* level3+wx *(bottom). (Center) Median value, upper quartile and lower quartile range of RB expressed as a box plot for the 5% bin interval of* etops25+ *(top) and* level3+wx *(bottom). (Right) Least squares fit of median RB values as related to the* etops25+ *(top) and* level3+wx *(bottom) Wx parameters. Background scatter (gray) represents data points of the two distributions.*

The ordered combination of Wx parameters seen in figure A.9-3 indicates that the first nine parameters produce a 10.3% error rate during training. Upon examination of error rates between the reduced and full ordered combination, the 0.9% increase does not yield a separation of the two standard deviations needed to warrant the exclusion of Wx parameters *small* and *l3andet25*. The full ordered combination was been presented to the KNN classifier for testing.

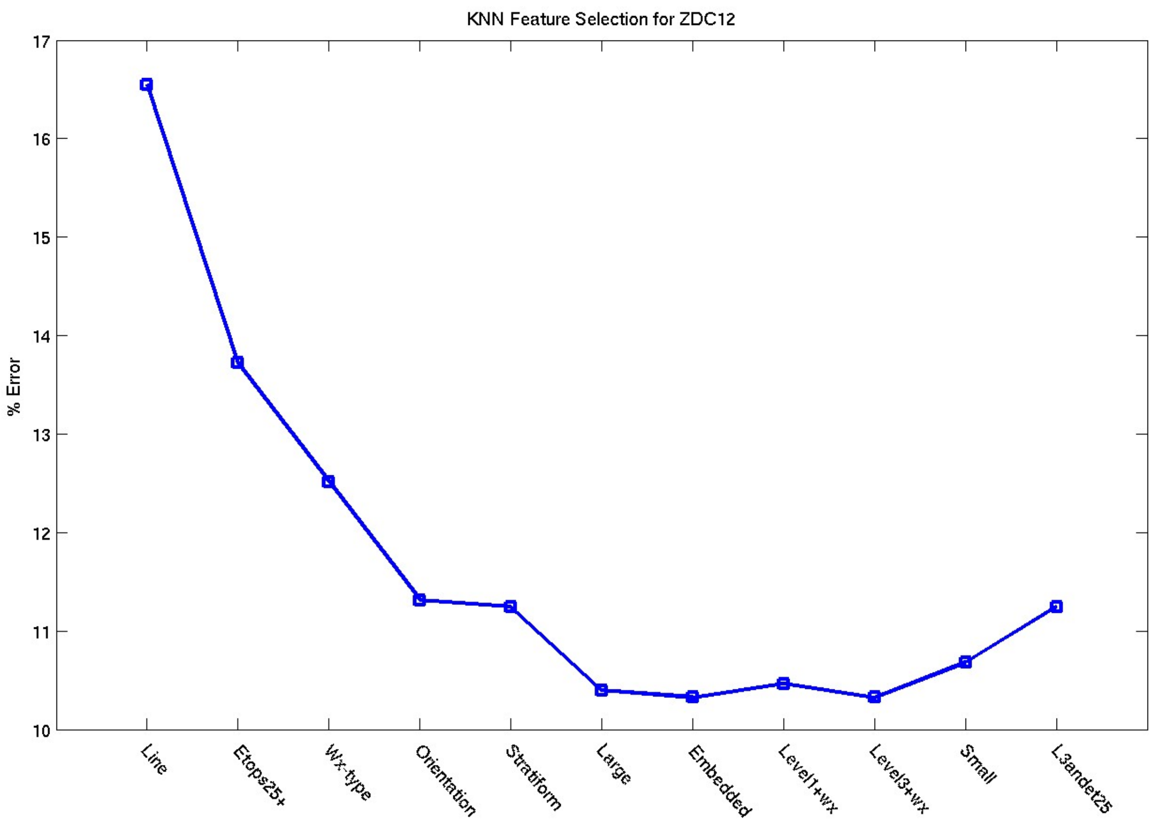

Figure A.9-3. Feature selection processing as performed by the KNN classifier. Utilizes a K=3, leave-one-out, cross-validation scheme. Error expressed as a percentage along the ordinate axis. Wx parameters are ordered in a combination that minimizes the training error rate. Wx parameters that fall to the right of the minimum increase the combined error. In this case, all Wx parameters are included in the best combination *set.*

Table A.9-2 compares the per RB interval errors of three single Wx parameter KNN models to a KNN model that utilizes the ordered combination of all Wx parameters. As with the other ATC sectors, results show that the *best combination* of Wx parameters determined through feature selection significantly reduces the classification error. For forecasting the RB of ZDC12, all RB intervals, except for the RB interval of [0–20%), show improved classification errors when the *best combination* of Wx parameters is used.

TABLE A.9-2

ZDC12 comparison table of four different KNN models brought through both training and testing phases of classification. Each column to the right of the "number of samples" column represents the error percentages produced by modeling RB as a function of the single explanatory parameters *level3+wx*, *l3andet25*, and *etops25+* as compared to the best combination of Wx parameters as determined through the feature selection process (left to right, respectively). Values down each column are per the RB interval error expressed as a percentage. The best combination of Wx parameters consistently yields the lowest error rates.

RB interval	# of samples	*level3+wx*	*l3andet25*	*etops25+*	*Best Combination*
[0–20%)	1404	0.71	1.07	2.14	4.27
[20–40%)	109	90.48	95.24	90.48	52.38
[40–60%)	733	100	80.77	92.31	57.69
[60–80%)	85	100	80	80	53.33
[80–100%]	43	75	75	75	25
Total Errors	---	19.37	17.66	19.09	13.68

Table A.9-3 shows the results for the KNN classification of RB for ATC sector ZDC12. When combined, the overall error rate for the RB classification of ZDC37 falls below 15%. Once again, middle range RB intervals between 20% and 80% yield the largest errors of the KNN classification. These three RB intervals all have calculated errors larger than 50%. The RB interval of [0–20%) has a low 4.27% error. The [80–100%] RB only incorrectly classified 25% of the patterns for that particular class, but due to the small sample size, the error result for this interval cannot be considered representative.

TABLE A.9-3

KNN (K = 3) test results for ZDC12 consisting of the classification confusion matrix to the left and per class statistics to the right. Red highlighted numbers along the diagonal of the confusion matrix indicate correctly classified instances of RB. Numbers that fall to either side of the diagonal are incorrectly classified RB. Red highlighted column to the right indicates the per class error. The number at the bottom of this column is the overall error rate of the classification (13.68%).

```
TEST:ZDC12.test    Time: 0.08 secs  RMS Err: 0.234  Err: 13.68%
K-Nearest Neighbor (K=3) classifier: 20 cases - trained on 80% of data tested on 20% ECHO-BSD
----------------------------------------------------------------------------------------------
Desired|   Computed Class
Class  |   0   1   2   3   4  Total  Class  Patterns  #Errors  %Errors  StdDev   RMSE  Label
----------------------------------------------------------------------------------------------
  0_20 | 269  12                281    0      281        12       4.27   ( 1.2)   0.131   0_20
 20_40 |   6  10   5             21    1       21        11      52.38   (10.9)   0.458  20_40
 40_60 |   1   9  11   5         26    2       26        15      57.69   ( 9.7)   0.480  40_60
 60_80 |       1   7   7         15    3       15         8      53.33   (12.9)   0.462  60_80
80_100 |           1   1   6      8    4        8         2      25.00   (15.3)   0.316  80_100
----------------------------------------------------------------------------------------------
 Total | 276  32  24  13   6  351  Overall  351        48      13.68%  ( 1.8)   0.234
----------------------------------------------------------------------------------------------
```

KNN training and test results modeling RB as a function of the single Wx parameter *etops25+* are shown in the first image (bottom row of figure A.9-4). As with sectors ZAU24 and ZID82, because much of the data that makes up the training set is associated with the [0–20%) RB interval, it dominates the output of the single Wx parameter transfer function. Only sporadic increases to larger RB intervals occur between *etops25+* of 30% and 92%. Where *etops25+* exceeds 92%, the transfer function classifies exclusively at the upper RB interval of [80–100%].

Adding *level3+wx* as the second Wx parameter reveals the complex decision region constructed within the synthetic *etops25+* vs. *level3+wx* plane (second image, bottom row). Training data influencing the creation of this 2-D transfer function are shown in the scatter plot directly above.

Points of scatter plot indicate how far the training data extends into the *etops25+* vs. *level3+wx* input space (0–100% and 0–37%, respectively). Portions of the KNN decision regions that fall beyond the outlying points in the scatter are influenced mainly by those points and their associated RB values. This accounts for the large, broadly colored regions lying above the *level3+wx* data extent. While the complex decision regions are optimal for minimizing classification errors for the data set, the resulting decision regions are somewhat unrealistic estimators of the full ensemble of possible RB-Wx events.

Large decision regions have been constructed for the [0–20%), [60–80%), and [80–100%] RB intervals. The remaining intervals appear more as noise between these three large decision regions than anything else. This is the result of the highly mixed input points seen in the image directly above, with a relatively small number of data points being attributed to RB intervals of [20–40%) and [40–60%). Also these intervals appear in small clusters or as individual points scattered among larger populations of data associated with the other RB intervals, making the decision regions small and disjoint.

Because of the scattered nature of the input data, complexity of the decision regions is not affected by the inclusion of *wx-type* as the third Wx parameter (bottom row, third and fourth image of figure A.9-4). The addition of *wx-type* associated with line generally shifts decision regions toward higher RB intervals. W*x-type* associated with stratiform shifts decision regions toward lower RB intervals. Although the *wx-type* stratiform contributes to the generalization of classification decision regions for the other ATC sectors, it has not done so for ZDC12.

Figure A.9-4 shows that the KNN RB model for ZDC12 does not fit the expected functional dependence defined by the conceptual model in figure A.0-1. Decision regions of the KNN transfer function are disjoint and RB does not monotonically increase with increasing *etops25+* and/or *level3+wx*. Anomalies in the surfaces constructed by the KNN routine keep the model from being a realistic, statistically meaningful representation of RB for the ensemble weather process. A much greater number of experimental data points are clearly needed for this sector.

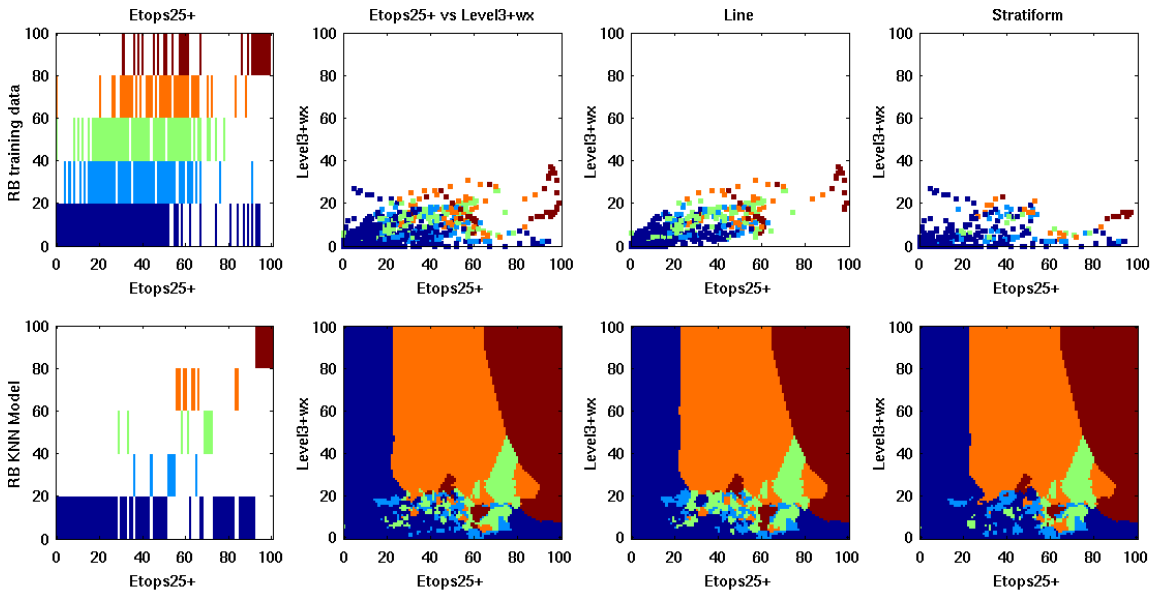

Figure A.9-4. (Top Row) ZDC12 training data distribution of discrete RB intervals as a function of etops25+, etops25+ *and* level3+wx, etops25+ *and* level3+wx *separated by* wx-type line, etops25+ *and* level3+wx *separated by* wx-type stratiform *(left to right, respectively). Colors differentiate between the five discrete RB intervals and are consistent throughout the figure. (Bottom Row) KNN transfer function of RB based on synthetic data covering full possible range of* etops25+, level3+wx, *and* wx-type. *For simplicity, poorly sampled* wx-types *small, large, and embedded are not shown. Complex decision regions in the last three images of the bottom row are colored by their respective RB interval.*

A.10 ZDC37

ZDC37 is one of two sectors within Washington center included in the Wx-RB study (figure A.10-1). ZDC37 consists of a dense route structure in comparison to its overall aerial coverage. Of the six high jet routes, five have an east-west orientation. The sole north-south crossing route is J53 (see figure A.10-1).

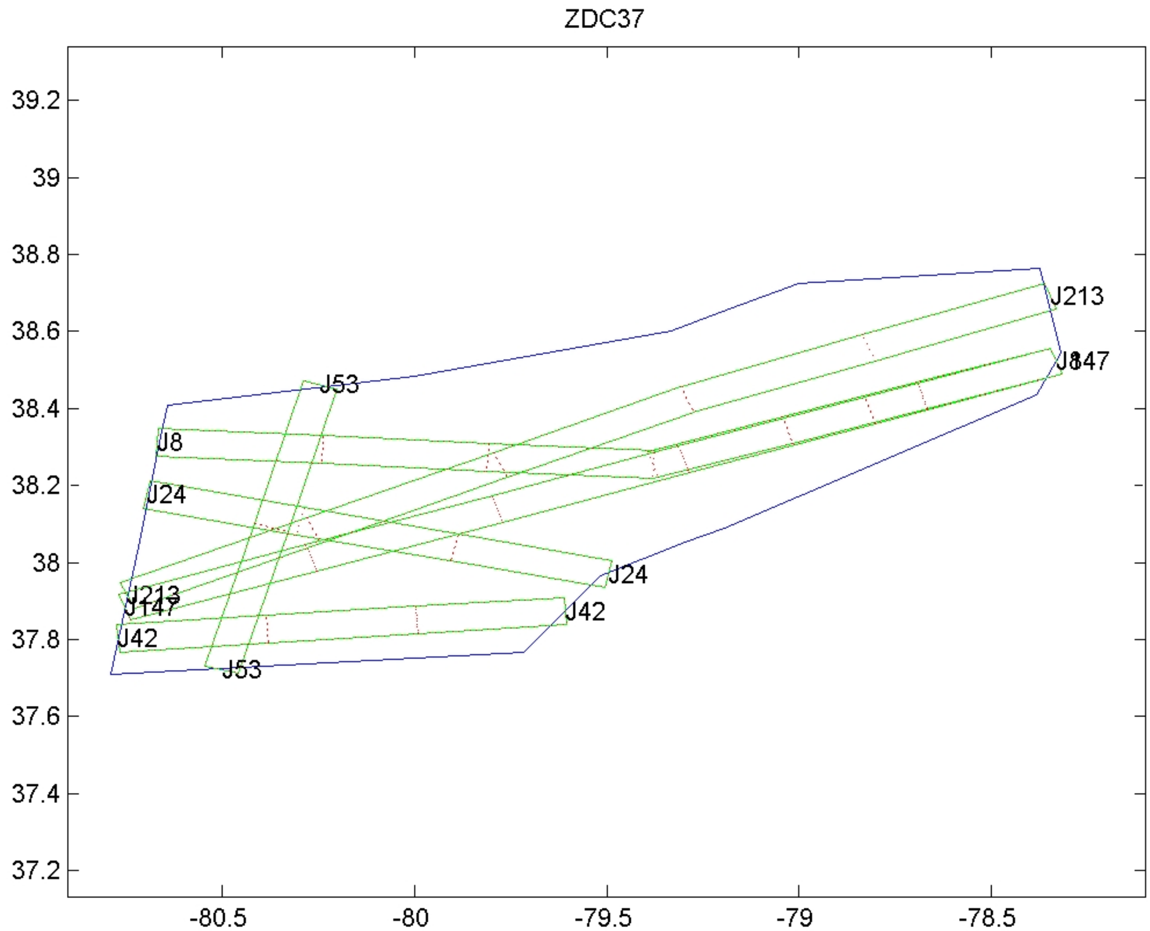

Figure A.10-1. ATC sector ZDC37 showing route orientation. Six high jet routes are in total.

As with all of the data compiled for the 10 ATC sectors in the Wx-RB modeling study, table A.10-1 indicates that parameters associated with high echo tops within a sector exhibit high explanatory power for the RB. For ZDC37, given all three classification routines listed in the above table, echo tops-derived parameters have explanatory percentages that do not fall below 89%. For the KNN routine, *etops25+* explains 91% of the variation seen in the RB of ZD37 when basing classification on that single parameter.

Lowest in the explanatory value of the KNN parameters is *level3+wx* with still a high explanatory percentage of 78%. The *level3+wx* ranking in explanatory power is not expected, given that VIL ≥ VIP level 3 is a major contributor to the calculation of RB. An explanation for this is that given the lack of data density for ZDC37, *level3+wx* by itself is a poor discriminator between RB intervals.

TABLE A.10-1

A comparison table of Gaussian, MLP, and KNN classifiers for ATC sector ZDC37. First column indicates classification routine. Second column indicates the overall error rate produced at the final testing phase of each classifier. Final column lists the Wx parameters in order of explanatory power over the variability seen in RB. Explanatory power is expressed as a percentage in the parentheses to the right of each Wx parameter. The KNN classifier, as in all ATC sector results, produces the lowest error rate and is highlighted in red.

Classifier	Error	Explanatory Power of Individual Features
Gaussian	9.32%	l3andet25 (89), embedded (89), large (89), small (89), wx-type (89), level3+wx (89), orientation (88), level1+wx (85), line (82), stratiform (78), etops25+ (72)
MLP	6.30%	l3andet25 (91), etops25+ (90), level3+wx (90), wx-type (89), embedded (89), stratiform (89), large (89), small (89), orientation (89), line (89), level1+wx (89)
KNN	5.04%	etops25+ (91), wx-type (89), embedded (89), stratiform (89), large (89), small (89), orientation (87), level1+wx (87), l3andet25 (85), line (84), level3+wx (78)

Similar to ZOB77, RB for ZDC37 is not spread across the full dynamic range of the *etops25+* Wx parameter. The histogram for ZDC37 in figure A.10-2 reveals that sampling captured only two Wx occurrences associated with the [80–100%] RB interval. Examination of the raw data indicates that both Wx occurrences hold a value at the low end of the RB interval (exactly 80%).

Box plot and probability distributions indicate that for low *etops25+* values, as with all other ATC sectors discussed earlier, the experimental RB data points are densely centered near zero (left and center images of figure A.10-2). RB outliers of 1.5*IQR can be seen in data bins from 0% to 25%. No box plots are displayed for the 0–5% and 5–10% discrete bins of *etops25+* because the median values and quartiles for these bins are essentially zero.

The quartiles of the box plot show a varying spread in RB exists throughout the range of *etops25+*. The largest RB spread occurs within the *etops25+* bin of 30–35% where the whiskers (1.5*IQR) of the box plot extend to all discrete RB intervals. This bin also happens to hold one of the two 80% RB values. Despite this variability, median RB values follow a linear upward trend with increasing *etops25+*.

RB for ZDC37 is distributed over a very shallow range of *level3+wx*. The spread of RB is limited to a maximum of 25% fractional Wx coverage (bottom row, left image of figure A.10-2). As with *etops25+*, the combination of box plot and probability distributions indicates that RB is densely centered near zero for low fractional coverage with no IQR being displayed for the 5% bin of RB.

Median slopes in the right column of figure A.10-2 indicate a positive trend in the relationship of RB to increasing fractional Wx coverage. Variability of the medians around the least squares fits is indicated by the r^2 values. As with all ATC sector RB distributions presented earlier, the positive least squares slope of median values for *level3+wx* vs. RB is steeper than that of *etops25+* vs. RB. Low variability is seen in the RB-Wx coverage relationship for ZDC37 and is reflected in the r^2 values of 0.945 and 0.941 for *etops25+* and *level3+wx*, respectively.

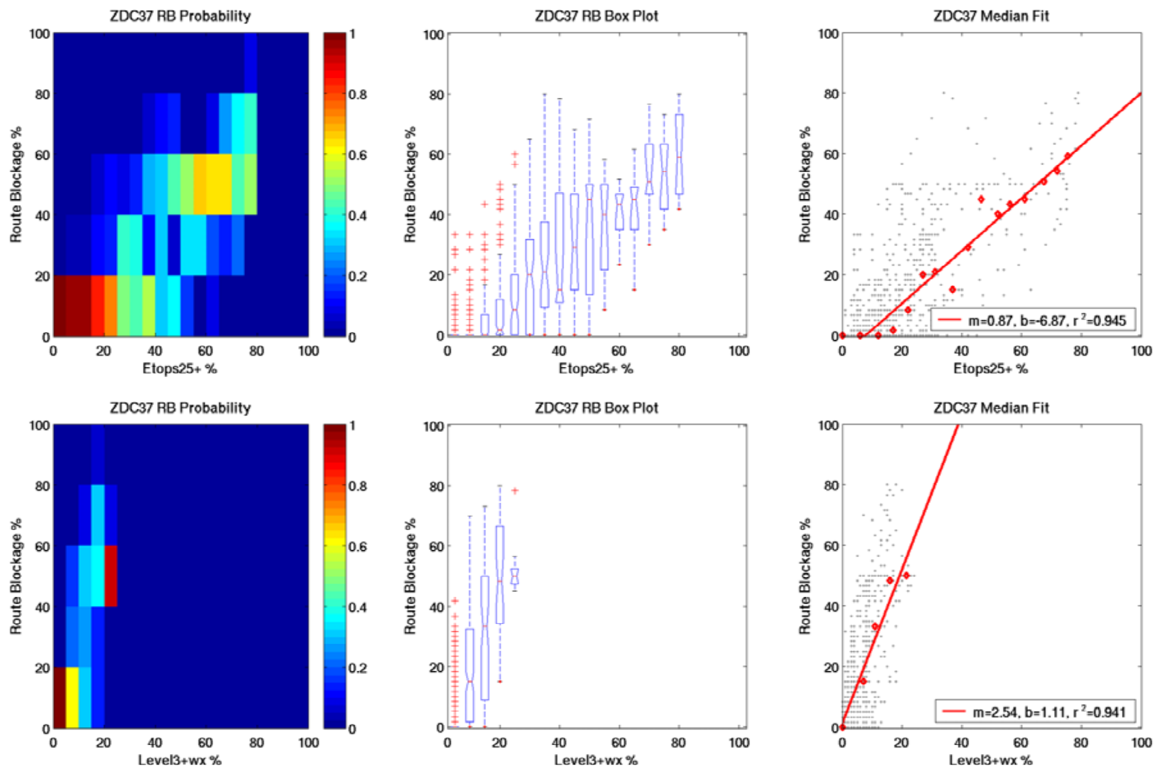

Figure A.10-2. ZDC37 distribution of RB as related to the Wx parameter etops25+ *(top row) and* level3+wx *(bottom row). (Left) Probability distribution of discrete RB (discrete RB as defined in section 2.4.5) along a 5% bin interval of* etops25+ *(top) and* level3+wx *(bottom). (Center) Median value, upper quartile and lower quartile range of RB expressed as a box plot for the 5% bin interval of* etops25+ *(top) and* level3+wx *(bottom). (Right) Least squares fit of median RB values as related to the* etops25+ *(top) and* level3+wx *(bottom) Wx parameters. Background scatter (gray) represents data points of the two distributions.*

For ZDC37, feature selection shows that the combination of parameters up to *level3+wx* minimizes the training error to 5.3% (figure A.10-3). Excluded from KNN classification are the remaining Wx parameters *wx-type*, *embedded*, *line*, and *orientation.* These parameters have been excluded as a result of the error increase of their inclusion being statistically significant.

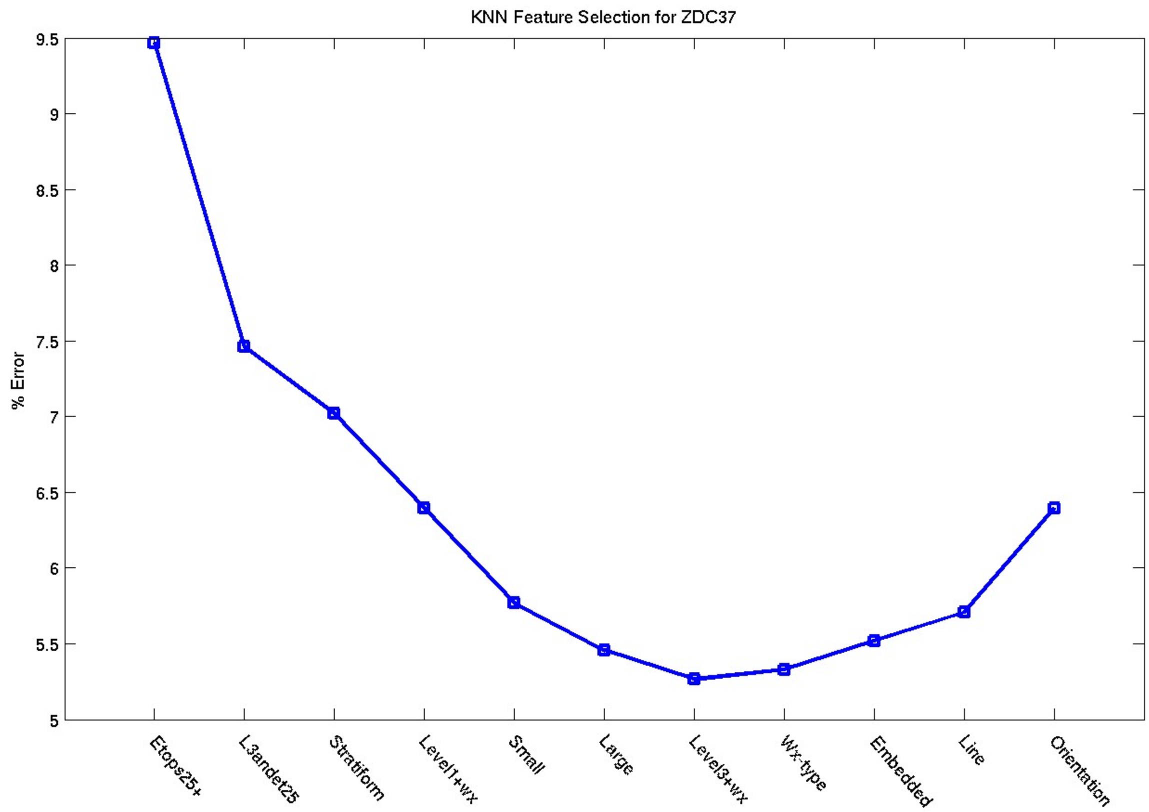

Figure A.10-3. Feature selection processing as performed by the KNN classifier. Utilizes a K=3, leave-one-out, cross-validation scheme. Error expressed as a percentage along the ordinate axis. Wx parameters are ordered in a combination that minimizes the training error rate. Wx parameters that fall to the right of the minimum increase the combined error and were not used in the best combination *parameter selection and were not used in the* best combination *parameter selection.*

Table A.10-2 compares the per RB interval errors of three single Wx parameter KNN models to a KNN model that utilizes the ordered *best combination* of Wx parameters. Results show that for modeling RB of ZDC37, all RB intervals show improved classification errors when the *best combination* of Wx parameters is used. Due to the small number of cases reflecting RB values beyond the [0–40%) interval, results summarized in table A.1-2 cannot be regarded as statistically meaningful for RB ≥ 60%.

TABLE A.10-2

ZDC37 comparison table of four different KNN models brought through both training and testing phases of classification. Each column to the right of the "number of samples" column represents the error percentages produced by modeling RB as a function of the single explanatory parameters *level3+wx*, *l3andet25*, and *etops25+* as compared to the best combination of Wx parameters determined through the feature selection process (left to right, respectively). Values down each column are per the RB interval error expressed as a percentage. The best combination of Wx parameters consistently yields the lowest error rates.

RB interval	# of samples	*level3+wx*	*l3andet25*	*etops25+*	*Best Combination*
[0–20%)	1764	17	6.8	2.27	1.42
[20–40%)	120	78.26	78.26	91.3	30.43
[40–60%)	86	76.47	47.06	82.35	41.18
[60–80%)	20	100	50	50	25
[80–100%]	2	NaN	NaN	NaN	NaN
Total Errors	---	23.93	13.1	11.34	5.04

As with ZOB77, the two patterns that make up the [80–100%] RB interval are included in the training data set of the classifier. Table A.10-3 shows that no patterns for this RB interval are made available for testing. A near-perfect classification has been achieved for the [0–20%) RB interval. The largest error of 41.18% occurs at the RB of [40–60%). The remaining two intervals include errors that are near or below 30%. While the overall RB error is a low 5.04%, small sampling again indicates that results for RB $\geq$ 60% cannot be regarded as statistically meaningful.

TABLE A.10-3

KNN (K = 3) test results for ZDC37 consisting of the classification confusion matrix to the left and per class statistics to the right. Red highlighted numbers along the diagonal of the confusion matrix indicate correctly classified instances of RB. Numbers that fall to either side of the diagonal are incorrectly classified RB. Red highlighted column to the right indicates the per class error. The number at the bottom of this column is the overall error rate of the classification (5.04%).

```
TEST:ZDC37.test    Time: 0.07 secs  RMS Err: 0.142  Err: 5.04%
K-Nearest Neighbor (K=3) classifier: 20 cases - trained on 80% of data tested on 20% ECHO-BSD
-------------------------------------------------------------------------------------------
Desired|   Computed Class
Class  |   0    1    2    3    4  Total  Class  Patterns  #Errors  %Errors  StdDev   RMSE  Label
-------------------------------------------------------------------------------------------
  0_20 | 348    5                  353      0      353        5      1.42  ( 0.6)  0.075   0_20
 20_40 |   3   16    4              23      1       23        7     30.43  ( 9.6)  0.349  20_40
 40_60 |        7   10              17      2       17        7     41.18  (11.9)  0.406  40_60
 60_80 |                  3    1     4      3        4        1     25.00  (21.7)  0.316  60_80
80_100 |                      **     0      4        0        *        *       *       *  80_100
-------------------------------------------------------------------------------------------
 Total | 351   28   14    3    1   397  Overall  397       20      5.04%  ( 1.1)  0.142
-------------------------------------------------------------------------------------------
```

Data distributions seen in the top row of figure A.10-4 indicate that collection efforts for ZDC37 did not capture events associated with coverage of *etops25+* greater than 80%. As was discussed earlier, only two occurrences of RB within the [80–100%] interval were calculated for this limited data. The [80–100%] occurrences can be seen in the *etops25+* vs. RB training data distribution of figure A.10-4 (top row, first image), but consequently have no impact on classification. As a result, the KNN routine is limited to the construction of four decision regions when applying the full range of possible coverage by Wx parameters *etops25+, level3+wx*, and possible *wx-types*.

RB as a function of the single Wx parameter *etops25+* (bottom row, first image) shows that low fractional coverage generally corresponds to the [0–20%) RB interval. A mixed RB region develops between an *etops25+* range of 30% and 75%, with the majority of classifications being made at the [20–40%) and [40–60%) RB intervals. Beyond 75% of *etops25+*, the KNN routine classifies RB at the [60–80%) interval continuously. Examining the full range of each RB interval, we see that a general increase to higher RB occurs with increasing *etops25+*.

Addition of *level3+wx* as a second Wx parameter reveals a complex decision region within the *etops25+* vs. *level3+wx* plane (bottom row, second image). Once again, decision regions are limited to the four lower RB intervals. Small patches of noise within these regions are the result of isolated clusters associated with similar RB mixing within the input space. Regions are largest at the [0–20%) and [40–60%) RB intervals.

The scatter plot indicates how far the experimental training data extends into the *etops25+* vs. *level3+wx* input space (0–78% and 0–24%, respectively). Portions of the KNN decision regions that fall beyond the outlying points in the scatter are influenced mainly by those points and their associated RB values. This accounts for the large, broadly colored regions lying above the *level3+wx* data extent. While this complex decision region works to reduce the test errors of the classifier, the resulting decision surfaces probably do not accurately depict the ensemble decision surfaces.

Addition of *wx-type* associated with line increases noise only slightly while expanding the size of the decision region associated with a [20–40%) RB interval (bottom row, third image). The *wx-type* associated with stratiform events only slightly generalizes decision regions and with no effect on the expansion or contraction of regions as seen in previously discussed sections (bottom row, fourth image).

Comparing figure A.10-4 to figure A.0-1 indicates the ZDC37 KNN RB transfer function applied to the synthetic data set does not fit the expected functional dependence defined by the conceptual model. Decision regions of the KNN transfer function are disjoint and RB does not monotonically increase with increasing *etops25+* and/or *level3+wx*. Mixing of the input space makes the surfaces discontinuous. No decision region is resolved for the [80–100%] RB interval, and this lack of experimental data points corresponding to RB in the interval [80–100%] keeps the model from being a realistic, statistically meaningful representation of RB based on the chosen Wx parameters.

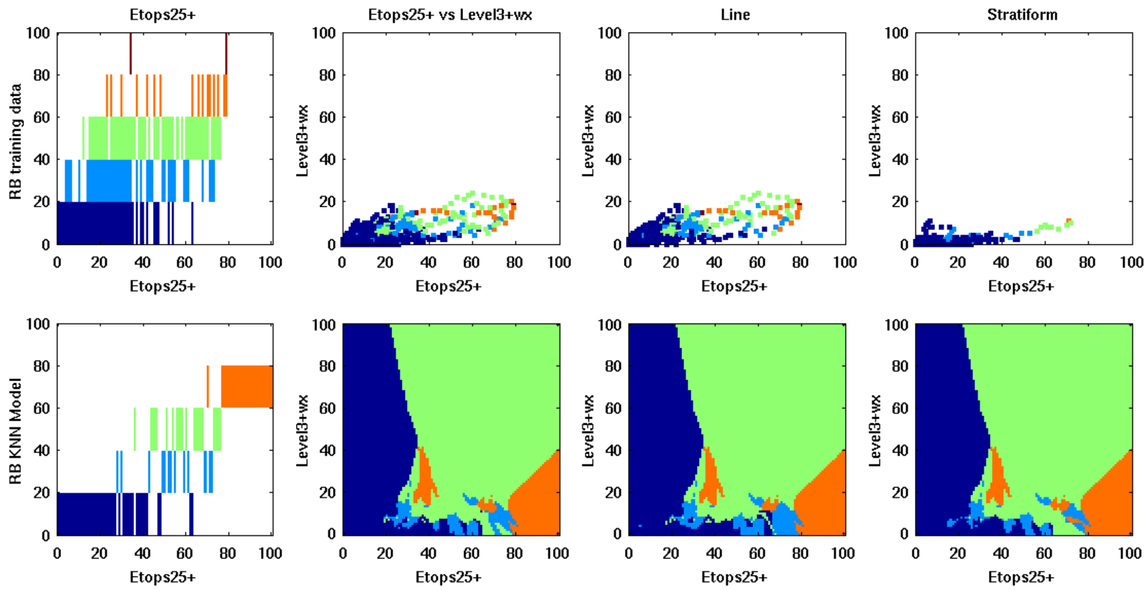

Figure A.10-4. (Top Row) ZDC37 training data distribution of discrete RB intervals as a function of etops25+, etops25+ *and* level3+wx, etops25+ *and* level3+wx *separated by* wx-type line, etops25+ *and* level3+wx *separated by* wx-type stratiform *(left to right, respectively). Colors differentiate between the five discrete RB intervals and are consistent throughout the figure. (Bottom Row) KNN transfer function of RB based on synthetic data covering full possible range of* etops25+, level3+wx, *and* wx-type. *For simplicity, poorly sampled* wx-types *small, large, and embedded are not shown. Complex decision regions in the last three images of the bottom row are colored by their respective RB interval.*

GLOSSARY

ARTCC	Air Route Traffic Control Center
ATC	Air Traffic Control
ATM	Air Traffic Management
CCA	Convective Constrained Area
CCFP	Collaborative Convective Forecast Product
CIWS	Corridor Integrated Weather System
ETMS	Enhanced Traffic Flow Management System
FAA	Federal Aviation Administration
FACET	Future ATM Concepts Evaluation Tool
IQR	Inner Quartile Range
KNN	K Nearest Neighbor
MIT	Miles-In-Trail
MLP	Multi-layer Perceptron
NAS	National Airspace System
NEXRAD	Next Generation Weather Radar
NWS	National Airspace System
PD	Probability
PPC	Practical Pattern Classification
RAPT	Route Availability Planning Tool
RB	Route Blockage
RCWF	Regional Convective Weather Forecast
SPT	Strategic Planning Team
TFM	Traffic Flow Management
WARP	Weather and Radar Processor
VIL	Vertically Integrated Liquid
VIP	Video Integrator Processor
VORTAC	VHF omnidirectional range station/tactical air navigation
Wc	Actual Weather Parameters
Wx	Weather
Wx-RB	Weather-Route Blockage
ZAU	Chicago ARTCC
ZBW	Boston ARTCC
ZDC	Washington ARTCC
ZID	Indianapolis ARTCC
ZNY	New York Center ARTCC
ZOB	Cleveland ARTCC

REFERENCES

DeLaura, R. and J. Evans, 2006: "An Exploratory Study of Modeling Enroute Pilot Convective Storm Flight Deviation Behavior," 12th Conference on Aviation, Range and Aerospace Meteorology, American Meteorological Society, Atlanta, GA.

DeLaura, R. and S. Allan, 2003: "Route selection decision support in convective weather: a case study of the effects of weather and operational assumptions on departure throughput," 5th Eurocontrol/FAA ATM R&D Seminar ATM-2003, Budapest, Hungary, http://atm2003.eurocontrol.fr/.

Dupree, W.J., M. Wolfson, R. Johnson, K. Theriault, B. Forman, B. Boldi, and C. Wilson, 2002: "Forecasting convective weather using multi-scale detectors and weather classification – enhancement to the MIT Lincoln Laboratory Terminal Convective Weather Forecast," 10th Conference on Aviation, Range, and Aerospace Meteorology, AMS, Portland, OR.

Fahey, T. and D. Rodenhuis, 2004: "Continual evolution of CCFP-User needs for extended range prediction, 11th Conference on Aviation, Range, and Aerospace Meteorology, Hyannis, MA.

Histon, J., R.J. Hansman, B. Gottlieb, H. Kleinwaks, S. Yenson, D. Delahaye, S. Puechmorel, 2002: "Structural Considerations and Cognitive Complexity in Air Traffic Control," 19th IEEE/AIAA Digital Avionics Systems Conference, Irvine, CA. (Can be downloaded from http://icat-server.mit.edu/Library/fullRecord.cgi?idDoc=203.)

Huberdeau, M. and J. Gentry, 2004: "Use of the Collaborative Convective Forecast Product in the Air Traffic Control Strategic Planning Process," April–June 2004, Air Traffic Control Association (ATCA) *Journal of ATC*, pp. 9–14.

Kukolich L.N. and R.P. Lippmann, 2004: *LNKnet User's Guide*, MIT Lincoln Laboratory, http://www.ll.mit.edu/IST/lnknet/usersguide.pdf.

Lippmann, R.P., L. Kukolich, and E Singer, 1993: "LNKnet Neural Network Machine Learning, and Statistical Software for Pattern Classification," *The Lincoln Laboratory Journal*, Vol. 6, No.2, pp 249–268.

Klingle-Wilson, D. and J. Evans, 2005: "Description of the Corridor Integrated Weather System (CIWS)," MIT Lincoln Laboratory Project Report ATC-317.

Mahoney, J.L., J.K. Hederson, B.G. Brown, J.E. Hart, A. Loughe, C. Fischer, and B. Sigren, 2002: "The Real-Time Verification System (RTVS) and its Application to Aviation Weather Forecast," 10th Conference on Aviation, Range, and Aerospace Meteorology, 13–16 May, Portland, OR.

Mahoney, J., S. Seseske, J. Hart, M. Kay, and B. Brown, 2004: "Defining observation fields for verification of spatial forecasts of convection: Part 2," 11th Conference on Aviation, Range, and Aerospace Meteorology, American Meteorological Society, Hyannis, MA.

Megenhardt, D. L., C. K. Mueller, N. A. Rehak, S. B. Trier, and D. Ahijevych, 2004: "NCWF-2 Probabilistic Forecasts," 11th Conference on Aviation, Range, and Aerospace Meteorology, American Meteorological Society, Hyannis, MA.

National Research Council, 2003: "Weather forecasting accuracy for FAA traffic flow management," National Academies Press.

Rhoda, D.A. and M. Pawlak, 1999: "An Assessment of Thunderstorm Penetrations and Deviations by Commercial Aircraft in the Terminal Area," MIT Lincoln Laboratory, Project Report NASA/A-2.

Rhoda, D., E. Kocab, and M. Pawlak, 2002: "Aircraft encounters with Thunderstorms in Enroute vs. Terminal Airspace Above Memphis, Tennessee," 10th Conference on Aviation, Range, and Aerospace Meteorology, American Meteorological Society, 13–16 May, Portland, OR

Robinson, M., J. Evans, B. Crowe, D. Klingle-Wilson, and S. Allan, 2004: "CIWS Operational Benefits 2002-3: Initial Estimates of Convective Weather Delay Reduction," MIT Lincoln Laboratory Project Report ATC-313.

Sims, D. and D. Rodenhuis, 2004: "Program Management for the Collaborative Convective Forecast Product (CCFP)," 11th Conference on Aviation, Range, and Aerospace Meteorology, American Meteorological Society, Hyannis, MA.

Troxel, S.W. and C.D. Engholm, 1990: "Vertical reflectivity profiles: Averaged storm structures and applications to fan-beam radar weather detection in the U.S.," 16th Conference on Severe Local Storms, American Meteorological Society, Kananaskis Park, Alta., Canada, pp. 213–218.

Wolfson, M.M., B. Forman, K. Calden, W. Dupree, R. Johnson, R. Boldi, C. Wilson, P. Bieringer, E. Mann, and J. Morgan, 2004: "Tactical 0–2 Hour Convective Weather Forecast for the FAA," 11th Conference on Aviation, Range, and Aerospace Meteorology, American Meteorological Society, Hyannis, MA.

Zobell, S., 2004: "Risk management decisions support for traffic flow management," 11th Conference on Aviation, Range, and Aerospace Meteorology, American Meteorological Society, Hyannis, MA.